Norwegian University
of Life Sciences

Master's Thesis 2021 60 ECTS
Faculty of Chemistry, Biotechnology and Food Science

Involvement of Ionotropic Glutamate- and TRPA1 receptors in Oligodendrocyte Response to Ischemia in Human Cerebral Organoids

Britina Kjuul Danielsen
Biotechnology

Involvement of Ionotropic Glutamate- and TRPA1 receptors to investigate the response of Oligodendrocytes to Ischemia in Human Cerebral Organoids

Oslo University Hospital, Department of Microbiology,

and

The Norwegian University of Life Science, Faculty of Chemistry, Biotechnology and Food Science

Acknowledgements

The work presented in this master thesis was carried out at the Department of Microbiology, Rikshospitalet, from August 2020 to May 2021 under the supervision of Johanne Egge Rinholm, PhD.

I would like to pay my special regards to my supervisor Johanne Egge Rinholm for giving me the opportunity to participate in this exciting project. Thank you for your encouragement and good and constructive feedback throughout this thesis. Your enthusiasm for your work and research experience was a motivation factor for me, and I highly appreciate all your help and advice.

I also want to express my gratitude to Niklas Meyer and Xiaolin Lin for help and guidance with growing cerebral organoids, and Emilie Rylund Glesaaen for teaching me lab techniques and tutoring me during this master project. You had always time when I struggled and for that I am profoundly grateful. Many thanks to Stig Ove Bøe and Anna Lång for teaching and assistance me with microscopy utilized at the core facility for advanced light microscopy at Gaustad.

I would also like to thank previous and current department managers Arne Klungland and Magnar Bjørås for the opportunity to write my thesis at Department of Microbiology, and to Lars Eide and Pernille Blicher at Department of Biomedical laboratory for allowing me to use the cell lab.

Lastly, I must express my gratefulness to the student office, for providing a lively and motivated working atmosphere. Special thanks to my lab- and writing partner Marie Landa Autsbø. Your company was always appreciated and thanks for turning frustrating situations into laughter. It has been a pleasure being a part of the Rinholm group,

Britina Kjuul Danielsen
Oslo, May 2021

Abstract

Stroke is the second leading cause of disability worldwide and is the most common cause of severe disability in Norway. 11 000 new cases occur every year in Norway, where 80-85 % are caused by cerebral artery blood clots or emboli, named ischemic stroke. Current treatment options for ischemic stroke are limited, and there is a need for new treatments that can reduce brain tissue damage after a stroke. Several neuroprotective agents have been developed, but none of the agents have passed clinical trials despite the success in preclinical studies. One reason for this could be because previous studies have ignored the importance of glial cells in stroke pathophysiology: the human brain has a much higher proportion of glial cells than other animals, and the number of oligodendrocytes is particularly high. Oligodendrocytes are the cells that myelinate axons and are crucial for neuronal signalling and their death leads to neuronal dysfunction. In stroke, neurons and oligodendrocytes are killed by mechanisms involving calcium overload, but new studies suggest that the upstream mechanisms differ between the two cell types. The different upstream mechanisms could explain the limited effects of neuroprotective agents on human stroke patients, since neuronal dysfunction will persist when oligodendrocytes are not rescued. Thus, saving the oligodendrocytes may be a significant factor in protecting brain tissue after an ischemic stroke and the scientific community urging to produce new experimental models to bridge the gap between animals and humans.

The aim of this thesis was to unravel mechanisms that cause oligodendrocyte injury in ischemic stroke. This was achieved by investigating the effect of inhibiting TRPA1-, NMDA- and AMPA receptors on oligodendrocyte survival after ischemia. Human cerebral organoids were produced from human induced pluripotent stem cells and were used as a model for the human brain. By immunohistochemistry, the results showed that inhibition of TRPA1 receptors increased the number of oligodendrocytes after ischemia. However, TRPA1 receptor inhibition also increased the overall number of apoptotic cells in non-ischemic conditions. By using RNA-FISH, TRPA1 receptor was detected in the human cerebral organoids, but methodological challenges prevented localization in specific cell types. Immunohistochemistry did not show any significant effect of NMDA- and AMPA receptor inhibition. Regardless, the results revealed large variations between the organoids and there is a need to improve the quality controls during development or include larger sample sizes in the experiments.

Abstrakt

Hjerneslag er den nest vanligste årsaken til uførhet verden og er den mest vanlige årsaken til alvorlig funksjonshemming i Norge. Hvert år er det 11 000 nye tilfeller i Norge hvor 80-85% er iskemiske hjerneslag, forårsaket av cerebral blodpropp eller emboli. Det er et stort behov for nye behandlingsformer som kan redusere ødeleggelsen av hjernevevet etter et slag, hvor nåværende behandling er svært begrenset. De siste årene har flere nevrobeskyttende midler blitt er utviklet, men ingen har blitt godkjent i kliniske studier til tross for preklinisk suksess. En av grunnene kan være at tidligere studier har ignorert viktigheten av gliacellene i hjerneslagets patofysiologi: menneskehjernen har en større andel gliaceller enn andre arter hvor antallet av oligodendrocytter er spesielt høyt. Oligodendrocytter er de cellene i sentralnervesystemet som myeliniserer aksonene og er helt avgjørende for nevronsignalisering hvor oligodendrocytt-død fører til nevronal dysfunksjon. Ved hjerneslag dør nevroner og oligodendrocytter av mekanismer som involverer kalsium-overflod, men nyere studier viser at oppstrømsmekanismen er ulik. Ulik oppstrømsmekanisme kan forklare den begrensende effekten av nevrobeskyttende midler hos mennesker fordi nevronal dysfunksjon vil vedvare hvis oligodendrocyttene ikke overlever. Dermed kan hindring av oligodendrocytt-død være en viktig faktor for å beskytte hjernevevet etter hjerneslag og forskningsmiljøet oppfordrer til å utforske nye, eksperimentelle metoder for å dekke avstanden mellom ulikhetene mennesker og dyr.

Målet med denne oppgaven var å avdekke mekanismer som forårsaker skade på oligodendrocytter ved iskemisk hjerneslag. Dette ble oppnådd ved å utforske effekten av oligodendrocyttene etter hjerneslag ved å blokkere TRPA1-, NMDA- og AMPA reseptorene. Humane cerebrale organoider var produsert fra human induserte pluripotente stamceller og var brukt som modell for den menneskelige hjernen. Ved å bruke immunohistokjemi viser resultatene at inhibering av TRPA1 reseptoren økte antallet av oligodendrocytter etter hjerneslag. Samtidig økte antallet av apoptotiske celler i organoider som ikke hadde fått indusert hjerneslag. Ved å bruke RNA-FISH ble TRPA1 reseptoren detektert i humane cerebrale organoider, men metodologiske utfordringer hindret lokalisering i spesifikke celletyper. Immunohistokjemi viste ingen signifikant effekt av å inhibere NMDA eller AMPA reseptorene. Resultatene viste likevel stor variasjon blant organoidene og det er dermed nødvendig å forbedre enten kvalitetskontroller gjennom organoide-dyrking eller inkludere større prøvemengder i eksperimentene.

Abbreviations

3D	three-dimensional
A96	A967076
AIF	apoptosis-inducing factor
AMPA	α-amino-3-hydroxy-5-methyl-4-isoxazole propionic acid
ANOVA	analysis of variance
AP5	D-2-amino-5-phosphonopentanoate
APC	Adenomatous polyposis coli
ATP	adenosine triphosphate
BDNF	brain-derived neurotrophic factor
Calcium	Ca2+
Cas-3	Cleaved Caspase-3
cDNA	complementary DNA
CNS	central nervous system
Ct	cycle threshold
DAPI	4`-6-diamidino-2-phenylindole
DAPK1	death-associated protein kinase 1
DMSO	dimethyl sulfoxide
dsDNA	double stranded DNA
EB	embryoid bodies
EBM	embryoid body medium
EtOH	Etanol
FISH	fluoresence in situ hybridisation
GAPDH	Glyceraldehyde 3-phosphate dehydrogenase
h	hour
HC-3	HC-030031
HGF	hepatocyte growth factor
hiPSC	human induced pluripotent stem cells
HK gene	housekeeping gene
IGF1	insulin-like growth factor 1
IHC	immunohistochemistry
MBP	Myelin basic protein
mRNA	messenger RNA
NBQX	3-dihydroxy-6-nitro-7sulphamoyl-benzo(F)quinoxaline
NDM	Neuronal differentiation medium
NG2	neuronal-glial antigen 2
NIM	Neural Induction Medium
NMDA	N-methyl-D-aspartate
NT-3	neurotrophin 3
OPC	oligodendrocyte prognitor cells
OPCM2	OPC medium 2
PBS	phosphate-buffered saline

PDGFRα	platelet-derived growth factor receptor alpha
PFA	paraformaldehyd
PLP	proteolipid protein
ROS	reactive oxygen species
RT-qPCR	Quantitativ reverese transcription PCR
TRP	transient receptor potential
TUJ-1	Neuron-specific class III beta-tubulin

Table of content

1. Introduction

1.1 The major cell types in the central nervous system

Human brain development begins during the third week of the gestation and is a prolonged process of neural progenitor cell differentiation and migration. Migration starts from the embryonic neuronal tube, and through a range of processes from molecular events of gene expressions to environmental input, they finally form the different brain regions and the spinal cord (1, 2). Both are essential for normal brain development and are characterized as complex series of organized processes, which operates to promote differentiation of neural structures and function throughout the development. By the end of the embryonic period, the establishment of the elementary brain structures and the central nervous system are complete, defining the major components in both the central and peripheral nervous system (1). The major cell types in the human central nervous system (CNS) are nerve cells and glial cells, where approximately 50% are glia (3), although this number are disputed. Nerve cells, also called neurons, have a cell body called soma, sensory dendrites and an axon, that interconnect with the surrounding cells. Neurons communicate with chemical and electrical signals and an integral part of this communication is the transmission of action potentials along their axons (4). Until Altman and colleagues finding in the 1960s, it was assumed that the adult brain was unable to generate new neurons (5, 6). Today, it is well-known that neurons cannot undergo mitosis, but new neurons are continuously generated throughout life. Research has showed neural stem and progenitor cells to present, having the capacity for long-term self-renewal. These stem cells are capable to generate multiple lineage cells, including glial cells, but how this adult neurogenesis on the molecular level is regulated are still controversial (6).

The glial cells in the CNS are also called “helping cells” and were for a long time thought to only function as passive supporters of neurons (7). Recently, researchers have found that glial cells are critical participants in the brain development as in the brain functions and survival. They contribute in the plasticity and in diseases, and presumably control the formation, timing and location of synapses in addition to regulate the blood vessel flow (8). In the central nervous system, the major glial cell types are astrocytes, microglia and oligodendrocytes. These have all diverse roles for development and maintenance of the nervous system. Astrocytes are the most abundant glial cell in the CNS and are essential for neuronal survival. They interact with both neurons and vasculature to take up nutrients from the blood to support the neurons and are

a part of the blood-brain barrier, important for the microenvironment in the CNS (9). Astrocytes also remove and recycle neurotransmitters and control the formation, strength and turnover of synapses, which are the chemical contact site for the neuronal communication (7, 8). Studies have also shown that astrocytes are required for survival and maintenance of oligodendrocytes and its myelin integrity, although this is still less defined *in vivo* (1*0).* Microglia are the resident immune cells of the CNS and have an important role during development, adulthood and aging (11). Together with astrocytes, microglia are important during synapse remodelling to achieve precise wiring (7). They are therefore, the first line of defence in the CNS located perivascular to manage fast screening for blood-borne substances and potential inflammatory stimuli in the brain (9). Oligodendrocytes and Schwann cells are the myelinating glia cells in the central and nervous systems, respectively. These cells allow rapid signal transmission in the neurons by wrapping their membrane in a multilamellar fashion, forming an electrical insulator around the axons (7, 12). I will later describe oligodendrocyte development and physiology in more detail.

1.2 Maturation and myelination of oligodendrocytes

As mentioned above, oligodendrocytes are the myelinating glia cells in the CNS. The central function of oligodendrocytes is to produce myelin that wraps around the axons, creating *myelin sheaths* in a concentric fashion. The myelin sheath is a lipid rich substance made from an extension of the oligodendrocytes plasma membrane where its function is to insulate the axons to allow rapid and efficient axon potential propagation along the axons (12, 13). The myelin sheaths are not continuous but separated evenly by regions of unmyelinated areas, called nodes of Ranvier. Due to the myelin, the axon potential that travels along the myelinated axon can "jump" from one node of Ranvier to the next, reducing time to transmit signals. Here, at the nodes, voltage-gated sodium channels are present helping ions to cross the membrane and thereby regenerating the action potential as well as increasing the conduction velocity, also named saltatory conduction (12). Neurons, or more precisely the axons, can be both myelinated and unmyelinated and are grouped into white and grey matter based on the myelin content. The white matter area contains the myelinated axons making interconnection with the neuron-rich grey matter (14). Oligodendrocytes myelinate axons during development as well as remyelinate after injury caused demyelination. This task is highly energy-demanding, thereby consuming a large amount of energy, such as glucose and lactate. However, despite this high energy need for myelin synthesis, this task is still favourable due to the reduction in the energy required for action potential in myelinated axons (15). In addition to allow efficient axon potential

propagation, studies have shown that oligodendrocytes also provide trophic and metabolic support to the underlying axon by transporting lactate, which has shown to be critical for axon survival (16).

Each mature oligodendrocyte generates up to 60 myelinating processes and thereby interconnect to many axons from just one cell. These myelinating processes vary in lengths from 20-200 μm long and can wrap the axon up to 100 times, making the oligodendrocyte the largest cell in the entire body when outstretched (14).

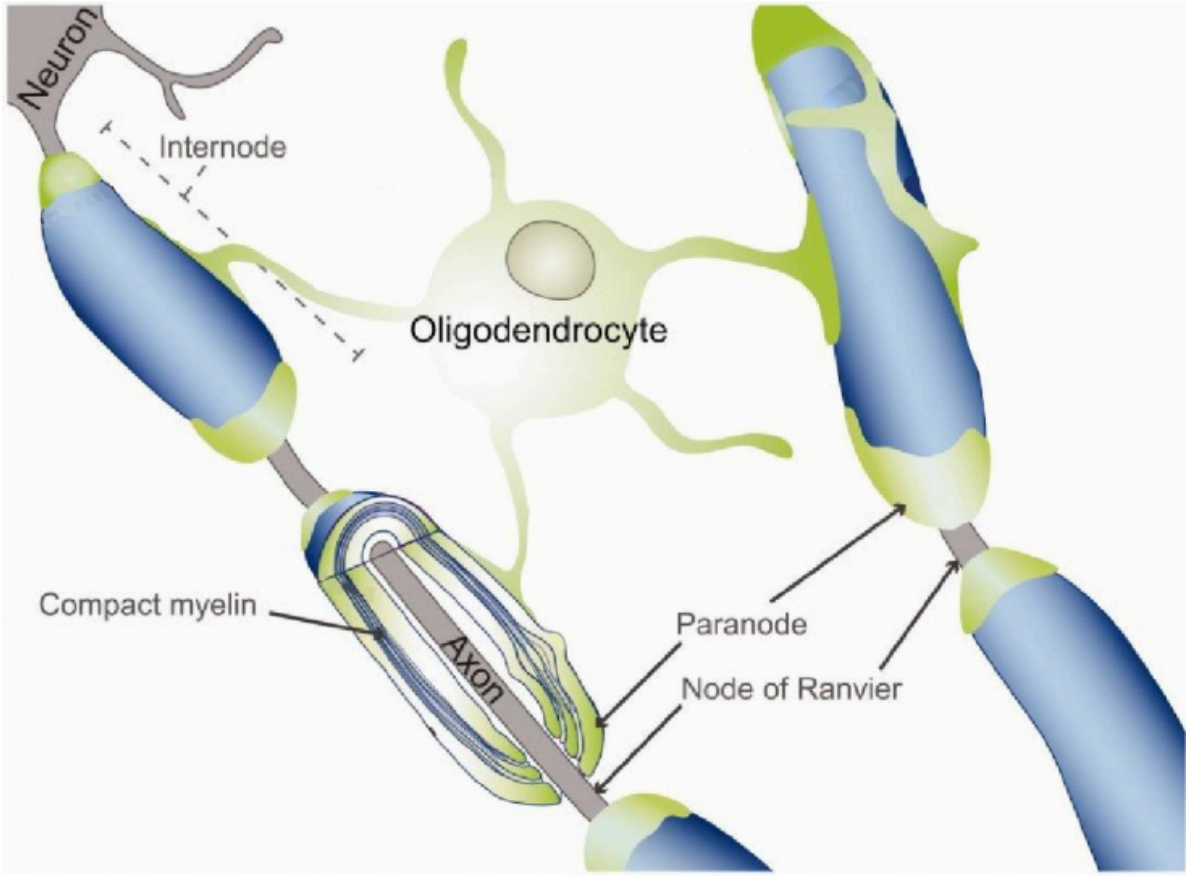

Figure 1: Illustration of mature oligodendrocyte with myelinating processes. Myelinating oligodendrocytes wrap their lipid rich membrane around axons in multiple layers making compact myelin sheets. Each oligodendrocyte can myelinate multiple axons, where one segment of myelin is called an internode. The myelin membranes are less densely wrapped at the paranodes, which flank the nodes of Ranvier. Adapted from Rinholm et at. 2016 (17).

In mammalian CNS, oligodendrocyte linage cells develop from neural progenitor cells from the ventricular germinal zones of the embryonic neural tube (13) which further transform into radial glia cells, generating progenitor cells for oligodendrocytes, astrocytes and neurons (7). After neurons have been generated, the radial glia cells start to differentiate into oligodendrocyte precursor cells (OPC) or astrocytes, controlled by release of numerous secreted

signals that act together to control the cell fate spatially and temporally (7). OPCs then migrate and proliferate away from these zones into developing white and grey matter.

For OPCs to become mature, myelinating oligodendrocytes, they further differentiate into late oligodendrocyte precursor cells, via pre-myelinating oligodendrocytes and finally to mature oligodendrocytes, showed in figure 2 (12, 13). Throughout the different developmental stages, the oligodendrocytes express different proteins and transcriptional factors that can be used as markers of the developmental stages. Early OPCs express a polysialoganglioside (A2B5) on the cells surface and is a highly specific marker for the oligodendrocyte lineage in the brain (12). These cells can differentiate into both astrocytes and oligodendrocytes, depending on the environmental signals (12). Together with A2B5, Olig1, Olig 2 and SOX10 are all transcription markers for the early OPCs and are expressed throughout the linage into mature oligodendrocytes. When OPCs start to differentiate into late OPCs, the A2B5 expression ceases and starts expressing platelet-derived growth factor receptor alpha (PDGFR- α) and neuron-glial antigen 2 (NG2) (13). As the late OPCs start to differentiate into immature oligodendrocytes, the cells begin to express a mixed antigen called O4, localized at the cell surface and in the myelin, thereby expressed in the mature oligodendrocyte as well (18). From the pre-myelinated stage, the oligodendrocytes start to express an antigen called O1, a glycolipid found in the myelin, and both the NG2 and PDGFR-α will no longer be expressed. Mature oligodendrocytes are finally capable to myelinate axons and can be localised by the marker myelin basic protein (MBP), which is at this time highly expressed together with a protein called proteolipid protein (PLP). Adenomatous polyposis coli (APC) is a tumour suppressor gene found in multiple cell types and can be used as a marker for mature oligodendrocytes, localised in the oligodendrocytes cytoplasm (19). These different markers are highly used for identification of oligodendrocyte lineage cells in research, when the different developmental stages can be easy detected by their selective proteins.

OPCs expressing the NG2 antigen are present in both white and grey matter throughout development and into adulthood (20). They represent a large population of resident progenitor cells being capable of rapidly react to injury with the potential to repopulate the lesion by proliferation. Researchers have also discovered neuron-glial synapses in NG2-glia, indicating neurotransmitter-mediated signalling between neurons and NG2-glia, and may have a modulatory role in the development of these glial cells. Although, they precise physiological role(s) are still undefined. The best established role of NG2-glia is to generate oligodendrocytes

and are therefore often referred to OPCs. Besides this, NG2-glia can also produce astrocytes, depending on the developmental stage and the brain area, or remain self-renewing NG2-glia cells (20).

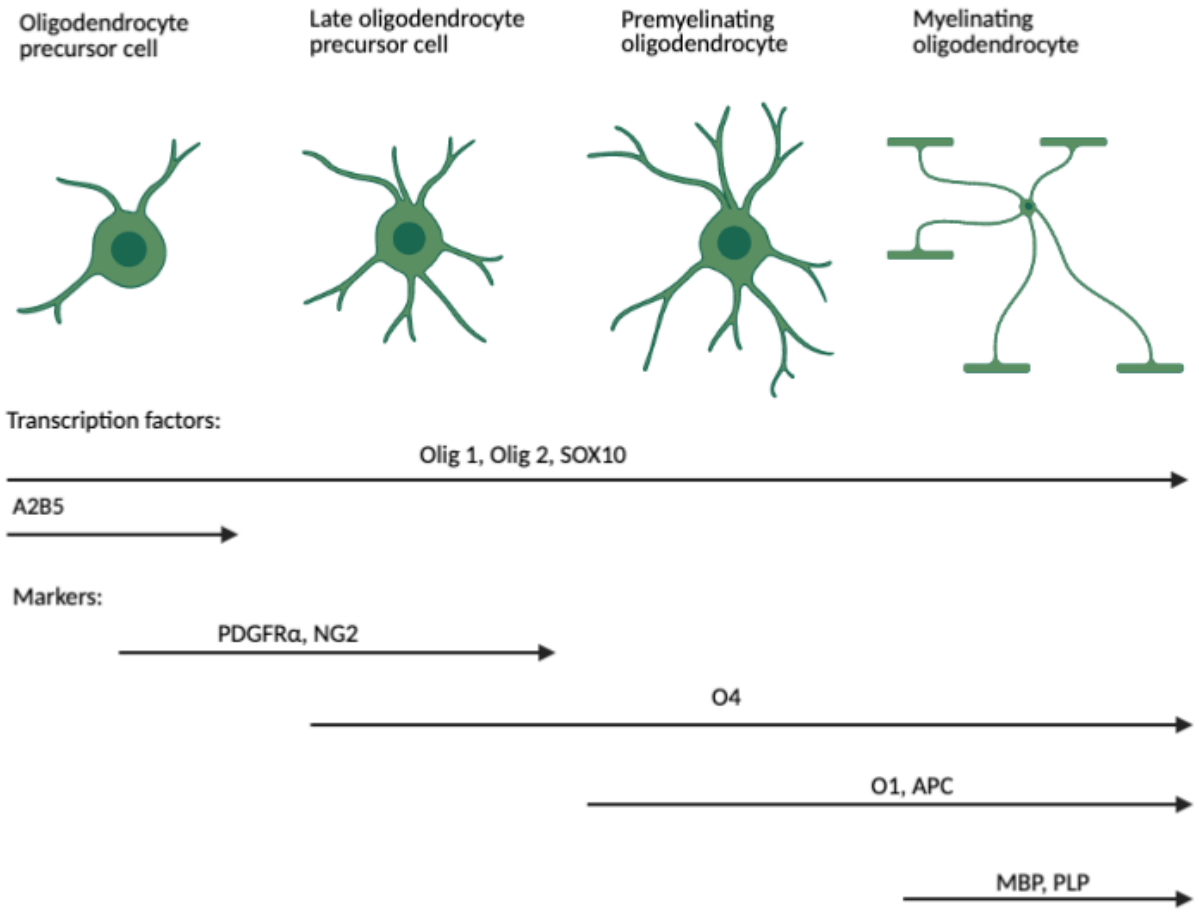

Figure 1: **Overview of the oligodendrocyte differentiation steps with corresponding transcription factors and specific markers**. A subset of different proteins or transcription factors are expressed in oligodendrocyte lineage cells and is often used as markers to detect and localize the oligodendrocytes at the different developmental stages. Modified from Kuhn et al. 2019 (12).

1.3 Ischemic stroke

Stroke is a common worldwide cerebrovascular disease and is a major cause of death and disability (21). It is a condition whereby the blood flow to a part of the brain is entirely blocked or reduced. This can be caused by two distinct reasons: occlusion of the blood vessels or a rupture, namely ischemic and haemorrhagic, receptively, and the rest of this chapter will focus on ischemic stroke. The majority of the stroke incidences today are ischemic strokes, reasonable for to up to 70-80% of the incidences globally (21). A study from 2013 showed a significant increase in the number of "disability-adjusted-life-years" in patients suffering from stroke globally between 1990-2013, and a mortality rate of 25% (22). Unfortunately, today, treatments

for ischemic stroke are limited where thrombolysis, platelet inhibitors and surgically removing of the thrombosis are the only options and need to be executed within few hours after symptoms for treatment success.

The brain is fully dependent on glucose and oxygen that are distributed to the brain through the blood stream. Glucose enters the cells cytoplasm through glucose transporters where glycolysis breaks down the glucose to small metabolites called pyruvate, and oxygen is needed for the complete degradation of fats, carbohydrates and amino acids by oxidative phosphorylation. The glycolysis generates a small number of energy-carrying molecules, adenosine triphosphate (ATP). The pyruvate metabolite can further be processed in the cell´s mitochondria to make a larger number of ATP molecules by the oxidative phosphorylation via the tricarboxylic acid cycle (23). These ATP molecules are highly necessary for normal maintenance of ion-gradient homeostasis across the cell membrane and is essential for diverse cellular processes, particularly in the central nervous system. For the neurons, is it extremely important for their axon potential propagation and recovery, together with neurotransmitter synthesis and as well as for other demands not signalling related (23, 24). During ischemia, blood supply to a part of the brain is reduced or stopped due to a blocked vein, resulting in low concentrations of nutrients and oxygen in the affected tissue. The glycolysis pathway thereby convert from aerobic to anaerobic glycolysis and highly reduce the efficiency of ATP production (23).

The affected area is called *ischemic core* and is fatally injured and will subsequently causing cell death by necrosis (25). Around this area, a region of less affected tissue is located with reduced blood flow but remains metabolic active, called the *penumbra*. This part of the brain is in focus for poststroke treatment which potentially can salvage the tissue from dying due to longer lifetime for the cells before eventually excitotoxicity kill them (25).

1.4 Mechanisms of excitotoxic cell death in ischemic stroke

As the ischemic core grows during an ischemic event, the penumbra grows with it, and reduced blood flow in the penumbra can lead to apoptotic cell death hours and days following the stroke. During stroke glucose cannot enter the cell for energy production, leading to low levels of ATP. Na^+/K^+ -ATPases consume ATPs to maintain the ion-gradient homeostasis in all cells, and will in ischemic onsets become dysfunctional, resulting in depolarization of the membrane (26). Neurotransmitters are released into the synaptic cleft due to the depolarization, illustrated in

figure 3. Usually, excess of neurotransmitters is removed by neurotransmitter transporters to keep this level under tight control and eliminate constantly activated neurons when increased levels are toxic for the cell. These are located at the pre-and postsynaptic cell and on astrocytes in close location for rapid uptake when released to the synaptic cleft (27). But due to the ion-gradient change across the cell membrane, the neurotransmitter transporters are reversed, resulting in excessive release of neurotransmitters (27).

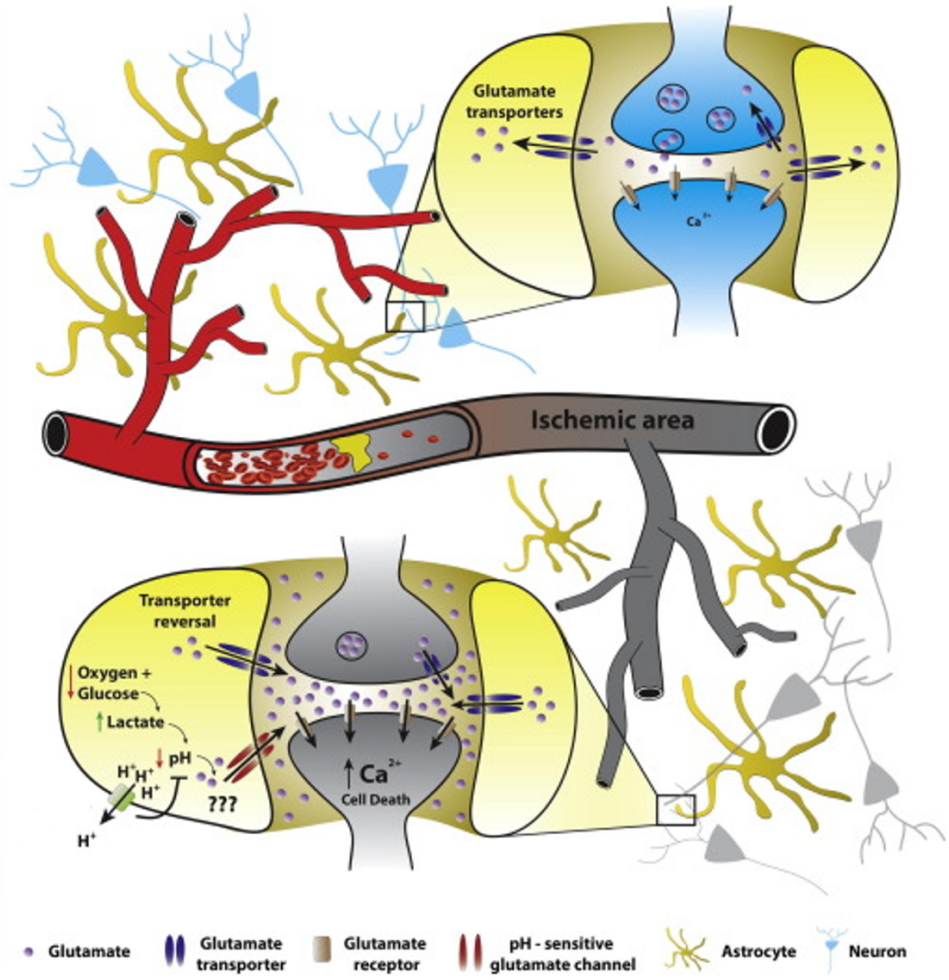

Figure 3: Illustration of ischemia-induced excitotoxicity. As the blood supply are being blocked during ischemic stroke, oxygen, glucose and ATP level decline in the ischemic area. As a result, astrocytes accumulate lactate levels, acidifying the intracellular space and is correlated with neuronal cell death when alkalization is capable of attenuating the neurotoxic effect. Glial glutamate release due to declining cytoplasmic pH remains to be elucidated. Normal ion-gradient homeostasis halts in the absence of ATP and as a consequence, glutamate transporters are reversed and expel glutamate from astrocytes and neurons into the synaptic cleft. Increased extracellular glutamate activate glutamate receptors on neurons and results in toxic influx of calcium. Adapted from Sloan et al 2014 (28).

N-metyl-D-aspartate (NMDA)-, α-amino-3-hydroxy-5-methyl-4-isoxazole propionic acid (AMPA)- and kainite receptors are activated by glutamate, leading to a change in the cell's ion gradient. In normal conditions, activation of these receptors is under tight control when they are essential for controlling the synaptic plasticity. But, during stroke, high levels of glutamate

result in Na^+ influx (and some Ca^{2+}) through the AMPA receptors, which further activates the NMDA receptors highly permeable for calcium (Ca^{2+}). K^+-ions are released from the cell as a result to the positive charge escalating in the cells cytoplasm (29). Ca^{2+} concentration is tightly regulated in physiological conditions, when high levels or prolonged rise can be toxic for the cells. As Ca^{2+} itself is a signalling molecule participating in regulating biological processes, it needs to be under tight control (29). Thereby, the constant influx of Ca^{2+} during stroke causes dysfunctional machinery that regulate this level, resulting in an excitotoxic cascade that contributes to cell death through either necrosis or apoptosis, depending on the mitochondrial functions and the recovered ATP level (30-32).

Mitochondria control every aspect for cell function, including managing redox status, modulating Ca2+ homeostasis, generating ATP and regulating response to cellular and environmental stresses (32). They are considered as the master regulator for stress-signalling and thereby being crucial regulators of cell survival. Mitochondria are expected to influence cellular apoptosis due to the release of proapoptotic factors to the cytoplasm. Apoptosis is a process that requires ATP and the cells have thereby a threshold value for when they can initiate apoptosis(33). Therefore, if the cells have lost a high ATP level, necrotic cell death will happen rather than apoptotic and trigger inflammation reaction in the tissue. As the most of ATP production happens in the mitochondria through ion transport processes across their double cell membrane, loss of ion-gradient homeostasis due to ischemic stroke depolarized the membranes and results in excessive production of reactive oxygen species (ROS) and decreased ATP generation. Cytotoxic accumulation of intracellular Ca^{2+} and the over production of ROS results in opening of mitochondrial transitions pores where apoptosis-inducing factor (AIF) and cytochrome c are released (32). These proteins further activate apoptosis by either activating caspases to induce DNA damage in the nucleus or mediate a large-scale DNA fragmentation, where caspase-3 is identified as the key mediator of apoptosis (34).

1.5 Mechanisms of oligodendrocyte death in ischemia

Oligodendrocytes and the other glial cells are all necessary for proper brain function and cell injury caused by ischemia will have impact on all these cell types (35). The pathway to cell death described above have been discovered in neurons, but the mechanism of how oligodendrocyte dies after ischemia are still controversial, and studies have shown that oligodendrocytes are more vulnerable to ischemia than neurons (36, 37). As mentioned above, high levels of intracellular Ca^{2+} is toxic for the cells, including the oligodendrocytes, and myelin

damages and oligodendrocyte death occurs in a Ca^{2+} dependent manner (38). The mechanisms that cause intracellular Ca^{2+} overload and cell death in oligodendrocytes have been under debate for decades. In 2005-2006, several studies showed that oligodendrocytes express NMDA receptors and suggested that the cell-death mechanisms are similar to those of neurons (39-41). However, in 2016, Hamilton et al showed in a mice model that intracellular Ca^{2+} does not rise through these receptors alone and additionally showed a downregulation of NMDA receptors in mature oligodendrocytes (38). Therefore, another receptor must be responsible for the influx. Hamilton et al. (2016) further showed that the accumulation of Ca^{2+} in the oligodendrocytes was pH-dependent, exhibiting that a rise in extracellular K^+ acidified the cells by K^+ influx through K^+-channels. The transient receptor potential (TRP) channel family share this property allowing Ca^{2+} into the cell, and the transient receptor potential cation channel subfamily A member 1 (TRPA1) and subfamily V member 3 (TRPV3) are the only one activated by intracellular H^+ (fig. 4). Together with metabolic changes and the decreased pH due to K^+ influx, TRPA1 activation rise intracellular Ca^{2+}, resulting in blockade of the action potential propagation due to myelin loss (38). By this study, Hamilton et al challenged the old model of oligodendrocyte death in ischemia. Still, more studies are needed to confirm or disprove this new hypothesis.

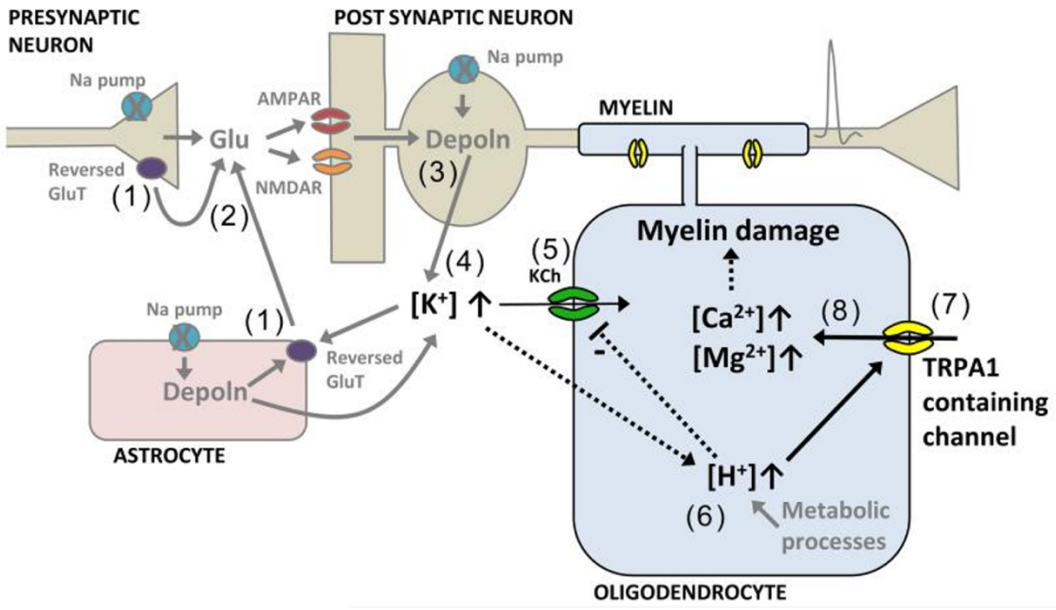

Figure 4: Illustration of Ca^{2+} influx in oligodendrocytes. Na^+/K^+-ATPases becomes dysfunctional due to energy loss during stroke, resulting in depolarization of the membrane and reversing of glutamate transporters (GluT) (1) and released glutamate (Glu) (2). Glutamate depolarizes the post synaptic neuron through NMDA and AMPA receptors and causes a neurotoxic rise of Ca^{2+} intracellular (3). This rises extracellular K^+ (4) which further causing an inward current (5) through K^+ channels in oligodendrocytes (5). This extracellular K^+ rise together with metabolic changes increase the H^+ concentrations in the oligodendrocytes (6) that further activate TRPA1 channels (7) resulting in an influx of Ca^{2+} and Mg^{2+} where the rise of Ca^{2+} (8) damage the myelin. Adapted from Hamilton et al. 2016 (38).

Oligodendrocytes have the highest content of protein-bound iron (Fe^{2+}), an important co-factor for cholesterol- and lipid synthesis, needed for myelin production (42). During stroke, in addition to being highly sensitive to the Ca2+ concentration, oxygen deficiency leads to free cytosolic Fe^{2+} causing reaction with hydrogen peroxide that catalyses to hydroxyl radicals (the Fenton reaction), an oxidant resulting in oxidative stress in the cell (43, 44). An additional way to promote apoptosis in the cell is realise of ceramide, a constituent in the myelin. Studies has shown that ceramide is a pro-apoptotic molecule, and accumulation due to myelin degradation during stroke lead to cell death by apoptosis (45).

1.6 Stroke therapy

Stroke research has been ongoing for decades, and the models and methods used have been improved every year. *In vivo* animal models for stroke research are today the most common model used worldwide, where rats and mice are the most used species (46). This has the advantage of simulating the complex ischemic cascade and allowing the researcher to control the durations and location of ischemic stroke, together with the possibility to test the animals function and behaviour during and after the event (47). In addition, cell cultures have been used and led to answers of the pathophysiology around ischemic stroke and are commonly used in in research today (48). However, animal models are still needed in order to study the interplay between the brain cell types and their signalling pathways, which is a limitation using cultured cells (46, 49).

The aim for stroke therapy is to restore the blood flow to the affected region and, if possible, modulate treatments that can stop the tissue for further destruction or repair the damaged area (50). Even though hundreds of neuroprotective agents have been tested and been effective on mice, no one have passed any clinical trials on humans (46). This can be due to the differences in the physiology between the mice and humans. Mice have a grey to white matter ratio of 90/10, which is only one fourth of what human brain contains, where in addition, humans have a much higher percentage of glia cells (3, 51). Mice also seems to differ in their metabolic activities and their genetic similarity compared with humans which play an important role in the search of neuroprotective agents (52). Despite the more recently knowledge about the importance of the glia cells, primary focus in mouse model studies have been on the neurons role and how to protect them from excitotoxicity (53). Therefore, these differences and the

limited focus on the glia cells could explain the insufficient effect of the therapeutic drugs developed during the last years when tested in humans (49, 53).

New strategies for treatment investigation have been on inhibiting various types of receptors responsible for excitatory neurotransmitter release or indirectly improves cell death in brain tissue. The NMDA receptor has been widely studied with the aim to save neurons, and can be inhibited to prevent glutamate to react and thereby reduce the Ca^{2+} influx (54). Even though plenty of antagonists have been reported as safe, some gave side effects in clinical trials and limited the use (54, 55). Other targets than the receptor itself have been tried including Ca^{2+} -channel antagonists (56), Na^{+} -channel antagonists and inhibiting glutamate release including synthesis of neuronal nitric oxide with the aim to reduce neuronal damage after stroke, all with poor or negative results in clinical trials (57). Other targets that have been tested in the excitotoxicity cascade are the NMDA subunit (58), the death-associated protein kinase 1 (DAPK1) (59) and prevention of free radicals evoked during stroke (60). A peptide called NA-1 disarranges the NMDA subunit and showing promising data, but larger clinical trials are needed to evaluate a neuroprotective effect. DAPK1 is another signalling pathway for apoptosis and rearrange with the NMDA receptor during stroke. This pathway has been considered as a potential target for inhibiting the initiation of apoptosis, but studies are not ready for any conclusions. The use of a free radical-trapping agents, NXT-059, to limit free radicals during stroke showed a promising treatment effect, but when tried in a larger clinical trial, the treatment showed an ineffective neuroprotectant in acute ischemic stroke (58-60). In addition of the primary focus of neuron protective agents, the pathway to apoptosis is comprehensive and one target to reduce the post-stroke damaged will not be enough.

The research on oligodendrocyte in ischemic stroke events have become wider in the last decades. A study from 2005 shows that inhibition of NMDA- and AMPA receptor reduced the glutamate-evoked current in oligodendrocytes (identified by the use of NG2, O4 and MBP markers), thereby suggesting NMDA and AMPA receptor presence in precursor, immature and mature oligodendrocytes in rats (39). Although these findings, the distribution of the NMDA receptor was reduced as the more differentiated the oligodendrocyte became and was only present in the mature oligodendrocytes myelinating processes (39). Although, at these processes, the intracellular space is narrow, and activation of NMDA receptors could give large rise of intracellular ion concentrations resulting in myelin damage. Blocking of both NMDA and AMPA receptor have thereby indicated to attenuated oligodendrocyte damage in rat and

cultured oligodendrocytes by reducing the influx of ions through the membrane, suggesting a potential therapeutic target for white matter injury (39, 61-63). Other studies have shown that glutamate receptors are involved in oligodendrocyte development and myelination (64, 65). Thereby, the therapeutic goal should not only attempt to reduce the potential injury in the penumbra after ischemia, but also focus on the proliferation mechanisms of new oligodendrocytes with the aim to remyelinate the damaged area. As described previously, NMDA- and AMPA receptors are not the only one responsible for the Ca^{2+} influx. TRPA1 activation duo to rise in intracellular H^{+} results in Ca^{2+} influx, thereby damaging oligodendrocytes. These receptors can therefore be a potential new therapeutic target in white matter ischemia, but few studies have examined the TRPA1 receptor contribution in human stroke (38, 54).

In summary, the functional anatomy and cellular distribution difference between animal models and humans could explain why no cell-protective treatments have passed any clinical trials. The need of development of new, improved *in vitro* human models taking all different brain cells into consideration are necessary to understand the complex cascades happening during and after stroke.

1.7 Human Cerebral Organoids

When studying the functioning of the brain and diseases, traditional methods such as animals-models and 2D-tissue culture techniques are used by neuroscience research for decades but have not given all the answers researchers are looking for. Animals and human brains have differences in structures and cell ratios, and cannot be fully representative for human disease pathology (52). 2D tissue culture techniques identify mechanistic pathways associated with simple phenomena and have given important and relevant insights in cell biology. However, 2D tissue cultures are not able to present the complete tissue since they only contain one or two different cell types in few layers. The human brain is a complex three-dimensional (3D) arrangement of cells and structured regions. To get a better understanding and visualization of the brain structures in vitro, a 3D brain model is necessary. At the beginning of the 20th century, Henry Wilson discovered dissociated sponge cells reassembled back to create a whole organism, and thereby, the explore of growing artificial organs started. (66). In the last decades, new methods of growing tissue have been examined, and the method developed by Lancaster and colleagues of growing cerebral organoids have now become known worldwide (67).

Cerebral organoids are 3D spherical organoid structures artificially grown by reprogram differentiated cells back to stem cells state, a method that was pioneered by Shiniya Yamanka, earning him the 2012 Nobel prize in medicine (68). The creation of human cerebral organoids starts with human induced pluripotent stem cells (hiPSC), that are generated by converting adult human fibroblast into stem cells by the activation of specific gene transcription factors (67, 69). By adding patterning factors to the different culture mediums, discreate brain regions can be developed with structures organized in a similar manner that resembles the human brain. Alongside controlling the differentiation of the hiPSCs with the use of different growth factors, the cells will eventually form embryonic bodies (EB), which start creating neuroectoderm and further mature into cerebral organoids (67). One drawback of using organoids is the lack of a vasculature system, and the nutrients must diffuse into the organoid. Eventually, the diffusion efficiency will be reduced as the organoids grow more substantial and thereby result in necrotic cores in organoids older than a couple of months (67).

The greatest advantage of using cerebral organoids as a research model is that they allow us to investigate the development and diseases on human brain tissue under conditions monitored by the researcher. The growth of organoids from Lancaster and colleagues protocol resembles the early developing human brain. This creates a good model for studying neurodevelopmental disorders, e.g. microcephaly, a condition where the brain is smaller in size, autism and epilepsy (67). Despite this young brain imitation, cerebral organoids give the opportunity to investigate neuronal tissue and the interplay between the different cell types *in vitro.* Even though animal models are still necessary for further neuroscience, cerebral organoids are to be expected as an important tool of future research to model human pathophysiology. In addition, this new *in vitro* model contributes to first of the 3Rs for research animal welfare: replacement, reduction and refinement, meaning that the use of research animal can in some be avoided (70, 71).

2. Aims

Current treatment options for ischemic stroke are limited, and there is a need for new treatments to reduce brain tissue damage after the ischemic stroke. As no neuroprotective agents have passed any clinical trials despite preclinical success, this suggests s a different pathophysiology between animal models and human brain tissue. Oligodendrocytes are crucial for neuronal signalling and the mechanisms leading to their cell death in ischemia are controversial. While several studies have suggested that ionotropic glutamate receptors are involved, others have pointed towards TRPA1 receptors.

Previous studies have shown that TRPA1 receptor are the dominant contributor in calcium overload in mice oligodendrocytes. Therefore, the overall aim for this thesis was to test the involvement of ionotropic glutamate- and TRPA1 receptors in oligodendrocyte response to ischemia in human cerebral organoid model. To answer this, different antagonists were used where the main goal was to test whether blocking one or more receptors had any influence on:

1. Total cell density and cell death

2. Density of oligodendrocyte lineage cells

Another aim was to localize the TRPA1 receptor in human brain tissue to investigate if the receptor was expressed in oligodendrocytes and other cells in the CNS.

3. Materials and Method

3.1 Experimental setup

Human cerebral organoids developed from induced pluripotent stem cells was used in this project to investigate the involvement of ionotropic glutamate and the TRPA1 receptors in oligodendrocytes in response to ischemic stroke.

First, human cerebral organoids were prepared and cultured for three months. Then, different durations of *in vitro* ischemia were induced; 5 hours and 11 hours, together with a control with no ischemia. In their 3-days recovery, antagonists were added to different organoid groups. The treatments were D-2-amino-5-phosphonopentanoate (AP5), 2,3-dioxo-6-nitro-7-sulphamoyl-benzo(F)quinoxaline (NBQX), HC-030031 (HC-3) and A967079 (A96) which are antagonists for the NMDA, AMPA and TRPA1 receptor, respectively. After these steps, the organoids were cut into thin sections or whole organoids were used to examine three experiments:

1) Immunohistochemistry (IHC) and confocal microscopy of the sections was accomplished, and quantitative analysis was done at total cell number and the oligodendrocytes together with qualitative analysis of the neurons. In addition, quantitative analysis of cell death was performed.

2) RNA fluorescence in-situ hybridization (RNA-FISH) was performed to localize the TRPA1 receptor in brain tissue cells.

3) Quantitative reverse transcription PCR (RT-qPCR) for quantification of oligodendrocyte lineage cells-, precursor oligodendrocytes-, neurons- and the TRPA1 mRNA expression in the cerebral organoids. Whole organoids induced to non or five hours of ischemia were used, treated with one of the receptor antagonists.

Illustration of experimental setup is shown in figure 5 and all solutions, equipment, and instruments used for these experiments are listed in appendix.

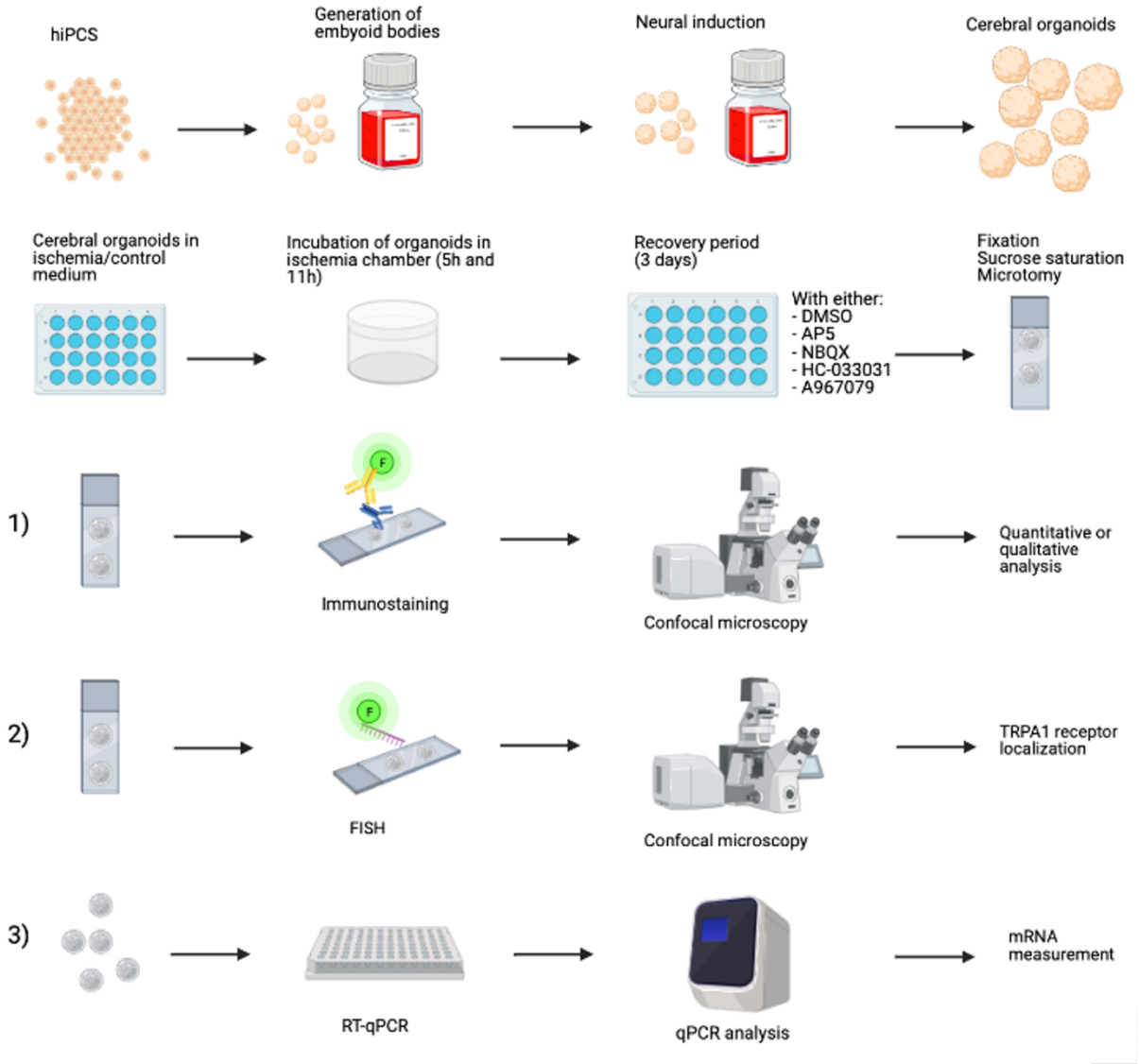

Figure 5: Schematic display of experimental setup. Cerebral organoids were grown for several months before induced to ischemia and receptor antagonists. Thereby, three different experiments were exhibited, including IHC, RNA-FISH, and RT-qPCR analysis.

3.2 Human cerebral organoids

Human cerebral organoids were cultured and used as our model to exhibit the different experiments. The protocol for growing organoids is a modified version of the original protocol by Lancaster and colleagues (67). Cerebral organoids were produced by using hiPSC provided by Magnar Bjørås, Institute for Clinical and Molecular Medicine at Norwegian University of Science and Technology (NTNU). The hiPSCs are maintained in six well plates containing hiPS culture medium (appendix section B) in standard cell culture incubators (37 ºC, 5% CO_2). The maintenance of the hiPSCs include daily changing of culture medium to provide nutrients and growth factors for the cells. Cell-passaging was exhibited approximately every four days

when the density of the cells gets so high (70% confluency) that the cells will eventually become less healthy due to lower access of nutrients and release of toxic chemicals. When passaging, a portion of the cells was transferred to a new well where the cells will have more space to grow and easy access to fresh nutrients. They were usually divided into multiple wells of a six-well plate which thereby creates colonies of the same cell line. Passaging thereby allows for multiplication of clones, maintenance of current clones and the possibility of initiating the protocol for growing human organoids. Each hiPSC clone has the possibility of surviving to passage number 100 (i.e day 400) but can be frozen and revitalised at any time before passage 80. This task was mostly exhibit by other lab members of this group. Figure 6 show an overview of the protocol, where the process of culturing cerebral organoids is divided into four main steps.

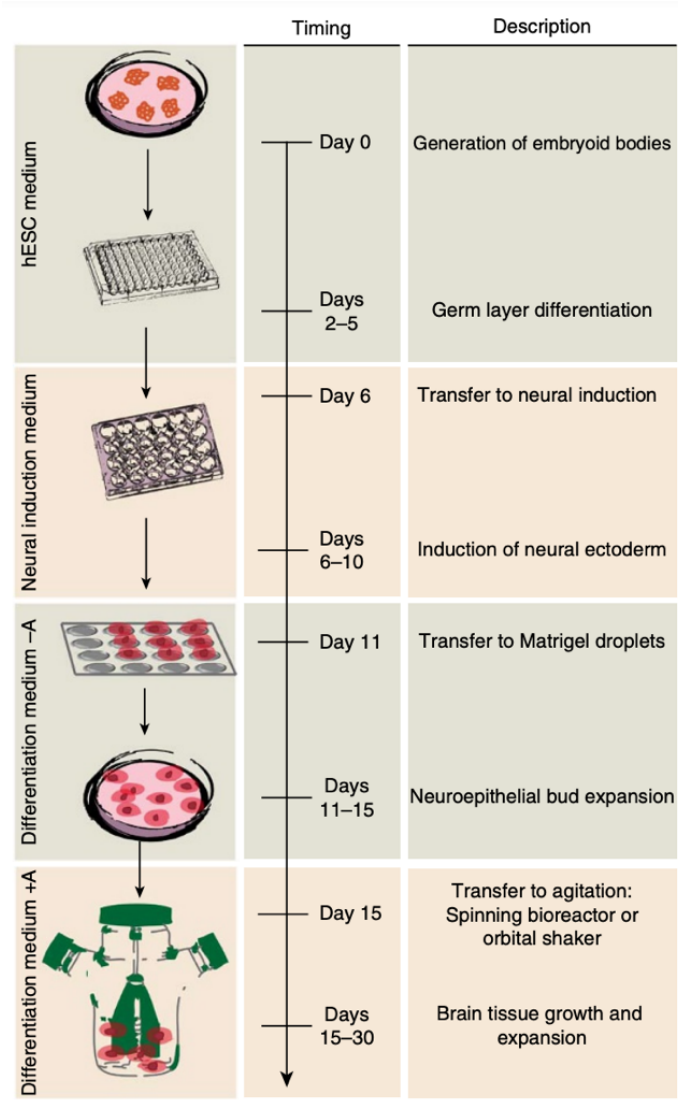

Figure 6: The four main steps of growing human cerebral organoids. A simplified overview of the process of culturing cerebral organoids showing the main steps at different timepoints. Culturing and maintenance of hiPSCs are not included. Modified from Lancaster et al. 2014 (67).

First, formation of embryonic bodies (EB) (3D aggregates of pluripotent stem cells) by making a single-cell solution of cell cultures and seeded onto a 96-well plate for aggregation. Secondly, the EBs were exposed to growth factors to trigger neural induction. Third step helps to support outgrowth of neuroepithelial buds and larger growth by planting the organoids into Matrigel droplets. The fourth and last step includes replacing the organoids into an orbital shaker for long-term maturation and development as well as boosting of oligodendrocyte precursor cells promotion. Different mediums are used in each stage, and quality control was performed to discard EBs with abnormal growth. Solutions used in this protocol are listed in the appendix (table S1 and section B for mediums content). All steps described below were done under sterile conditions.

Step 1: Generation of embryoid bodies (EB)

To develop EBs, hiPSC were grown in a six-well plate located in an incubator with 37°C and 5 % CO_2. The stem cells were incubated in an Essential 8 medium (E8) to the plate reached a confluent of 70-80%. Then, the E8 medium was first aspirated before 2 mL of Phosphate-buffered saline (PBS) was added to wash the plate. After washing, 1 mL of Accutase was added before placing the plate back into the incubator for 4-8 minutes to detach the cells from the plate. When completed, a 1 mL pipette tip was used to help the process even more by triturate and wash the plate to detach the remaining cells. After this step, the cell suspension was added to a 15 mL conical tube with 5 mL pre-warmed DMEM/F12 medium. The solutions were triturated up and down a few times to ensure single-cell suspension before centrifuging the cells at 1100RPM (270g) for 5 minutes.

The hiPSCs were further aspirated and resuspended in 2 mL of embryoid body medium (EBM) with included ROCK inhibitor and bFGF to avoid the cells from apoptosis due to single cell solutions. 20 µL of the cell suspension was taking out to count the number of cells using a hemocytometer (Countess 3, Invitrogen) by adding trypan-blue to the cell suspension. Nine thousand cells per well (150 µL) are favourable. Therefore, calculated cell suspension solution was added to a new tube to create the right concentration in EMB with ROCK and bFGF. The hiPSC suspension was then pipetted to a reservoir and a multichannel pipette added 150 µL of the solution to a low-attachment 96-well plate with round bottoms. The 96-well plate was further cultured in a 37°C incubator with 5% CO2. The EBM needed to change every other day by removing 100 µL of the medium from each well and replacing it with a fresh medium to

feed them and initiate germ layer differentiation. ROCK inhibitor (50 μM) and bFGF (4 ng/mL) were included in the medium in the first four days.

Step 2: Neuroepithelia Induction

Primitive neuroepithelial induction started six days after EB seeding, where EBs begun to form small embryonic bodies (fig 7A). Before replacing the EBM with neural induction medium (NIM), accumulated debris around the EBs was removed by triturating the suspension up and down. 130 μL of the EBM was then removed from the wells before 150 μL of NIM was added. This was repeated two days later to feed the EBs with a fresh medium.

Step 3: Matrigel embedding and neuroepithelial bud expansion

On day 10-15, the EBs needed to be Matrigel embedded, which resembles the extracellular environment and helps the EBs developing in a three-dimensional manner. The Matrigel was thawed on ice at 4°C in 1-2 hours before use and was kept on ice for the whole procedure. Parafilm sheet (Thermo Fisher Scientific) was used to make 4x4 grids for the Matrigel and placed into a 60 mm tissue culture dish. The EBs was transferred one by one from the low-attachment 96-well plate to an individually Parafilm pimple on the dish using a cut-off pipette. The excess medium from the transferring was aspirated off by using an uncut pipette before 20 μL of Matrigel droplets were added immediately to each EBs to avoid dehydration and structural damage. Directly, the EBs were centred in the Matrigel for the proper function of the gel, and the dish was placed in the incubator for 20-30 minutes for polymerizing of the Matrigel. The Matrigel droplets were removed from the sheet using the neuronal differentiation medium (NDM) without vitamin A to flush it off, and in total 5 mL of the NDM was added to a six-well plate. Each well contained around 10 EBs and these were placed back in the incubator for further culturing. The NDM was changed 48 and 96 hours later to maintain fresh medium to the wells by aspirating off the old medium and adding 5mL of new, fresh NDM.

Step 4: Transforming EBs for long-term culturing and expansion

The EBs can either be transformed to a spinner flask for long-term culture of >40 EBs or leave at the six-well plate if <40 EBs. In this project, the organoids were left in the six-well plate and medium change was needed every other day. The medium used for long-term culturing was NDM with vitamin A and 5 mL was added to each well every other day and entirely replaced and aspirated every four days. The six-well plates were placed on the shaker in the incubator for long-term maturation and development.

Two weeks into the long-term maturation step, additional growth factors were added to the NDM to promote oligodendrocyte precursor cell formation (OPC medium 1). This included brain-derived neurotrophic factor (BDNF), cyclic AMP (cAMP), PDGF-AA, hepatocyte growth factor (HGF), insulin-like growth factor 1 (IGF-1), neurotrophin 3 (NT-3) and triiodo-L-thyroine (T3). Medium change was performed every other day. 12 days later, the organoids were cultured in OPC medium 2 (OPCM2) contained only BDNF, cyclic AMP and T3. Medium change was done every other day for 7 days, and then every 4-5 day. The organoids could now be grown for as long as wanted. Our cerebral organoids were between three and four months old. The protocol for generation of cerebral organoids is a modified version from Lancaster et al. (67) with implemented oligodendrocyte promoting adapted from Arlotta et al. (72).

3.3 Quality of cerebral organoids

Organoids treated with the same compounds and grown in the same environmental conditions were likely to develop differently. Quality check during the culturing was therefore performed at different developmental stages to exclude unhealthy organoids before further processing. Quality check was done by inspecting the organoids under a tissue culture microscope (Olympus), and was done at several time points during the culturing. The morphology of the stem cell colonies is crucial for successful cerebral tissue formation. Evidence of differentiation should not be seen in the colonies where optimal features of pluripotency with clear boundaries and a uniform texture should be displayed (not shown).

From start day (0) until day 4, the EBs were quality checked by measuring their size using tissue culture microscope. The EBs was kept in EBM medium with ROCK and bFGF until their began to brighten or was >350-400um in diameter. On day five from start-day, an EB should show evidence of ectodermal differentiation by having a round, brightened and smooth surface tissue, and a darker core indicating non-ectodermal tissue. Healthy EBs had a diameter of approximately 350-600 μm (fig 7A). EBs without clear surfaces and showing sub-optimal features such as debris around the cells were considered unsuitable and were discarded (fig 7E). On day 10, or after 4-5 days in NIM, a healthy, early organoide should show clear transient neuroectoderm on the outer surface and smooth edges. Also, “buds” can be seen at this stage, showed in figure 7B, contained ectodermal tissue whiteout radially organization. Once neuroepithelium appeared, EBs needed to be transferred to Matrigel embedding as this can

affect later morphology of cerebral tissues. Early organoids lacking optically translucent neuroectoderm indicates failure of neural induction and do not fulfil the criteria for healthy development (fig 7F). In addition, too large organoids are neither suitable. After Matrigel embedding, the success of tissue formation is seen by bud formation of neuroepithelial outgrowths that are optically clear, in addition to non-neuroepithelial outgrowths and migrating cells (fig 7C). Organoids that failed to produce buds are disqualified and were removed from the culturing process. Figure 7G shows an organoid that instead displaying extended cell processes, being unqualified for further differentiating. Before OPC boosting, healthy organoids revealed neural tissues that had significantly expanded once embedding in the Matrigel, showed in figure 7D. After several weeks of differentiation, organoids with visible fluid-filled cysts (figure 7H) and lack of thickened neuroepithelium edges indicate differentiation failure and was discarded from the culturing.

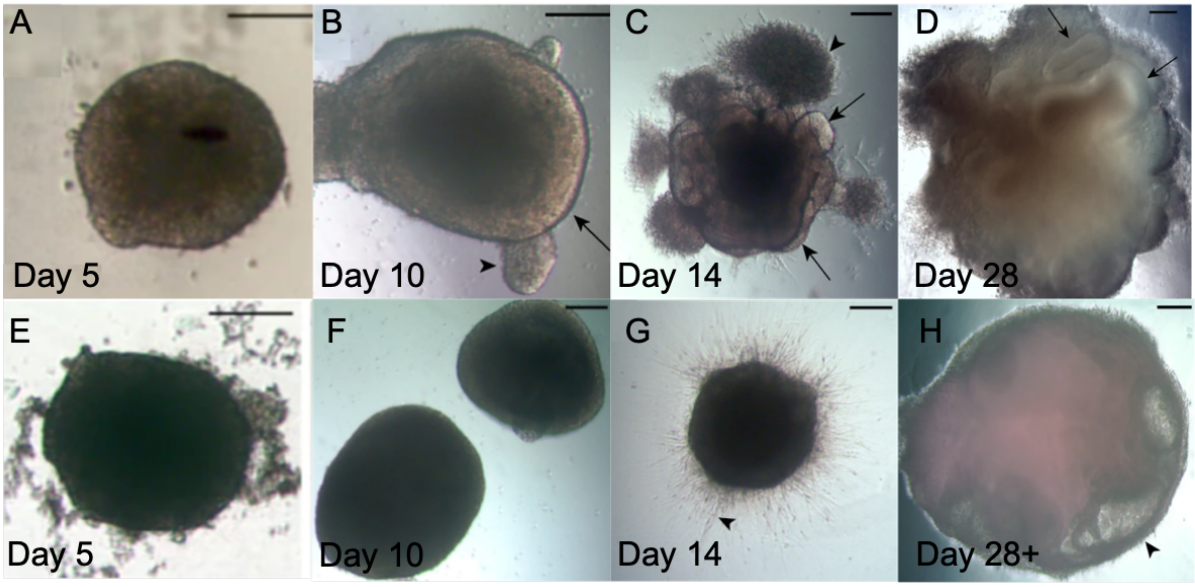

Figure 7: Progression of cerebral organoid development with optimal and unsuitable organoids at various stages. Cerebral organoid development needs to be quality checked at different stages before further culturing to ensure optimal growth. Figure **A-D** showing healthy developing organoids at different time points where **A** showing an EB at day 5 with evidence of ectodermal differentiation by having a round, brightened and smooth surface tissue. **B:** An early organoid with clear transient neuroectoderm on the outer surface and smooth edges (arrow) and bud-formation can be seen (arrowhead). **C:** After Matrigel embedding, bud formation of neuroepithelial outgrowths indicate healthy growth (arrows) in addition to non-neuroepithelial outgrowths and migrating cells (arrowhead). **D:** Organoid before OPC boosting revealing large neural tissues (arrows) once embedded in Matrigel. Figure **E-H** showing unsuitable organoids at the same steps as **A-D** where arrowheads indicate inappropriate features. Figure **E** showing an organoid having debris around the cells and **F** too big organoids. Scale bars: 200 µm. Modified from Lancaster et al 2014 (67).

3.4 Experimental setup for human cerebral organoid ischemia model

The ischemia experiments performed in this thesis used cerebral organoids as a model for the human brain. To simulate an ischemic stroke to the organoids, glucose and oxygen deprivation

were induced, which together mimic ischemia *in vitro* (73). The organoids were divided into three groups with different durations of ischemia: 5 hours, 11 hours, and a control group with no ischemia. The recovery time for all the groups were three days.

Ischemia setup:

All relevant equipment outside the hub were disinfected before any further work. This includes the Hypoxia Induction Chamber (STEMCELL), the Single Flow Meter (STEMCELL), and the Tygon tubing (STEMCELL) connected to the gas can. Then, the ischemic- and control medium was prepared, a variant of the cerebral differentiation medium, without the glucose for the ischemia group and standard medium for the control group (see appendix section B for solutions). 1 mL of ischemia- and control medium was prepared for the ischemia event and the recovery period for each organoid.

24-well low-attachment plates were placed in the hypoxia chamber field with 1 mL ischemic medium to each well with one organoid in it.

To ensure a humid environment and avoid evaporation of the medium during the experiments, some of the well was filled with sterilized water. In addition, in each plate had wells for rinsing the organoids before placing into the ischemic medium. After filling the wells with ischemia medium, the plates were placed on the top of a grid inside the hypoxia box. The hypoxia chamber was precisely closed and connected to a gas tank contained 95% nitrogen and 5% CO2. Before the valves were sealed, the chamber was flushed with gas for three minutes at 30 PSI to remove the oxygen. The chamber was then placed in the incubator at 37 °C for 45 minutes to equilibrate the medium of all oxygen and obtain physiological temperature.

After the equilibration, the organoids selected for the ischemia experiment were placed from their previous environment into the cleaning well before placing them into the ischemic medium using a cut-off pipette. The hypoxia chamber was then sealed and flushed with the nitrogen-CO2 gas for three minutes at 30 psi for equilibration before the hypoxia chamber was placed in the incubator for the wanted duration of ischemia. The control groups with the control medium were placed back into the incubator. When the ischemic duration was done, the organoids were taken out from their ischemic medium and placed in a petri-dish with OPCM2 on a shaker for three days for recovery. Medium change to OPCM2 was also done for the control organoids. The selected antagonists were included in the medium and was given to their respective

organoid groups during these days. An overall setup of ischemic durations and antagonists is listed in table 1.

3.5 Treatments

After the duration of ischemia was induced to the organoids, antagonists were added to their medium. NMDA, AMPA, TRPA1 antagonists or dimethyl sulfoxide (DMSO) were added to the OPCM2 for the recovery days and was substituted until fixation. DMSO is a colourless solution used as a solvent detergent and was used to solve the antagonist in our treatments. DMSO is therefore added to the control group of the organoids. In the first batch of culturing organoids, AP5 and NBQX was loaded together, as for HC-3 and A96. Next batch, all these antagonists were divided into individual groups. An overview of the treatments and ischemic durations is listed in table 1.

Table 1: Treatment setup for cerebral organoid cultures

Ischemic duration	Batch 1: antagonists	Batch 2: antagonists
0 hour	DMSO	DMSO
	AP5 + NBQX	AP5
		NBQX
	HC-3 + A96	HC-3
		A96
5 hours	DMSO	DMSO
	AP5 + NBQX	AP5
		NBQX
	HC-3 + A96	HC-3
		A96
11 hours	DMSO	-
	AP5 + NBQX	-
		-
	HC-3 + A96	-
		-

3.6 Sample preparations

Fixation

Organoids for IHC and RNA-FISH analysis needed to be prevented from degradation and were substituted in a fixative medium that will preserve the tissue's proteins and amino acids' structures and was substituted after their recovery time. The fixation will stop any further biochemical reactions from occurring and preserve the tissue from degradation (decaying) and

make the cells permeable to staining solutions (74). The medium used for this purpose is reactive aldehydes, either pareformaldehyde (PFA) or glutaraldehyde, or a mix of both. Aldehydes make covalent bonds with proteins and the free groups on the amino acids, which will then cross-link and make the tissue more stable and "locked" in their position. These are called "methylene bridges," and the reactions with proteins and amino acids are highly complex (75). Glutaraldehyde gives stronger bindings than formaldehyde but is not the best choice when using fluorescence immunolabeling as it induces autofluorescence (74, 75). Formaldehyde gives good tissue preservation and has a high degree of tissue penetration, making it a commonly used fixative (76). The organoids used for immunohistochemistry had been immersion fixed in 4% PFA for 2 hours and were stored in 0,4% PFA at 4°C until further processing. For RNA-FISH analysis, the organoids were only fixated in 4% PFA (24 hours) before additional processes were performed, and fresh tissue was used for RT-qPCR analysis.

Cryo-preservation and microtomy

For visualizing the organoids in the microscope, they need to be cut into thin sections with an appropriate size for microscopy. Thin sections were cut by using cryostat-microtome (CryoStar NX70, Thermo Scientific), a frozen technique that maintains a low temperature in the cutting chamber. Before using the cryostat, the tissue must be preserved to prevent it from being destroyed by ice crystal formation when water freezes and expands. Cryoprotecting of the tissue was achieved with the addition of sucrose to the organoids. Here, three concentrations of sucrose-solution were used: 10%, 20%, and 30% diluted in PBS to make the suitable concentrations.

First, the organoids were placed in a 10% sucrose solution for 1 hour or until they had sunk to the bottom of their wells. Then, the next step was to substitute this with 20% sucrose solution for three hours. The final step was to put the organoids in 30% sucrose solution and store them in the fridge overnight to make sure that they had absorbed the sucrose before sectioning. Without this cryoprotective step, the cell membrane could break and produce holes within the cells, thereby losing some extracellular matrix. Sucrose saturation was done stepwise concerning the sucrose concentrations to avoid any pressure caused by the osmolarity differences along the cell membranes, which could negatively impact the tissue morphology. A cryostat is a good method for preserve the antigenicity, which makes it very applicable for immunohistochemistry (77). The tissue was placed on a sample plate mounted with a Ned50

medium (Mercedes Scientific). The cryostat cut the organoids into 16 and 15 µm thick sections for IHC and RNA-FISH, respectively, in a chamber that holds -20°C. The sections were collected on SuperFrost Plus slides (Thermo Fischer Scientific) and stored at -20°C for IHC or -80°C for RNA-FISH.

3.7 Immunohistochemistry

Immunostaining is a widely used technique that became known in 1941 (76) and has since then been used in research and clinical applications. The fundamental concept of IHC is to detect specific antigens in histological tissue sections using labelled antibodies for visualizing particular cell types, cell compartments, or proteins in the tissue. Antigen-antibody reactions can be achieved in two different ways; direct or indirect. By doing it the direct way, the antigen of interest will become visible by binding to a respective antibody conjugated to a reporter label, e.g., a fluorophore (78). This signal can then be detected in a microscope by its fluorophore intensity. However, this 1-step process is quick but lacks sufficient detection sensitivity, and the signal strength is relatively low. The indirect way gives higher sensitivity and an increased reaction intensity and is, therefore, more often used. This higher sensitivity is achieved by using two antibodies: a primary and secondary antibody (79). The unlabelled primary antibody binds to the antigen of interest. The secondary antibody is multiply labelled with, e.g., fluorophores and binds specifically to the immunoglobulin domain of the primary antibodies. When using the indirect antigen- antibody method, it is essential to use secondary antibodies that are made against the same animal that the primary antibody was made in (the host animal). Simplified, primary antibodies are made by immunizing decided animals of antigens of interest. The animal produces antibodies that can further be used for the detection of antigens in samples. Secondary antibodies are raised against the host species used to generate the primary antibody, and thereby made in species other than the host where goat are often used (74).

When using conjugated fluorophores as a reporter label, it is important to choose the right excitations wavelength. The fluorophores absorb light energy of a specific wavelength which results in the excitation of fluorophore's electrons. The fluorophores then re-emit the absorbed light energy at a longer wavelength, which then can be detected in a fluorescence microscope. Thus, the secondary antibodies must have diverse excitation wavelengths to avoid crossover detection

3.7.1 Immunohistochemistry protocol

The organoids sections were taken out from the freezer to thaw at room temperature for 5-10 minutes. Some antigens need antigen retrieval, and for those, 10 mM citrate buffer (pH 6) in a small container was pre-heated to 85°C using a water bath. The organoid sections were washed for 10 minutes in PBS before they were put in the pre-heated citrate container, leaving for 25 minutes before they were taking out to cool to room temperature in the buffer liquid. For organoid sections without the need for antigen retrieval, this step was excluded, and the rest of this procedure was done at room temperature. After the antigen retrieval step, the slides were rinsed two times in PBS for 10 minutes and further dried with tissue paper (Kimwipes) without touching the organoid sections. The sections were encircled twice with a liquid blocker pen, ImmEdgeTM -pen (Thermo Fischer Scientific). This fluid is made of lipids and will prevent water-based solutions from floating away from the sections and minimize the amount of staining solution. The samples were then placed in a moisture chamber, and blocking solution (10% normal goat serum, 1% bovine serum albumin, 0,5% Triton-X-100 in PBS) was added to the sections and incubated for one hour. This step is essential to avoid unspecific bindings of the antibodies since they might weakly bind to other proteins than the protein of (80). The next step was to remove the blocking and add the solution containing the primary antibodies which incubated overnight in a moisture chamber at room temperature. Primary and secondary antibodies were diluted in a solution containing 3% normal goat serum, 1% bovine serum albumin, 0,5% Triton-X-100 in PBS.

The next day, the slides were rinsed three times for 10 minutes in PBS and checked for the integrity of the liquid blocker-pen before adding fluorescent secondary antibodies and 4`-6-diamidino-2-phenylindole (DAPI). The secondary antibodies with DAPI were incubated for 1 hour in a moisture chamber before rinsed three times for 10 minutes in PBS. After the slides were dried, they were mounted with ProLong^{TM} Glass Antifade Mountant (Thermo Fisher Scientific) and cover glass to support the tissue. Nail polish was used to glue cover glass and slides together and help to maintain the mounting moisture over time. The slides were stored dark at 4°C until microscopy and then at -20°C for long-term storage.

IHC was performed on 3,5 months old cerebral organoids, and different primary antibodies were utilized to detect the cells of interest: rabbit anti-SOX10 (1:400, Abcam), mouse anti-NG2 (1:200, Millipore), mouse anti-TUJ-1(1:1000, R&D systems/Bio-Techne) and rabbit anti-Cleaved Caspase-3 (1:200, Abcam) were used. Secondary antibodies used were AlexaFlour

488 goat anti-rabbit (Thermo Fisher Scientific) and AlexaFlour 555 goat anti-mouse (Thermo Fisher Scientific). DAPI (Sigma-Aldrich) was used to mark all cell nuclei. In this project, both monoclonal and polyclonal antibodies were used. Polyclonal antibodies are favourable when giving higher antibody affinity against the antigen due to the recognition of multiple epitopes and thereby having high sensitivity for detection of low-quantity proteins (81).

Confocal microscopy was performed on stained sections (described below), and 3-6 images were taken from each organoid depending on the organoids size. The centre of the organoids was not imaged due to naturally occurred necrotic cores. Correct staining was verified by microscopy to check for expected labelling based on the literature. All equipment and solutions used in IHC are listed in the appendix.

3.7.2 Imaging and data processing

Confocal microscope

Imaging of the stained sections was done by the use of a confocal microscope. A confocal microscope is a type of fluorescence microscope that uses a laser as an illumination source. For imaging the samples, the laser illuminates the sample point by point, line by line, which emits light with specific wavelengths, thereby increasing fluorophore excitation accuracy. This is an essential difference from a conventional epifluorescence microscope, where the whole image is being illuminated simultaneously. By using a confocal microscope, the system focuses a spot of light onto the specimen in a specific depth. This spot is in the focal plane and will be in *confocal* with a pinhole located under the detector. The detector will therefore precisely detect the emitted rays from the illuminated, focused spot from the sample. No other signals will pass this pinhole and thereby will not be depicted. These features will result in a higher resolution, particularly in the Z-axis, compared with conventional fluorescence microscopy (82). In IHC and RNA-FISH experiments, a Leica TCS SP8 STED confocal microscope was used with Leica LASX software, and images were captured with a 20x (aperture: 0.75) or 40x (aperture: 1.30) oil objective giving 200x and 400x magnitude, respectively, depending on the lenses available in the lab. The organoid sections used in this project were 16 µm thick, which is ideal for studying cell types and structures in a confocal microscope (74). Z-stacks obtained from the microscope varied from 4-10 images depending on the experiment, each 1 µm thick.

Image analysis by ImageJ

In order to analyse the images taken with the confocal microscope, a Java-based open-source image processing program was utilized. This program is called ImageJ and is a much-used scientific tool for image processing and analysis (83), developed at the National Institute of Health and the Laboratory for Optical and Computational Instrumentation (84). Pictures taking from the confocal microscope give Leica TIF files and can be easily uploaded into the open ImageJ software for processing. These are raster images that consists of an assigned pixel location with a range of colour values. The number of pixels per inch specifies the resolution, and the colour value information in each pixel is described in the bit depth of the image. The bit depth can be 8, 16 or 32, giving a colour value range from 0-255, 0-65535, and 0-4294967295, receptively. From the confocal microscope, each laser channel makes greyscale images segmented by intensity and structure and show areas of interest. In this project, 8-bit pictures were used with 1024x1024 pixels.

For quantitative analysis of objects, image segmentation or fluorescence intensity measure can be executed. Fluorescence intensity measurements are relevant options, but the variation of the fluorescence will vary depending on where in the z-stack the picture is gathered. Slices are in contact with light before and during experiments, resulting in a loss of their ability to fluoresce and is a permanent issue called photo-bleaching resulting in reduced intensity. Segmentations evaluate the size, shape and direction of the objects in the section. Individually threshold algorithms were used to segment the images in the different experimental groups, and because of this, the picture processing was done blinded to avoid any selection bias for the analysis.

Quantification of oligodendrocytes lineage cell, total cell density and cell death as well as nuclei sizes in the different treated organoids was performed by using threshold algorithms and the analyse particles plug-in to extract information. For measurement of the TUJ-1 staining, assessment of the tissue quality was executed by individually score the images from 1 to 5, where 5 is top score meaning good quality, where taking tissue fragmentation in consideration (see section 4.2.4 for visualized score-setting).

Statistical analyses.

After the data from ImageJ was moved to Microsoft Excel, we unblinded the data and organized them into experimental groups. The total number of each cell type was counted and further divided the number on the total area to get number of cells/0.1mm^2. This was done for all the

immunohistochemistry analysis, except TUJ-1 staining, where only qualitative measuring was exhibited. GraphPad Prism was used for the statistical analysis and constructions of graphs. As there were more than two groups, a one-way analysis of variance (ANOVA) was conducted to test for statistically significant differences between group means. The Dunnett´s test for multiple comparisons of one-way ANOVA was done as a post-hoc analysis to see which groups varied significantly from the control group. All the graphs and results are shown as mean ± errors bars representing the standard error of mean (SEM) and p-values where analysis of variance was conducted.

3.8 RNA-fluorescence in situ hybridization

Fluorescence in situ hybridization is a method developed for the detection of DNA sequences or mRNA transcripts in cultured cells, tissue sections, or whole-mount preparations. This is achieved by using the nucleic acid thermodynamics principles whereby annealing of two complementary strands of nucleic acids forms duplexes under proper conditions, known as a hybrid (85, 86). FISH analysis takes advantage of these phenomena where DNA or RNA probes are used to visualize target DNA or mRNA in the sample, a method known as in situ hybridization (ISH). At the beginning, a radioactive probe was used to visualize the endogenous DNA or RNA, which both require a long time of exposure and were harmful to human health (87). Later, when the technique had been developed over time, fluorophore-related probes were established and could be detected with fluorescence microscopy, today known as FISH (88). Modern FISH protocols can today label positions of genes on chromosomes, identify microorganism and diagnose diseases, and in addition visualize gene expression in situ, referred to as RNA-FISH (86, 89). In this thesis, the RNA-FISH analysis was used to localize mRNA expression of TRPA1 in the cerebral organoids and mice sections. Co-staining with markers for oligodendrocyte lineage cells and neurons exhibited to localize which cells expressing this receptor. The choice of TRPA1 receptor probe was done with recommendation from ACD-Bio-techne support, and was quality checked for sequence specificity in BLAST (see appendix for probe cat. no).

3.8.1 RNA-FISH protocol with implemented IHC

The organoids were fixed in 4% PFA for 24 hours and directly transferred for sucrose feeding before sectioning was done using cryostat-microtome (see chapter 3.6 for more details). 0,4% PFA was excluded as it may reverse the fixation process and activate some RNases. 14 um

thick sections were made, and only one section was placed on the slides. The slides were stored at -80°C until analysis. The need for lower store temperature is to prevent degradation of the RNA in cells, where it has been shown activation of RNases at -20ºC, which are nucleases that degrade RNA to smaller fragments (90).

Cerebral organoids sections from the control group were taken out from the freezer and washed in 1X PBS (5 min) before they were baked in a heating incubator (Termaks AS) at 60°C for 30 minutes. After incubation, the slides were post-fixed by immersing them in pre-chilled 4% PFA in a fume hood for 15 minutes. Next was to dehydrate the tissue by immersing them in different concentrations of ethanol (50% EtOH for 5 minutes at room temperature, then 70% EtOH so two times 100% EtOH with the same conditions). When the slides were completely dehydrated, 2-3 drops of RNAscope Hydrogen Peroxide (ACD Bio-techne) were added to each section and incubated for 10 minutes at room temperature before it was washed away with distilled water. Mildly boiling (98-102°C) RNAscope 1X Co-Detection Target Retrieval Reagent (ACD Bio-techne) was further used for target retrieval. The slides were boiled for 10-15 minutes covered with a foil and the temperature was correlated the hole period with a thermometer. After the retrieval period, distilled water and phosphate-buffered saline with Tween 20 (PBS-T) was used to wash the slides. Hydrophobic barrier was drawn around the sections using an ImmEdge™ -pen (Thermo Fischer Scientific). At this point, primary antibodies were added and incubated overnight at 4°C in dark environment.

The following day, the slides were washed in PBS-T for two minutes, repeated with fresh PBS-T followed by immersion in 10% Neutral Buffered Formalin (NBF) at room temperature for 30 minutes. PBS-T was then used for washing two times for 2 minutes before RNAscope Protease Plus (ACD Bio-Techne) was applied. The slides were loaded into an RNAscope®EZ-Batch™Slide Holder (ACD Bio-Techne), and three drops of Protease Plus were added to each section. The slide holder was placed into a HybEZ™Humidity Control Tray (ACD Bio-Techne) containing a humidifying paper moistened with distilled water and placed in a HybEZ™Oven (ACD Bio-Techne) for incubation for 30 minutes at 40°C. 200 mL of distilled water was used to wash the Slide Holder containing the slides after incubation in an RNAscope®EZ-Batch™ Wash tray (ACD Bio).

At this stage, preparations of the tissue were complete to run the RNAscope® assay. The sections were incubated with Probe mix for TRPA1 for 2 hours by adding 4-6 drops to each

section. RNAscope® Multiplex FL v2 AMP 1 and 2 (ACD Bio-Techne) incubated for 30 minutes each and RNAscope® Multiplex FL v2 AMP3 (ACD Bio-Techne) 15 minutes, followed by RNAscope® Multiplex FL v2 HRP-C1 (ACD Bio-Techne) for 15 minutes. Opal™ 570 mixed with Tyramide Signal Amplification (TSA) buffer (ACD Bio-Techne) to get a concentration of 1:1500 were added and incubated in 30 minutes. Finally, the RNAscope® Multiplex FL v2 HRP blocker (ACD Bio-Techne) was applied and incubated for 15 minutes. The HybEZ™ Oven was used for all incubations and was done at 40°C. The slides were washed with freshly made 1X RNAscope® Wash Buffer (ACD Bio-Techne) in the wash tray between each incubation for two times 2 minutes. The final step was to add fluorophore-conjugated secondary antibodies diluted in Co-Detection Antibody Diluent and incubated at room temperature for 30 minutes. PBS-T was then used to wash the slides (2 minutes at room temperature twice). After gently dried tissue paper (Kimwise), two drops of RNAscope® Multiplex FL v2 DAPI (ACD Bio-Techne) were added and incubated for 30 seconds at room temperature. One drop ProLong™ Glass Antifade Mountant (Thermo Fisher Scientific) was added to the sections, and a cover glass was placed on the slides and followed sealed with nail polish to maintain the moister. The sections were stored dark at 4°C until microscopy.

Primary antibodies used in RNA-FISH analysis with implemented IHC was rabbit anti-Olig2 (1:100, Milipore) and mouse anti-TUJ-1 (1:200, R&D Systems). Secondary antibodies were Alexa Flour 488 anti-rabbit (1:400, Thermo Fisher Scientific) and Alexa Flour 555 anti-mouse (1:400, Thermo Fisher Scientific)

3.8.2 Imaging and data processing

Imaging of the stained sections was done by the use of Leica TCS SP8 STED confocal microscope with Leica LASX (see section 3.7.2 Imaging and data processing for more details). and the images were taken with a 40x objective (aperture: 1.30). For TRPA1 localization executed by RNA-FISH analysis, ImageJ was used to collect and edit the images taken from the confocal microscope and to investigate closer which cell type expressed the TRPA1 mRNA.

3.9 Quantitative reverse transcription polymerase chain reaction

Quantitative revers-transcription polymerase chain reaction (RT-qPCR) analysis is a widely used tool utilized to measure levels of up-and downregulated genes at mRNA levels and is a refinement of the original Polymerase Chain Reaction (PCR) developed in the mid '80s (91).

Changes in an organism´s metabolism or its environment can change its gene expression at the mRNA level. Being highly transient molecules, mRNA is an efficient candidate to represent gene expression at a specific time.

The basic principle of this technique is to first transcribe total RNA into complementary DNA (cDNA) before quantification. Then, specific DNA targets are amplified in a PCR reaction where RT-qPCR takes advantage of fluorescent reporter dyes. These dyes will monitor the product formed during the course of the reaction, and the fluorescent intensity is proportional to the amount of amplified DNA. Fluorescence signals above a certain computer-chosen threshold are considered as valid and indicate the levels of the mRNA sequence of interest at the inception (91). RT-qPCR was in this study used in order to determine the mRNA expression of SOX10, NG2, TUJ-1, and the TRPA1 receptor in the organoids treated with different antagonists after 5h of induced ischemia, together with a no-ischemia control.

3.9.1 RNA purification and cDNA construction

For RT-qPCR analysis, fixations of cells are not recommended when formaldehyde alters the structure and integrity of the RNA and DNA as well as RNA degradation can occur (92). Therefore, organoids used for RT-qPCR analysis was taken from their recovery medium and was immediately processed as to the protocol. As RNeasy Plus Mini Kit (QIAGEN) showed low mRNA content after isolation, mRNA from the different treated cerebral organoids were extracted using TRIzol (Thermo Fisher Scientific), a phenol-based solution that separates biological samples into their protein, DNA and RNA content. This task was performed by another lab member and will therefore not be described.

While on ice, NanoDrop™ Spectrophotometer was used to measure the RNA purification and concentration (ng/µL) from the extraction. RNA purity is a critical step to avoid downstream applications where contamination can affect the DNA synthesis. The DNA and RNA have a maximum absorbance at 260nm, while proteins and other molecules have their maximum absorbance at 230 nm and 280 nm. NanoDrop™ Spectrophotometer therefore measured the ratio between 260/280 nm and 260/230 nm absorbance in the samples to quality check for RNA purity. Pure RNA should give a 260/280 ratio of 2, and pure DNA have a ratio of 1.8 where lower values could indicate presence of phenols or proteins. The 260/230 ratio is a secondary measure of purity where ratios lower than 2.0-2.2 (clean RNA) indicate contaminants.

To analyse mRNA expression in a sample, mRNA needs to be converted to cDNA by reverse transcription when SYBR® Green to binds to only double-stranded DNA (dsDNA). For cDNA construction, 50 ng/µL concentrations of the mRNA were aliquoted, diluted in RNase-free water (QIAGEN). 10 µL of 50 ng/µL mRNA was mixed with buffer, dNTPs, random primers, reverse transcriptase, and RNase free water retrieved from High-Capacity cDNA Reverse Transcription Kit (Thermo Fisher Scientific). Reverse transcribed to cDNA was done by using 2720 Thermal Cycler (Thermo Fisher Scientific). See appendix for reaction volume and PCR program.

3.9.2 RT-qPCR

For quantification of SOX10, NG2, TUJ-1, and TRPA1 in different treated cerebral organoids, 25 ng/µL amplified cDNA were mixed with PowerUp™ SYBR™ Green Master Mix (Thermo Fischer Scientific), RNase Free Water (QIAGEN), forward- and reverse primer. Further, this mix was pipetted in duplexes in a MicroAMP® Fast 96-well Reaction Plate (Thermo Fischer Scientific) and sealed with MicroAmp™ Optical Adhesive Film (Thermo Fischer Scientific). Although triplets are favourable when pipetting replicates, this could not be achieved due to limited space on the reaction plate to avoid potential analytical errors if included more plates. The reaction plate was briefly centrifuged in Microplate Centrifuge (VWR International) in advance of the RT-qPCR analysis to eliminate excess air in the sample and was carried out in StepOnePlus™ RealTime PCR System (Thermo Fisher Scientific).

Choice of primer for mRNA quantification of SOX10, NG2, TUJ-1, and TRPA1 was made by using the primer-BLAST application to optimize the RT-qPCR analysis. This was achieved to avoid non-specific primer pair amplification and to check for further specifications for the primers. This included the choice of similar melt-temperature (Tm) between the forward and reverse primer and should not differ more than 5 ºC between all and have a Tm within 57-63 ºC. In addition, primer length of 20-24 bp, GC content within 40-60%, and amplification size range be between 70-200 bp were other specifications. In addition, exon-exon boundary primers were chosen to eliminate genomic DNA amplification in our samples.

To eliminate potential unspecific binding of the SYBR® Green to another dsDNA in the sample, the melt curve program was used. This graph shows the change in the fluorescence that arises when dsDNA connected to SYBR® Green melt to single-stranded DNA under the denaturation phase. The melt curve was further used to check for equal melt temperatures for

each gene that will arise for the specific amplified product, where different melt curves will detect unspecific binding.

3.9.3 Calculation of gene expression

To calculate the relative fold mRNA expression in each cerebral organoid, the delta-delta Ct method was used. The fluorescence signals above the computer-chosen threshold indicate the levels of the mRNA sequence. This is given by the qPCR machine (StepOnePlus™ RealTime PCR System (Thermo Fisher Scientific)) and is carried out as Ct-values (cycle threshold). The Ct-values are the cycle number where the fluorescence generated from the PCR reaction is distinguishable from the background noise. The data was carried out in Microsoft Excel for calculations. The overall formula to calculate the relative fold gene expression is known as $2^{-\Delta\Delta Ct}$. To perform this measurement, a housekeeping (HK) gene must be included in the analysis as an endogenous control and thereby corrects for proper pipetting and dilution. Glyceraldehyde 3-phosphate dehydrogenase (GAPDH) was used in this experiment. The endogenous control gene is assumed to be present in all samples at a constant concentration that is resistant to biological fluctuations in the organism.

The first step to calculate the relative gene expression was to average the Ct values for the technical replicates of each sample, including the HK gene. Next step was to calculate delta Ct (ΔCt) for each sample, by using the average Ct values. This was done by subtract average Ct value from the gene of interest by the average Ct value from the HK gene, thereby normalized the value. In the third step, the delta-delta Ct (ΔΔCt) value for all the sample were calculated, by selecting a calibrator/refence gene. By doing this, all the results will be presented relative to that samples average Ct values. In this experiment, DMSO treated cerebral organoids with 0h of ischemia was chosen as our refence gene and the average ΔCt was measured. This value (average ΔCt of the refence gene) was further used to measure the ΔΔCt value of each sample by divide the ΔCt value of each sample to the average ΔCt of the refence gene.

To calculate the fold gene expression values, 2 to the power of negative ΔΔCt values was measured. For easier investigate the gene expression levels between the groups and compared with control group, the $2^{-\Delta\Delta Ct}$ values from each group was normalized to one of the DMSO treated cerebral organoid sample (the organoid with lowest Ct value was selected). Followed, the data was transformed to GraphPad Prism for constructions of graphs.

Biological replicates were only 2 (n = 2). Therefore, no statistical analysis was performed showing only mean normalization value to 0h DMSO ± SEM. Ct values within each sample were not allowed to vary more than 0,3-0,4 Ct units, where values above 0,4 was excluded. Ct values between 30-40 were expected to have more variability, therefore, the values could deviate up to 1,5 Ct units before excluded. Every gene included a negative template control. This control includes all PCR reagents except the cDNA template, substituted with nuclease-free water and would identify ant set-up contamination and primer dimerization. Reaction conditions for PCR and RT-qPCR analysis, primer sequences, kits and reactions volumes are listed the appendix.

4. Results

4.1 Organoid morphology

Organoids that had passed the quality check described in Methods were used for analysis. Healthy organoids at age 3.5 months are shown in figure 8A, having smooth surfaces in addition to variations in their sizes. Overall, immunostained sections from these organoids showed areas containing neurons and glia cells, as expected (fig. 8B-C). Even though their morphology seemed to indicate healthy growth, investigation of stained sections showed that some organoids had areas of, most likely, cells not differentiated into neuroepithelial tissue (fig. 8D-F). Since these presumed non-neuronal regions were present only in a limited area and were easy to identify, the organoids were still used, but the non-neuronal regions were excluded from quantification in IHC experiments.

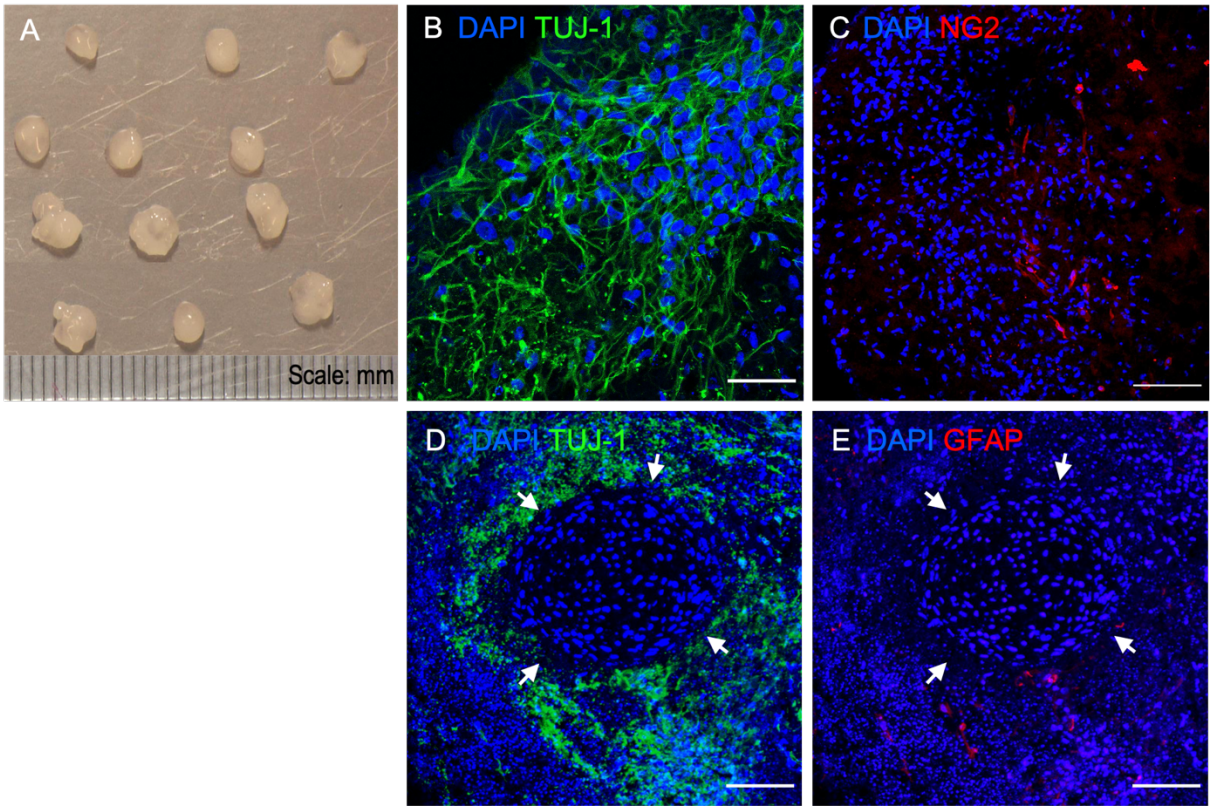

Figure 8: Healthy cerebral organoids showing neuronal tissue and areas of presumed non-neuroepithelial cells. A: Healthy, mature organoids at age 3,5 months showing smooth surfaces with a size between 2-7 mm in diameter. Figure **B** and **C** showing confocal images of immunostained cerebral organoid sections (from control experiments with no ischemia) with DAPI (blue), TUJ-1 (green, **B**) and NG2 (red, **C**), showing both nerve- and oligodendrocyte precursor cells to be present as expected in cerebral organoids. **D-E**: Sections immunostained with DAPI, TUJ-1 and astrocyte marker (GFAP, red) showing evidence of no neural tissue formation in some areas (arrows). Picture **A** obtained from J. E. Rinholm. Scale bars: 50 µm (**B**) and 100 µm (**C-E**).

In addition, some organoids seemed to develop cavity-like structures resembling the ventricular zones in mice when stained with DAPI (not shown) (93). The growth of these structures in

cerebral organoids has been documented in other studies (69, 94, 95). Since these areas had no cells, they were excluded in IHC analysis.

4.2 The role of glutamate- and ionotropic receptors on ischemia-induced cerebral organoids

Ischemia was induced to cerebral organoids to investigate the role of NMDA-, AMPA- and TRPA1 on total cells, oligodendrocytes, neurons, and cell death after an ischemic event. The organoids used in this study were exposed to different durations of ischemia (0h, 5h, and 11h) together with antagonists for the receptors (NMDA: AP5, AMPA: NBQX, TRPA1: HC-3 and A96), and IHC was performed.

4.2.1 The effect of ischemia and receptor inhibition on total cell number and nuclei size

To investigate whether ischemia would lead to a loss of cells in the organoids, sections were stained with DAPI, which labels all cell nuclei in the tissue, and quantified the total cell density. There was a considerable variation of cell density between different organoids. However, no significant change in cell density in organoids treated with five or eleven hours of ischemia compared with the no-ischemia, although the average number of cells was somewhat lower in 5h ischemia group (fig. 9A, Mean DAPI/0.1mm^2: DMSO 0h; 18.10 ± 3.08, n = 5, DMSO 5h; 12.42 ± 3.1, n = 4, p = 0.22 compared with DMSO 0h and DMSO 11h; 17.22 ± 1.76, n = 7, p = 0.94 compared with DMSO 0h). This indicates that ischemia did not lead to cell loss.

We also assessed whether the different drug treatment would affect cell density. The average cell density did not significantly differ after HC-3+A96 treatment in the no-ischemia group compared with the DMSO treated group (fig. 9B, Mean DAPI/0.1mm^2: DMSO 0h; 18.10 ± 3.08, n = 5, (HC-3+A96 0h; 14.72 ± 1.51, n = 5, p = 0.55). There was also no effect on cell density by HC-3+A96 treatments after 5h ischemia (fig. 9C, Mean DAPI/0.1mm^2: DMSO 5h; 12.43 ± 3.10, n = 5, HC-3+A96 5h; 15.75 ± 2.31, n = 5, p = 0.55) or 11h of ischemia (fig. 9D, Mean DAPI/0,1mm^2: DMSO 5h; 17.23 ± 1.75, n = 7, HC-3+A96 11h; 15.33 ± 2.88, n = 5, p = 0.80).

In the no-ischemia group treated with AP5+NBQX antagonists, there was no statistically differences in cell density (fig. 9B, Mean DAPI/0.1mm^2: DMSO 0h; 18.10 ± 3.08, n = 5, AP5+NBQX 0h; 22.34 ± 2.42, n = 6, p = 0.38). Although the average mean density was somewhat higher after 5h of ischemia, this was not statistically significant (fig. 9C, Mean

DAPI/0,1mm^2: DMSO 5h; 12.43 ± 3.10, n = 4, AP5+NBQX 5h; 18.11 ± 2.61, n = 5, p = 0.22). At 11h ischemia, there was no observable difference after AP5+NBQX treatment (fig. 9D, Mean DAPI/0.1mm^2: DMSO 11h; 17.23 ± 1.75, n = 7, AP5+NBQX 11h; 13.97 ± 2.69, n = 5, p = 0.53).

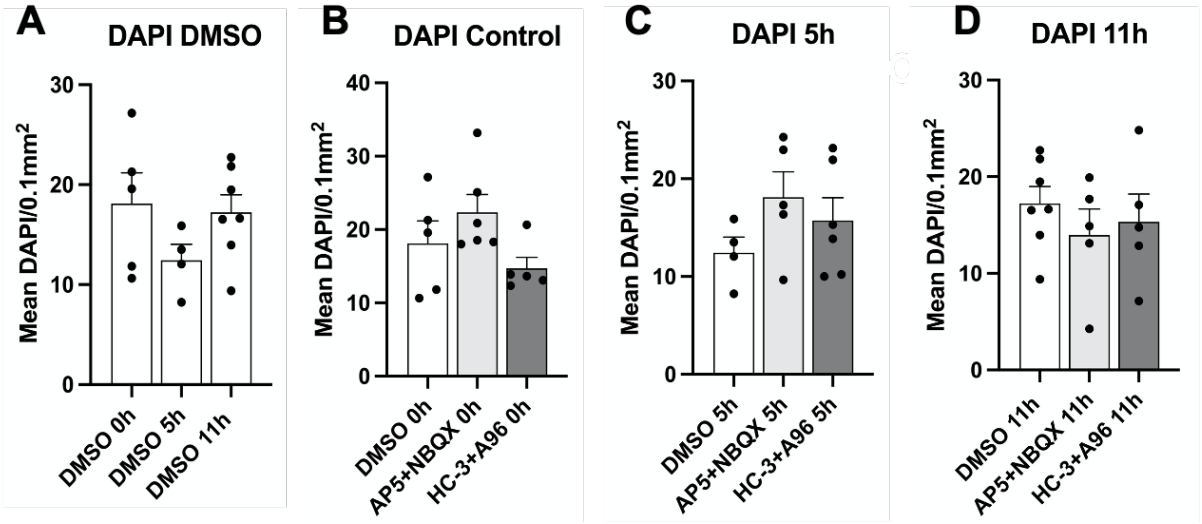

Figure 9: Cell density did not differ significantly between experimental groups. A-D: Quantification of cell density (mean ± SEM) per 0.1mm^2 in sections from organoids that underwent different durations of ischemia and drug treatments. **A**: Cell density after different durations of ischemia (no drug added). **B-D**: Cell density after treatment with either glutamate inhibitors (AP5+NBQX) or TRPA1 inhibitors (HC-3+A96) after no ischemia (0h**, B**) after 5h ischemia (**C**) or after 11h ischemia (**D**). Each data point (filled circle) represents one organoide. Statistical significance was calculated using a one-way ANOVA with Dunnett´s multiple comparison post-hoc test showing no significant difference in the total dell density between groups.

However, we noted that nuclei in the ischemia-treated groups appeared smaller and more fragmented than nuclei in the no-ischemia group (fig 10 A-C), indicating damaged or dying cells. A statistically significant smaller mean nuclei size (measured by square pixels) was observed between both five and eleven hours of ischemia compared with the no-ischemia (fig. 10A-C, D, Mean nuclei size (square pixels): DMSO 0h; 39.01 ± 3.48, n = 5, DMSO 5h; 27.05 ± 1.74, n = 4, p = 0.004 compared with DMSO 0h and DMSO 11h; 20.38 ± 0.49, n = 7, p < 0,0001 compared with DMSO 0h). This indicates that ischemia leads to smaller and more fragmented nuclei.

We also assessed whether the different drug treatment would affect the nuclei size. The average nucleus size was not statistically significant different after HC-3+A96 treatment in the no-ischemia group compared with the DMSO 0h (fig. 10E: Mean nuclei size (square pixels): DMSO 0h; 39.01 ± 3.48, n = 5, HC-3+A96 0h; 33.46 ± 1.28, n = 5, p = 0.34) or in the 5h ischemic group (fig. 10F: Mean nuclei size (square pixels): DMSO 5h; 27.05 ± 1.74, n = 4, HC-

3+A96 5h; 33.92 ± 2.97, n = 6, p = 0.29). After 11h of ischemia there was no observed differences (fig. 10G: Mean nuclei size (square pixels): DMSO 11h; 20.38 ± 0.49, n = 7, HC-3+A96 11h; 21.60 ± 0.93, n = 5, p = 0.44).

Organoids treated with AP5+NBQX antagonists did not shown any differences in mean nuclei size compared with the DMSO in the non-ischemia group (fig. 10E: Mean nuclei size (square pixels): DMSO 0h; 39.01 ± 3.48, n = 5, AP5+NBQX 0h; 44.38 ± 3.15, n = 6, p = 0.33). After 5h of ischemia, there was a trend towards higher mean nuclei size, but this was not statistically significant (fig. 10F: Mean nuclei size (square pixels): DMSO 5h; 27.05 ± 1.74, n = 4, AP5+NBQX 5h; 38.45 ± 4.28, n = 5, p = 0,07), and after 11h of ischemia there was no effect of AP5+NBQX treatment (fig. 10G: Mean nuclei size (square pixels): DMSO 11h; 20.38 ± 0.49, n = 7, AP5+NBQX 11h; 19.10 ± 0.95, n = 5, p = 0.40).

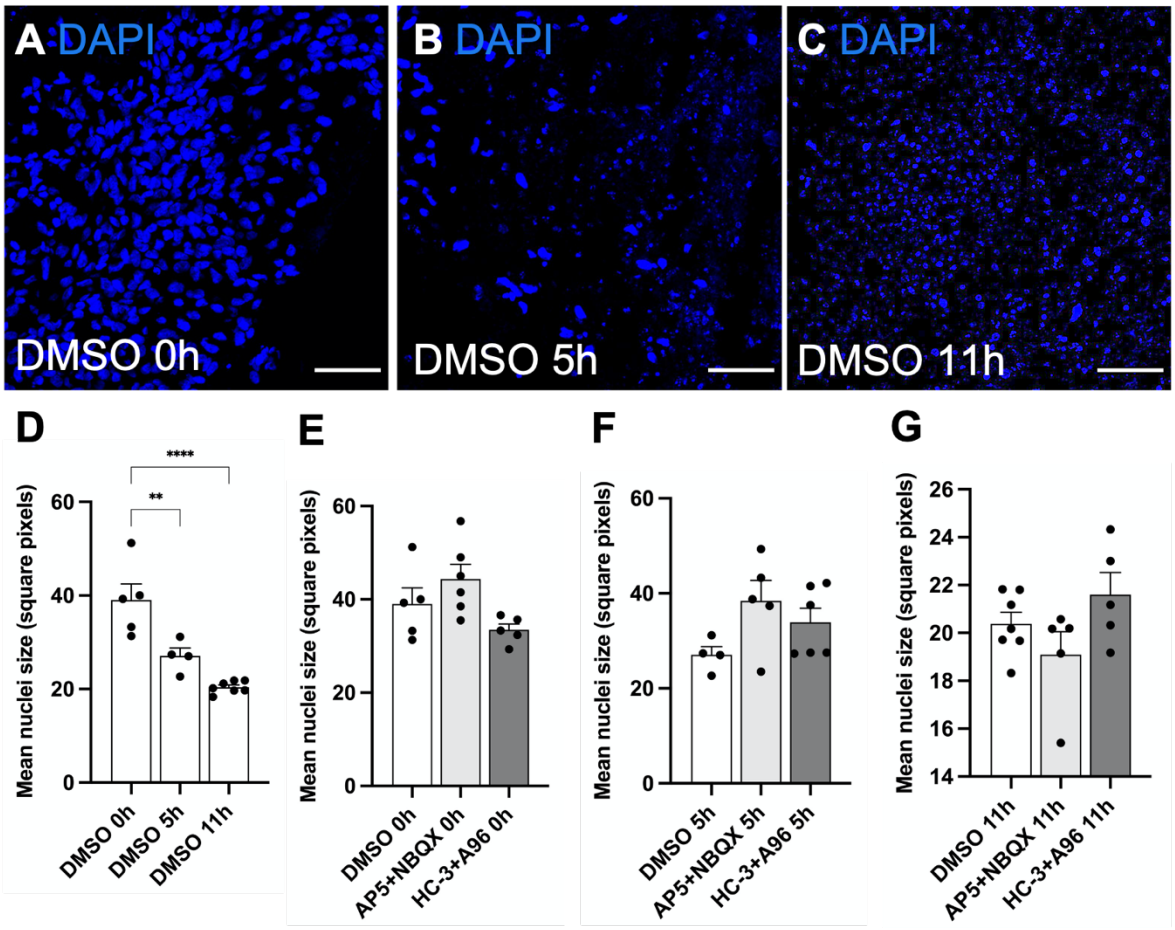

Figure 10: Mean nuclei size did significantly decrease between the ischemic durations. A-C: Confocal images of cerebral organoids sections immunostained with DAPI (blue, all nuclei) from control (**A**), 5h (**B**) and 11h (**C**) of ischemic durations showing decreased nucleus size with increasing ischemia. **D-G**: Quantification of mean nuclei size displaying mean size (square pixels) ± SEM between the DMSO treated groups (**D**) and in the control- (**E**) 5h- (**F**) and 11h groups (G) with either glutamate inhibitors (AP5+NBQX) or TRPA1 inhibitors (HC-3+A96). Each data point (filled circle) represents one organoide. Statistical significance was calculated using a one-way ANOVA with Dunnett´s multiple comparison post-hoc test (**p<0,01, **** p<0,0001). Scale bare 50µm.

To sum up, quantification of mean nuclei sizes showed a significant decrease in size after introducing ischemia. Treatments did not reveal to influence the nuclei size. Nevertheless, a trend was detected with AP5+NBQX treatment after 5h of ischemia. There was also a large variation in cell density between organoids. Although there seemed to be some altered mean cell densities due to ischemia and drugs, these were not statistically significant. Because of the considerable variation in cell density, I have chosen to present the quantitative immunostainings in the sections below as number as positive cells/area (cells/0.1mm^2) rather than the number of positive cells/numbers of DAPI nuclei.

4.2.2 The role of NMDA-, AMPA and TRPA1 receptors on apoptosis

To verify the ischemia model and evaluate the role of NMDA, AMPA and the TRPA1 receptors have on general apoptosis, sections from the different treatment groups were immunostained with cleaved caspase-3 (cas-3), a protein activated during apoptosis (34).

Sections from organoids treated with five or eleven hours of ischemia had a significantly higher number of cas-3+ cells compared with the no-ischemia control (fig. 11. A, D, G, J, Cas-3+ cells/0.1mm^2: DMSO 0h; 0.47 ± 0.10, n = 5, DMSO 5h; 4.15 ± 1.06, n = 4, p = 0.002 compared with DMSO 0h and DMSO 11h; 3.02 ± 0.46, n = 7, p = 0.01 compared with DMSO 0h), demonstrating that these durations of ischemia led to increased apoptosis. Surprisingly, in the no-ischemia group, we detected a significant increase of cas-3+ cells in the HC-3+A96 treated organoids compared with the DMSO, with approximately three times more cas-3+ cells (fig. 11. A, C, K, Cas-3+ cells/0.1mm^2: DMSO 0h; 0.47 ± 0.10, n = 5, HC-3+A96 0h; 1.58 ± 0.13, n = 5, p = <0.0001). The average number of cas-3+ cells was also somewhat higher after HC-3+A96 treatment in the 5h ischemia group, although this was not statistically significant (fig. 11. D, F, L, Cas-3+ cells/0.1mm^2: DMSO 5h; 4.15 ± 1.06, n = 4, HC-3+A96 5h; 7.46 ± 1.97, n = 6, p = 0.19). At 11h ischemia there was no effect of HC-3+A96 treatment (fig. 11. G, I, M, Cas-3+ cells/0.1mm^2: DMSO 11h; 3.02 ± 0.46, n = 7, HC-3+A96 11h; 2.16 ± 0.28, n = 6, p = 0,24). This suggest that TRPA1 receptor inhibition increases apoptosis in non-ischemic conditions, but this effect disappears with increasing ischemia. It should be noted that there is a difference in the y-axis scale in fig. 11 J-M: the effect of HC-3+A96 on apoptosis is far lower than that of five or eleven hours of ischemia.

AP5+NBQX treatment had no effect on apoptosis in the no-ischemia group (fig. 11. A-B, K, Cas-3+ cells/0.1mm^2: DMSO 0h; 0.47 ± 0.10, n = 5, AP5+NBQX 0h; 0.69 ± 0.13, n = 6, p =

0,35). At 5h ischemia, there was somewhat lower apoptotic cells after AP5+NBQX treatment, although not statistically significant (fig. 11. D-E, L, Cas-3+ cells/0.1mm^2: DMSO 5h; 4.15 ± 1.06, n = 4, AP5+NBQX 5h; 1.21 ± 0.27, n = 5, p = 0,28). In the 11h ischemia group, we did not detect any significant differences (fig. 11. G-H, M, Cas-3+ cells/0.1mm^2: DMSO 11h; 3.02 ± 0.46, n = 7, AP5+NBQX 11h; 1.79 ± 0.30, n = 5, p = 0.08).

In conclusion, these data show that the density of apoptotic (cas-3+) cells increased in response to ischemia, as expected. In addition, there was an increase in apoptotic cells in the non-ischemic group treated with TRPA1 antagonists, but not in the ischemic induced organoids. In order to investigate which cell types died from apoptosis with these treatments, co-staining with oligodendrocyte and neuron marker was tried carried out. Unfortunately, this was not achievable due to different preparation criteria for different antibodies and demanding co-localization analysis. Therefore, we cannot conclude which cell type died from the ischemic events but instead proceeded to quantify cell density of oligodendrocytes.

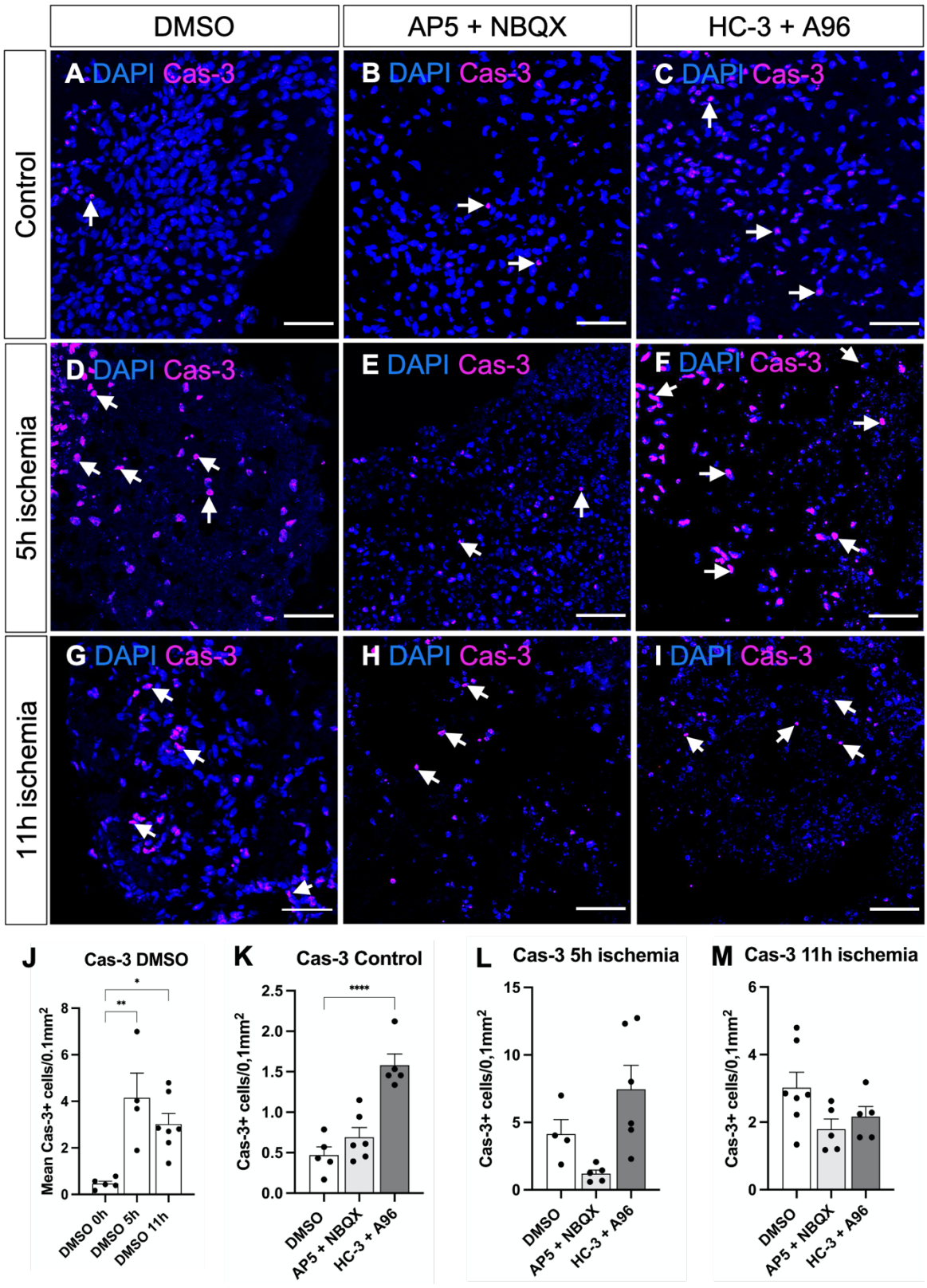

Figure 11: Cleaved caspase-3 quantification for investigation of apoptotic cells. A-I: Confocal images of cerebral organoids sections from control (**A-C**), 5h (**D-F**) and 11h ischemia groups (**G-I**) with additionally antagonists for glutamate receptors (AP5+NBQX, **B**, **E**, **H**) and TRPA1 receptors (HC-3+A96, **C**, **F**, **I**) or DMSO (Ctrl, **A**, **D**, **G**). Sections are immunostained with cas-3 (magenta) and DAPI (blue) showing positive cas-3 cells (white arrows). **J-M:** Quantification of cas-3+ cells per 0.1mm^2 displaying mean number ± SEM between the DMSO treated ischemic groups (**J**) and in the control- (**K**) 5h- (**L**) and 11h groups (**M**). Each data point (filled circle) represents one organoide. Statistical significance was calculated using a one-way ANOVA with Dunnett´s multiple comparison post-hoc test (*p<0,05, **p<0,01, **** p<0,0001). Scale bare 50µm.

4.2.3 Effect of ischemia and receptor inhibition on oligodendrocyte density

To study how inhibition of glutamate or TRPA1 receptors might influence the density of oligodendrocytes, organoids were treated as described above and sections were stained with the general oligodendrocyte marker SOX10, which labels all oligodendrocyte lineage cells. There was a large variation in oligodendrocyte density between organoids. Although, the mean SOX10+ cells were somewhat lower after introducing ischemia, this was not significant (fig. 12. A, D, G, J, SOX10+ cells/0.1mm^2: DMSO 0h; 1.34 ± 0.72, n = 5, DMSO 5h; 0.86 ± 0.33, n = 5, p = 0.65 compared with DMSO 0h and DMSO 11h; 0.23 ± 0.10, n = 7, p = 0.12 compared with DMSO 0h).

In the no-ischemia group, HC-3+A96 treatment had no significant effect on SOX10 cell density (fig. 12. A, C, K, SOX10+ cells/0.1mm^2: DMSO 0h; 1.34 ± 0.72, n = 5, HC-3+A96 0h; 0.76 ± 0.28, n = 5, p = 0.44). However, when ischemia was introduced, organoids with HC-3+A96 treatment had a significantly higher number of SOX10+ cells. In the 5h ischemia group, organoids with HC-3+A96 treatment had almost a three-fold increase number of SOX10+ cells (fig. 12. D, F, L, SOX10+ cells/0.1mm^2: DMSO 5h; 0.86 ± 0.33, n= 5, HC-3+A96 5h; 2.39 ± 0.53, n = 6, p = 0.03), and 11h ischemia group had a four-fold increase (fig. 12. G, I, M, SOX10+ cells/0.1mm^2: DMSO 11h; 0.23 ± 0.09, n= 7, HC-3+A96 11h; 1.00 ± 0.23, n = 6, p = 0.007). This shows that inhibition of TRPA1 receptors can increase oligodendrocyte density after ischemia.

AP5+NBQX treatment did not significantly affect SOX10 cell density in the no-ischemia group (fig. 12. A-B, K, SOX10+ cells/0.1mm^2: DMSO 0h; 1.34 ± 0.72, n = 5, AP5+NBQX 0h; 2.18 ± 0.51, n = 6, p = 0.75). Also, after 5 and 11 hours of ischemia AP5+NBQX treatment had no effect (for the five-hour group: fig. 12. D-E, L, SOX10+ cells/0.1mm^2: DMSO 5h; 0.86 ± 0.33, n = 5, AP5+NBQX 5h; 0.33 ± 0.09, n = 5, p = 0.57, and between the eleven-hour group: fig. 12. G-H, M, SOX10+ cells/0.1mm^2: DMSO 11h; 0.23 ± 0.10, n = 7, AP5+NBQX 11h; 0.32 ± 0.13, n = 5, p = 0.90). This suggest that NMDA or AMPA receptor inhibition have no effect on the number of oligodendrocytes after ischemic events.

We also wanted to investigate the role of these receptors on oligodendrocyte precursor cells, by using the marker NG2. There was a large variation in the density of NG2+ cells between different organoids, with many organoids expressing NG2+ cells close to zero (fig 13). Sections from organoids treated with five or eleven hours of ischemia without any treatments did not

detect any statistically significant increase of NG2+ cells, although the mean density of NG2+ cells was somewhat higher in the 5h ischemic group (Fig. 13. A, D, G, J, NG2+ cells/0.1mm^2: DMSO 0h; 0.018 ± 0.015, n= 5, DMSO 5h; 0.111 ± 0.068, n = 5, p = 0.17 compared with DMSO 0h and DMSO 11h; 0.008 ± 0.006, n = 7, p = 0.97 compared with DMSO 0h).

In the no-ischemia group, we did not detect a significant increase in NG2+ cells with HC-3+A96 treatment compared with the DMSO (fig. 13. A, C, K, NG2+ cells/0.1mm^2: DMSO 0h; 0.018 ± 0.015, n= 5, HC-3+A96 0h; 0.085 ± 0.047, n = 5, p = 0.72). HC-3+A96 treatment had no effect on increased NG2+ cells in 5h ischemia group (fig. 13. D, F, L, NG2+ cells/0.1mm^2: DMSO 5h; 0.111 ± 0.068, n = 5, HC-3+A96 5h; 0.109 ± 0.049, n = 6, p = 0.99). However, a statistically significant increase in NG2+ cells were detected in 11h ischemic group, with a 12-fold increase compared with the DMSO (fig. 13. G, I, M, NG2+ cells/0.1mm^2: DMSO 11h; 0.008 ± 0.006, n = 7, HC-3+A96 11h; 0.126 ± 0.054, n = 6, p = 0.03), suggesting that TRPA1 receptor inhibition increase density of OPCs after eleven hours of ischemia.

The AP5+NBQX treatment in non-ischemic condition detected a trend towards a higher number of NG2+ cells, although this was not statistically significant (fig. 13. A-B, L, NG2+ cells/0.1mm^2: DMSO 0h; 0.018 ± 0.015, n= 5, AP5+NBQX 0h; 0.228 ± 0.093, n = 6, p = 0.07 compared with DMSO 0h). After 5 and eleven hours of ischemia, there was no effect of AP5+NBQX treatment on the density of NG2+ cells (fig. 13. D-E, K, NG2+ cells/0.1mm^2: DMSO 5h; 0.111 ± 0.068, n = 5, AP5+NBQX 5h; 0.014 ± 0.009, n = 5, p = 0.32 compared with DMSO 5h and for 11h: fig. 13. G-H, M, NG2+ cells/0.1mm^2: DMSO 11h; 0.008 ± 0.006, n = 7, AP5+NBQX 11h; 0.012 ± 0.012, n = 5, p = 0.99 compared with DMSO 11h).

In sum, organoids treated with TRPA1 antagonists showed a significant increase in the density of SOX10+ cells after an ischemic event (5h and 11h) and NG2+ cells in the organoids induced with 11h of ischemia. Although large variation between different organoids, this suggests that the receptor can improve oligodendrocytes density after ischemia.

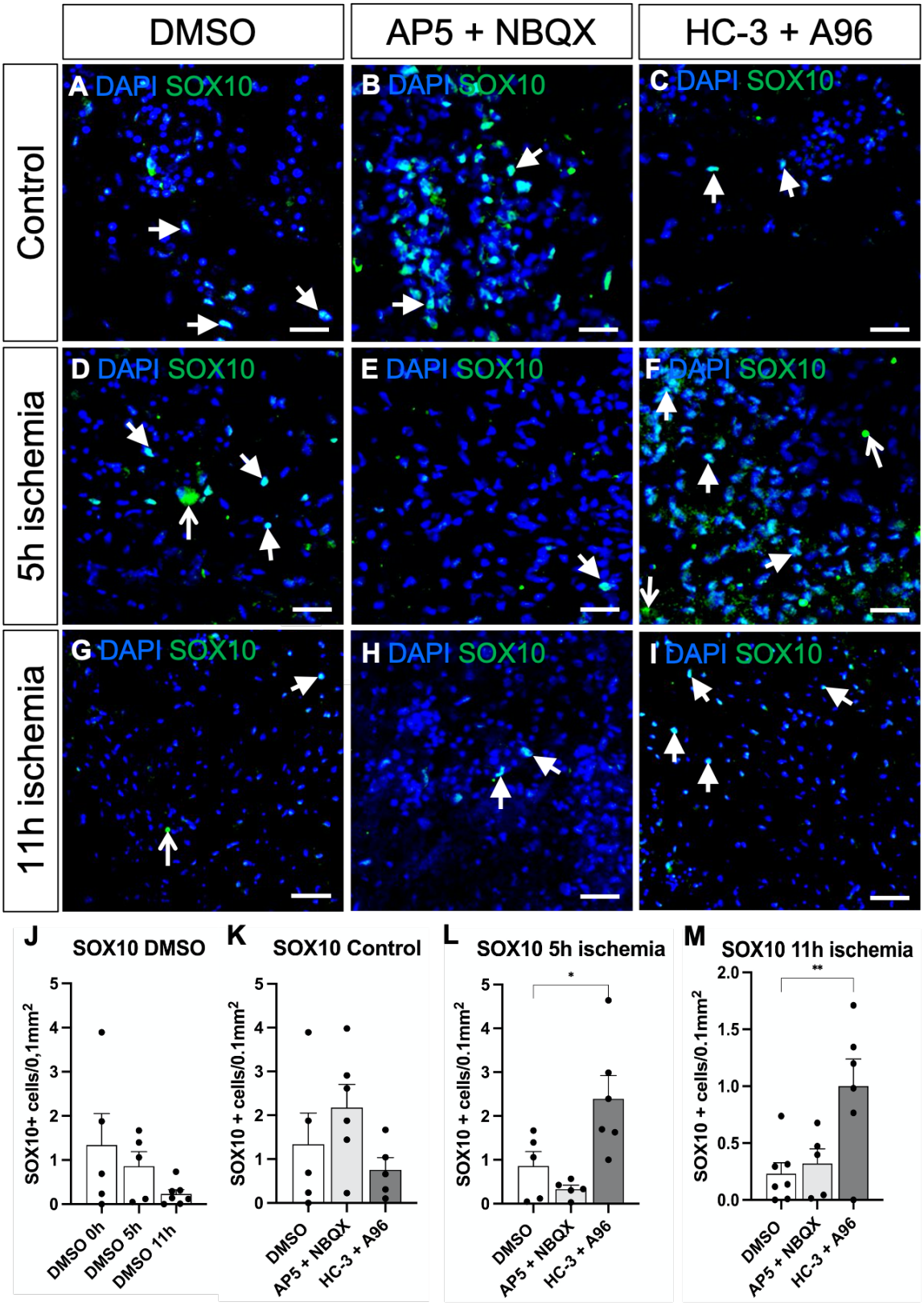

Figure 12: Density of SOX10 positive cells increased with TRPA1 antagonists. A-I:Confocal images of cerebral organoids sections from control (**A-C**), 5h (**D-F**) and 11h ischemia (**G-I**) groups with additionally antagonists for glutamate receptors (AP5+NBQX, **B**, **E**, **H**) and TRPA1 receptors (HC-3+A96, **C**, **D**, **I**) or DMSO (Ctrl, **A**, **D**, **G**). Sections are immunostained with DAPI (blue) and SOX10 (green) showing positive SOX10 cells (filled arrows) and poor staining (open arrows). **J-M**: Quantification of SOX10+ cells per 0,1mm^2 displaying mean number ± SEM between the DMSO treated ischemic groups (**J**) and in the control- (**K**) 5h- (**L**) and 11h group (**M**). Each data point (filled circle) represents one organoide. Statistical significance was calculated using a one-way ANOVA with Dunnett´s multiple comparison post-hoc test (*p<0,05, **p<0,01). Scale bare 50µm.

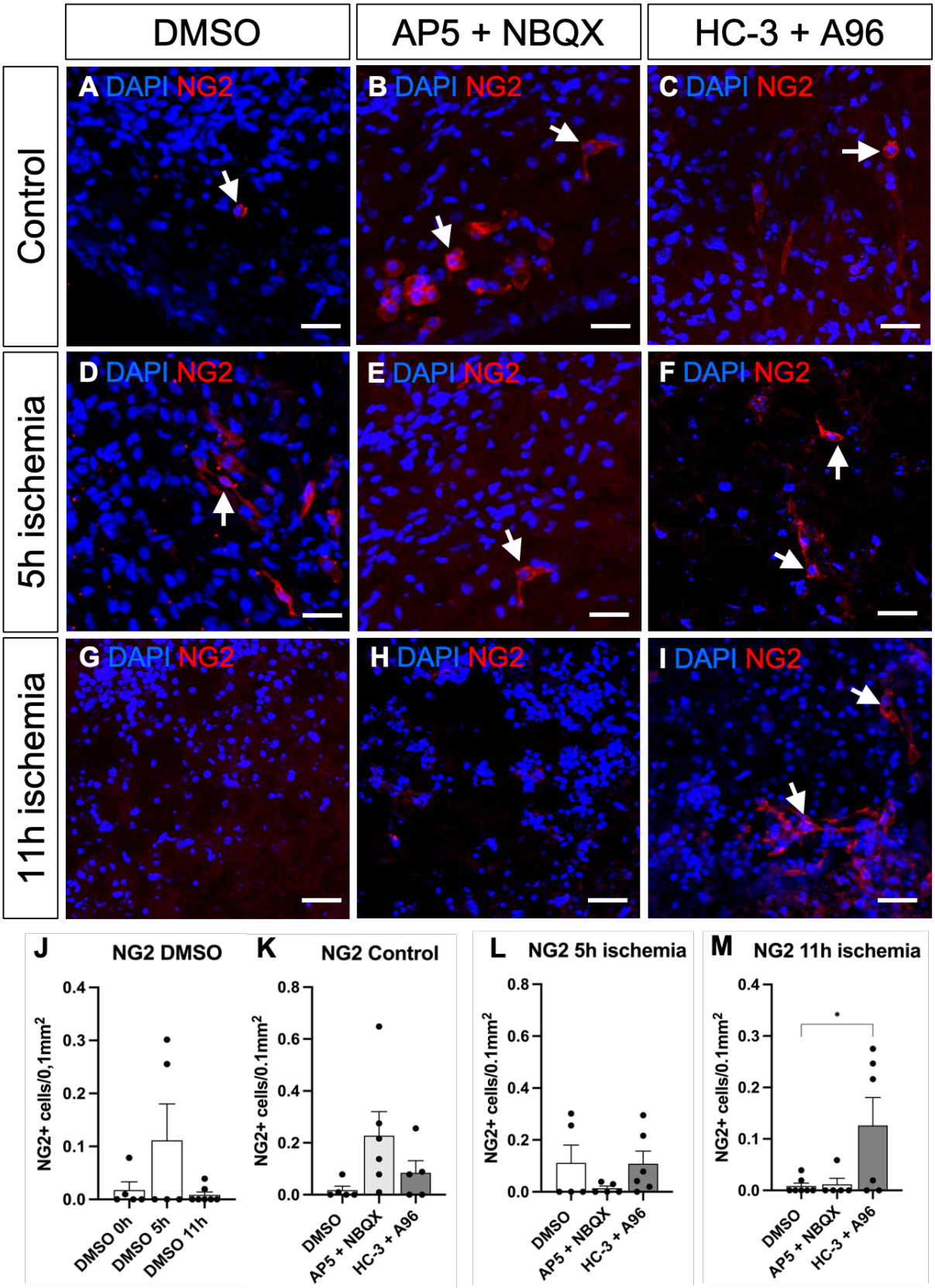

Figure 13: TRPA1 antagonist increased the density of oligodendrocyte precursor cells in 11h ischemic group. A-I: Confocal images of cerebral organoids sections from control (**A-C**), 5h (**D-F**) and 11h ischemia (**G-I**) groups with additionally antagonists for glutamate receptors (AP5+NBQX, **B**, **E**, **H**) and TRPA1 receptors (HC-3+A96, **C**, **E**, **I**) or DMSO (Ctrl, **A**, **D**, **G**). Sections are immunostained with DAPI (blue) and NG2 (red) showing positive NG2 cells (white arrows). **J-M**: Quantification of NG2+ cells per 0,1mm^2 displaying mean number ± SEM between the DMSO treated ischemic groups (**J**) and in the control- (**K**) 5h- (**L**) and 11h group (**M**). Each data point (filled circle) represents one organoide. Statistical significance was calculated using a one-way ANOVA with Dunnett´s multiple comparison post-hoc test (*p<0,05). Scale bare 50µm.

4.2.4 The effect of ischemia and receptor inhibition on neurons

To study how inhibition of glutamate or TRPA1 receptor might influenced the quality of the neurons, organoids were treated as described above and sections were stained with TUJ-1, a class III ß-tubulin marker, which stains the microtubules elements in the neurons (96). Quantitative analysis of TUJ-1+ neurons was not achievable due to high density of TUJ-1 staining; therefore, qualitative studies were carried out for this marker. One method used to identify and quantify deteriorated neurons is to manually score the extent of both intact and degenerated axons, the area of most microtubules together with the dendrites (97, 98). Damaged or degenerated cells are observed as fragmented, sometimes with swelling of the axonal extended processes (97, 99). For qualitative analysis of the neurons, sections from each group were given a score from 1-5 that resembles the percentage of damaged neurons in the section (score 1; 80-100% fragmented TUJ-1 staining, score 2; 60-80%, score 3; to 40-60%, score 4; to 20-40% and score 5; 0-20%). See figure 11A-E for examples of axonal score setting 5-1. The scoring was carried out blinded, such that the group identity of each image was unknown during the scoring process.

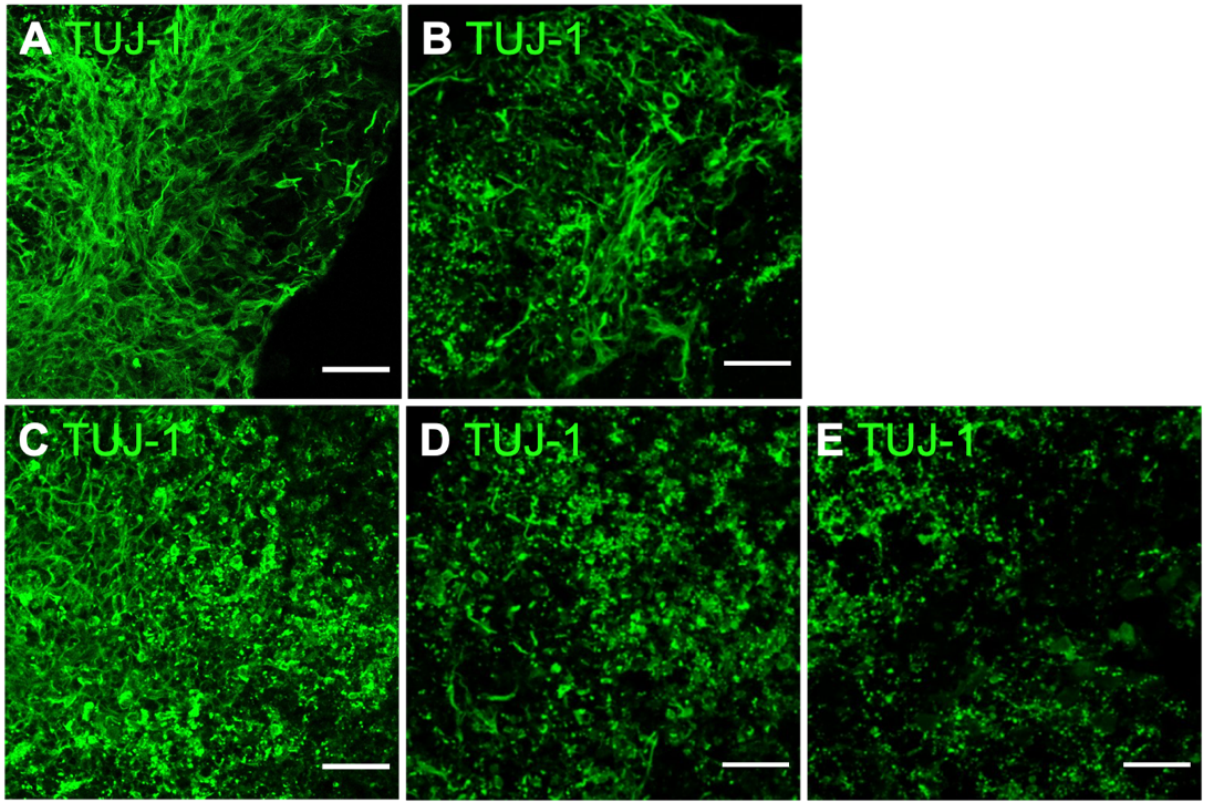

Figure 14: Qualitative score setting of TUJ-1+ cells. A-D: Confocal images of cerebral organoids sections stained with TUJ-1 (green) showing examples of different neuron-quality score where **A:** showing score 5 (0-20% fragmented TUJ-1 staining). **B:** score 4 (20-40% fragmented). **C:** score 3 (40-60% fragmented). **D:** score 3 (60-80% fragmented) and **E:** showing score 1 (80-100% fragmented). Scale bar 50µm.

Sections from organoids treated with five or eleven hours of ischemia had a significantly lower tissue quality score compared with the no-ischemia control (fig. 15. A, D, G, J, TUJ-1 quality: DMSO 0h; 4.06 ± 0.30, n = 5, DMSO 5h; 1.40 ± 0.23, n = 4, $p<0.0001$ compared with DMSO 0h and DMSO 11h; 1.45 ± 0.10, n = 7, $p <0.0001$ compared with DMSO 0h), demonstrating that ischemia led to degenerated neurons.

In the no-ischemia group, organoids treated with HC-3+A96 had a statistically significant decrease in neuron quality (fig. 15. A, D, K, TUJ-1 quality: DMSO 0h; 4.06 ± 0.30, n= 5, HC-3+A96 0h; 2.89 ± 0.18, n = 5, p = 0.008), with about 28% decreased neuronal quality, indicating more degenerated neurons. At 5h and 11h ischemia, there was no significant effect of HC-3+A96 treatment (fig. 15. D, F, L, TUJ-1 quality: DMSO 5h; 1.40 ± 0.23, n = 4, HC-3+A96 5h; 2.27 ± 0.26, n = 6, p = 0.26 and for the eleven-hour group fig. 15. G, I, M, TUJ-1 quality: DMSO 11h; 1.45 ± 0.10, n = 7, HC-3+A96 11h; 1.45 ± 0.12, n = 5, p > 0.99).

AP5+NBQX treatment had no effect on TUJ-1 quality in non-ischemic conditions (fig. 15. A-B, K, TUJ-1 quality: DMSO 0h; 4.06 ± 0.30, n =5, AP5+NBQX 0h; 4.14 ± 0.21, n = 6, p = 0.96). There was also no significant effect of AP5+NBQX treatment after ischemia (fig. 15. D-E, L, TUJ-1 quality: DMSO 5h; 1.40 ± 0.23, n = 4, AP5+NBQX 5h; 2.54 ± 0.59, n = 5, p = 0.14 and for the eleven-hour group fig. 15. G-H, M, TUJ-1 quality: DMSO 11h; 1.45 ± 0.10, n = 7, AP5+NBQX 11h; 1.25 ± 0.13, n = 5, p = 0.38).

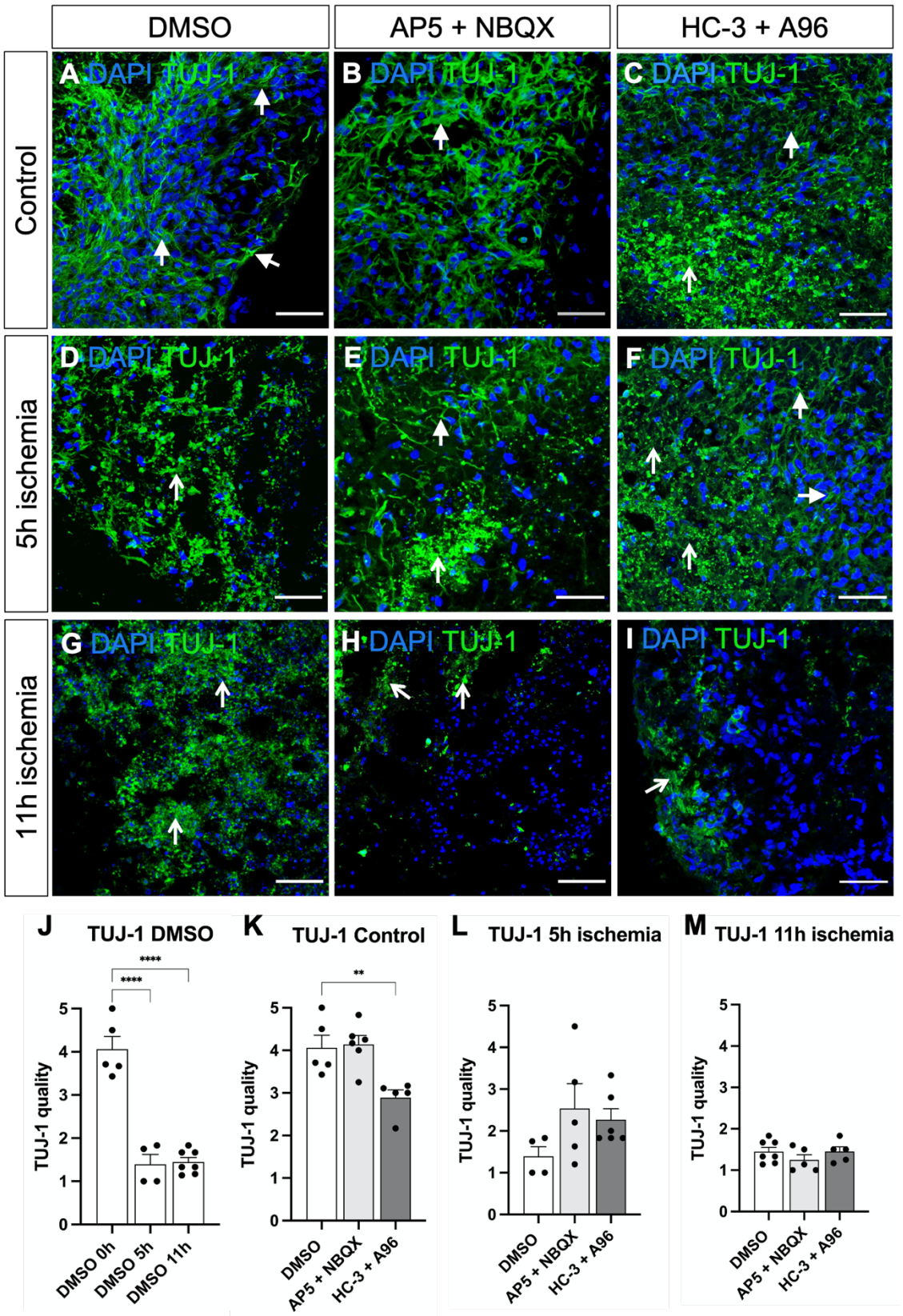

Figure 15: Qualitative analyses of neuronal tissue showing degenerated axons after ischemia. A-I: Confocal images of cerebral organoids sections from control (**A-C**), 5h (**D-F**) and 11h ischemia groups (**G-I**) with additionally antagonists for glutamate receptors (AP5+NBQX, **B**, **E**, **H**) and TRPA1 receptors (HC-3+A96, **C**, **F**, **I**) or DMSO (Ctrl, **A**, **D**, **G**). Sections are immunostained with TUJ-1 (green) and DAPI (blue) showing the mean neuronal quality (score) of each group based on fragmented TUJ-1staining. Healthy tissues are shown with filled arrows and fragmented or degenerated with open arrows. **J-M**: Graphs displaying the mean quality score ± SEM between the DMSO treated ischemic groups (**J**) and in the control- (**K**) 5h- (**L**) and 11h group (**M**). Statistical significance was calculated using a one-way ANOVA with Dunnett´s multiple comparison post-hoc test (**p<0,01, **** p<0,0001). Scale bare 50µm.

4.3 Localisation of TRPA1 receptors in cerebral organoids

TRPA1 receptors are known to be present in sensory neurons and are linked to their role in pain and neurogenic inflammation (100). But newer studies have shown a range of different cell types expressing TRPA1 receptors, and a study from Hamilton et al. (38) showed TRPA1 receptors in mouse oligodendrocytes. To my knowledge, localization of the TRPA1 receptor has not been studied in the human CNS. Since antibodies to TRPA1 have shown to be unspecific (38), RNA-FISH was performed on cerebral organoids to examine their presence. To localize TRPA1 expression in specific CNS cells, RNA-FISH combined with immunohistochemistry was carried out. Sections from mice were included in this experiment as a control, co-stained for oligodendrocytes linage cells. Images taken with a confocal microscope revealed expression of TRPA1 mRNA in oligodendrocytes (Olig2+ cells) in corpus callosum (fig 16A-C), as shown previously (38). We also detected TRPA1 in oligodendrocytes in the neocortex in mice (fig 16D-F), indicating TRPA1 mRNA expression in both white and grey matter oligodendrocytes. A negative control was included to quality check probe signal. As no signals were detected (not shown), correct probe hybridization was assumed.

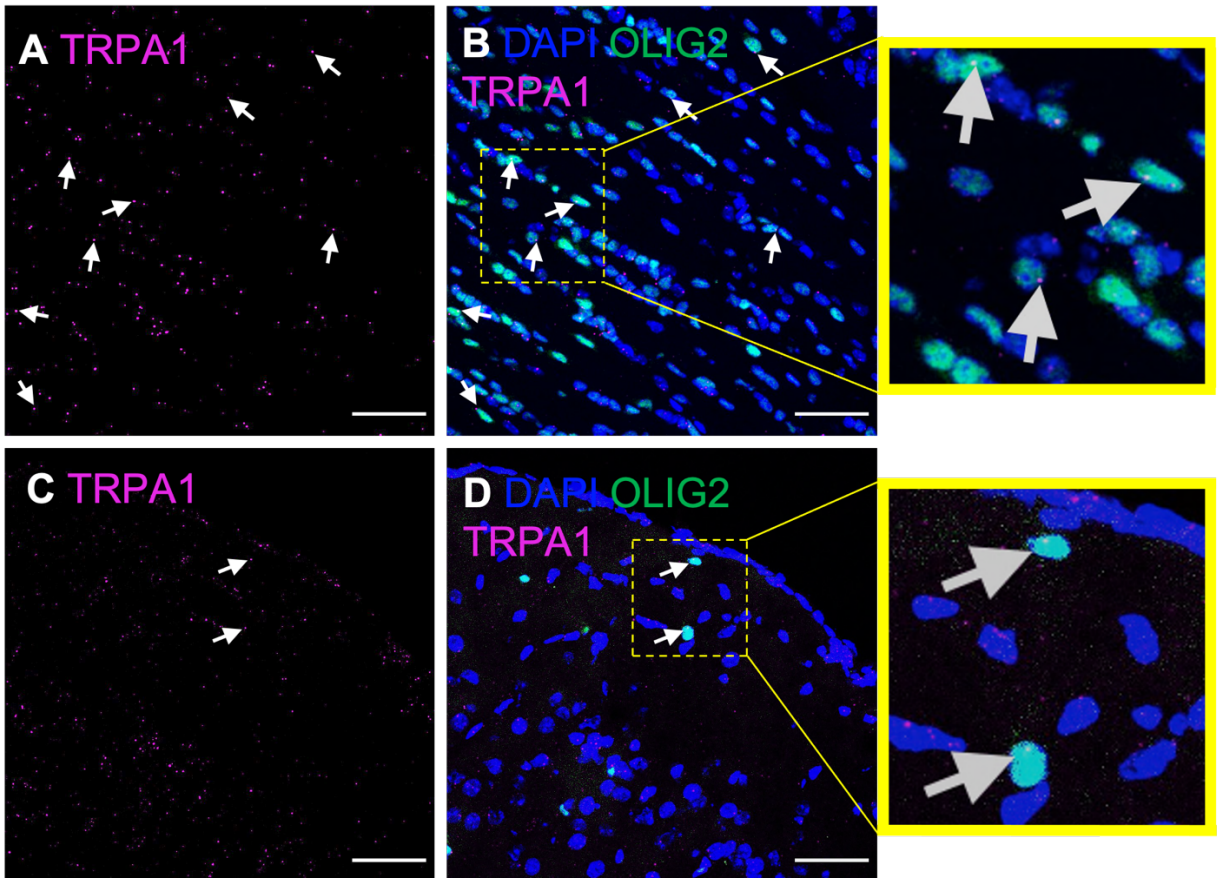

Figure 16: Mouse section from corpus callosum and neocortex stained with combined RNA-FISH and IHC showing TRPA1 receptor mRNA in oligodendrocytes. A-D: Confocal images of mice sections of corpus callosum are shown in **A-B** (white matter) and cortex **C-D** (grey matter) immunostained with DAPI (blue), Olig2 (green) and hybridized with TRPA1

FISH-probe (magenta). White arrows indicate the expression of TRPA1 receptor. Merged image showing expression of TRPA1 messenger RNA in Olig2+ cells in corpus callosum (**B**) and in neocortex (**D**). Scale bar 50µm.

In addition, other CNS cells showed the expression of TRPA1 mRNA, although not identified with immunostaining. The neuron marker TUJ-1 was included in our experiment to test TRPA1 expression in neurons. Unfortunately, the TUJ-1 antibody did not work when implemented in our combined FISH and immunostaining protocol (not shown). Therefore, a potential mRNA expression of TRPA1 in mouse CNS neurons could not be revealed.

RNA-FISH revealed a strong TRPA1 expression in a subset of cells in the cerebral organoids, shown in figure 17A-C. However, co-detection with oligodendrocyte lineage cell markers (Olig2, SOX10, O4) or neuron marker (TUJ-1) did not succeed when implemented in the FISH analysis of organoids (not shown). Thus, we cannot reveal which cell types that express this receptor. A negative control was included to quality check correct probe hybridization (Fig. 17D-F).

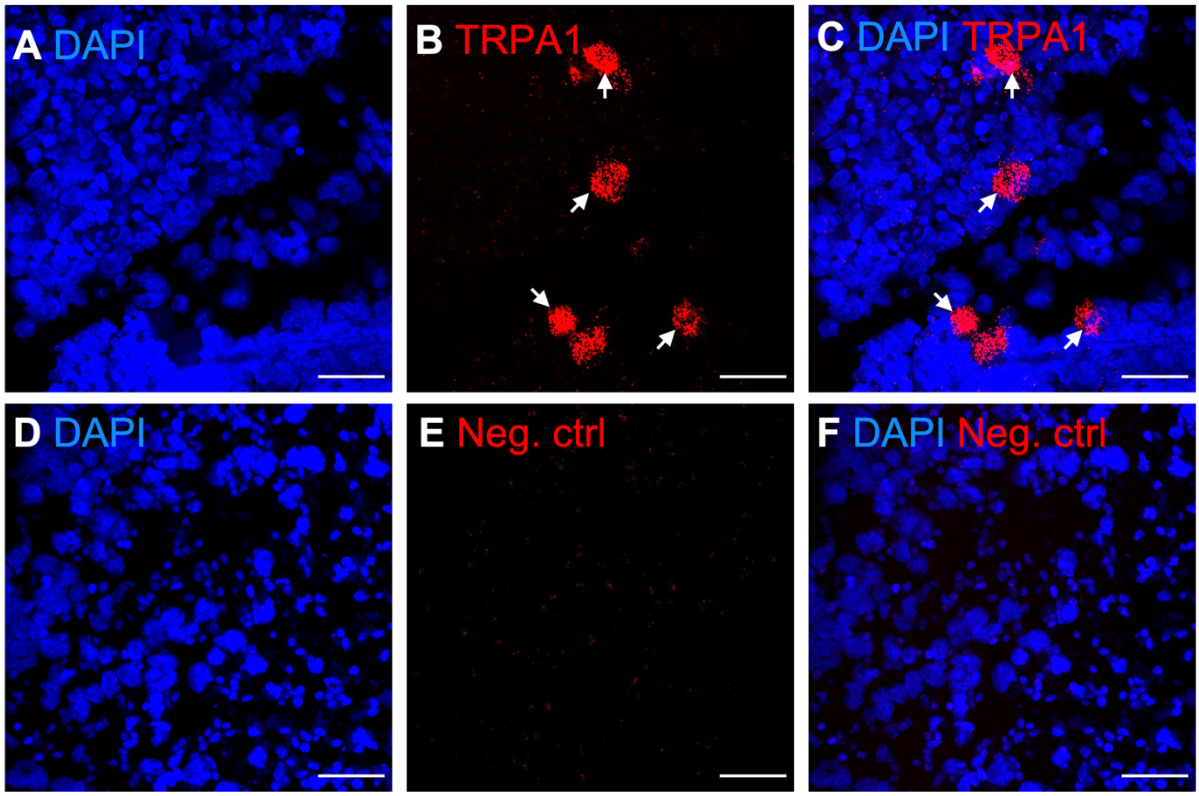

Figure 17: *in situ* hybridization for TRPA1 receptor showed expression in cerebral organoids. Confocal images of cerebral organoids labelled with DAPI (blue) and TRPA1 probe (red) are shown in **A** and **B** and merged image in **C**. White arrows indicate mRNA expression of TRPA1 receptor. Negative ctrl (**D**-**F**) showing DAPI (**D**) and no probe signal (**E**). Merged image is shown in **F**. Scale bar 50µm.

4.4 mRNA expression analysis using RT-qPCR to examine the relative gene expression

While immunohistochemistry revealed various levels of SOX10+-, NG2+ cells, and neuron qualities in differently treated organoids, we wanted to perform RT-qPCR analysis to assess the transcript levels of these genes. Moreover, since RNA-FISH analysis showed TRPA1 mRNA expression in cerebral organoids, we went on to investigate whether ischemia and receptor inhibition could affect the expression of TRPA1. Due to a low number of organoids available for these experiments, organoids treated with 5h of ischemia and control groups were examined and were limited to two biological replicates (two organoids) per treatment. Statistical analysis was therefore not performed, but a visual presentation of the data can be seen in figure 18A-D showing the relative expression of each gene. All mRNA expression is relative to the DMSO 0h expression for all groups (relative to the group with highest Ct value). Unfortunately, 5h ischemic organoids with the HC-3 antagonist showed low and contaminated mRNA and were excluded from the experiment.

SOX10 showed large variations within the biological replicates in the non-ischemic groups (0h) and can therefore not conclude about any obvious tendency in the mRNA expression between the groups (Fig. 18. A, Relative SOX10 expression: 0h AP5: 0.23 ± 0.03, n = 2, 0h NBQX; 0.29 ± 0.07, n = 2, 0h HC-3; 0.24 ± 0.07, n = 2, 0h A96: 0.29 ± 0.06, n = 2, 5h DMSO: 0.24 ± 0.19, n = 2, 5h AP5: 0.36 ± 0.30, n = 2, 5h NBQX: 0.30 ± 0.16, n = 2, 5h A96: 0.37 ± 0.26, n = 2). The general gene expression for SOX10 had Ct values between 25-34, where values from 30 Ct cycles indicate low gene expression. This means that SOX10 expression again varied, but indicate in general a low expression, when over 1/3 of the organoids had values of 30 or higher.

The mRNA expression of NG2 also showed variations within the 0h ischemic groups. Even though no statistical analysis was performed, a tendency of less mRNA expression can be seen in all the 5h groups when compared with the 0h ischemic groups (Fig 16. B, Relative NG2 expression: 0h AP5: 0.62 ± 0.24, n = 2, 0h NBQX; 0.53 ± 0.41, n = 2, 0h HC-3; 1.03 ± 0.77, n = 2, 0h A96: 0.51 ± 0.32, n = 2, 5h DMSO: 0.16 ± 0.09, n = 2, 5h AP5: 0.08 ± 0.04, n = 2, 5h NBQX: 0.06 ± 0.04, n = 2, 5h A96: 0.12 ± 0.07, n = 2). The Ct values for NG2 expression was somewhat lower compared to SOX10, having values between 23-27 indicate more expression of NG2 mRNA than SOX10 in the organoids.

TUJ-1 mRNA expression also showed large variations between groups, especially in the 5h ischemic treated organoids. Even though one replicate of each group showed low TUJ-1 expression in the 5h ischemic groups, the others had up to 28-fold increased expression compared with the DMSO 0h group. This observation could suggest that TUJ-1 expression might increase after ischemia, but more replicates are needed to confirm this observation (Fig. 18. C, Relative TUJ-1 expression: 0h AP5: 0.32 ± 0.09, n = 2, 0h NBQX; 1,06 ± 0,45, n = 2, 0h HC-3; 1,60 ± 0,98, n = 2, 0h A96: 1,10 ± 0,75, n = 2, 5h DMSO: 3,37 ± 3,35, n = 2, 5h AP5: 13,38 ± 13,13, n = 2, 5h NBQX: 6,98 ± 6,31, n = 2, 5h A96: 4,34 ± 3,32, n = 2). The general gene expression for TUJ-1 had Ct values between 17-22, indicating more expression of this gene compared with both SOX10 and NG2.

TRPA1 expression detected more variation in the 5h ischemic group than in the 0h group. No conclusion of any trends in the mRNA expression between the non-ischemic and the ischemic group can be made (Fig 16. D, Relative TRPA1 expression: 0h AP5: 0.23 ± 0,03, n = 2, 0h NBQX; 0,29 ± 0,07, n = 2, 0h HC-3; 0,23 ± 0,07, n = 2, 0h A96: 0,29 ± 0,06, n = 2, 5h DMSO: 0,24 ± 0,19, n = 2, 5h AP5: 0,36 ± 0,30, n = 2, 5h NBQX: 0,29 ± 0,16, n = 2, 5h A96: 0,37 ± 0,26 n = 2). TRPA1 had in general low expression in the organoids, having Ct values from 27-31.

In sum, RT-qPCR analysis on cerebral organoids showed a high degree of in-group variation. Although some trends could be seen in how expression level was influenced by ischemia, a potential effect of the different drug treatments could not be properly evaluated. More organoids need to be included in the experiment for statistical analysis before any conclusion can be made.

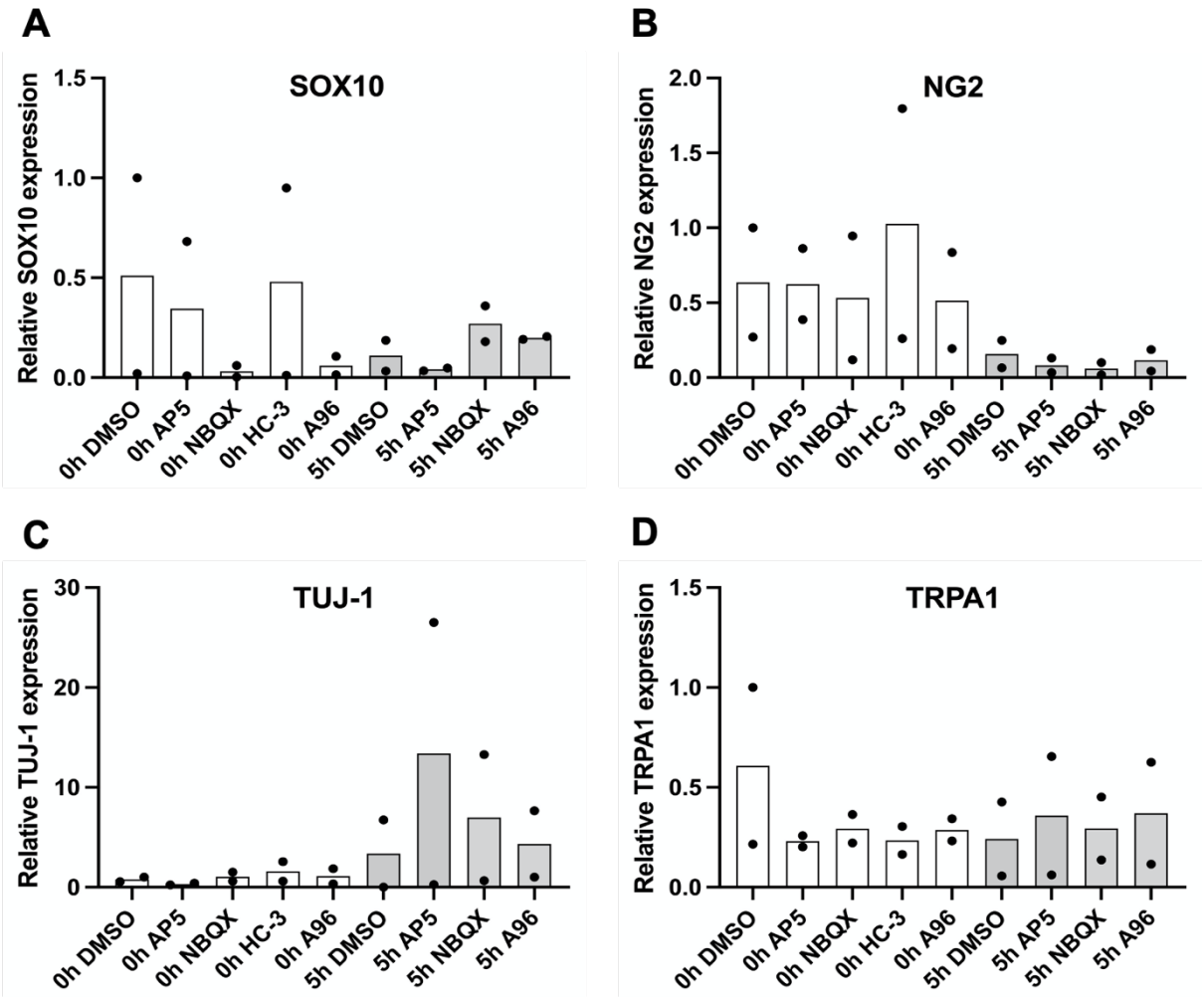

Figure 18: RT-qPCR analysis detecting mRNA levels of SOX10, NG2, TUJ-1 and TRPA1. Detection of SOX10 (A), NG2 (B), TUJ-1 (C) and TRPA1 (D) transcript levels in cerebral organoids induced with 5h of ischemia and control groups (0h). Organoids were treated with antagonists for the NMDA-, AMPA- or the TRPA1 receptor or DMSO. All values are relative to the control group (0h DMSO) and normalized to internal GAPDH expression. Graphs bars shows mean value between replicates (n = 2) and black dot represent each sample. Relative expression is calculated from the DMSO 0h treated organoid with lowest Ct value.

5. Discussion

Oligodendrocytes are the myelinating glial cells in the CNS and are crucial for rapid neuronal signalling. Oligodendrocytes are highly sensitive to injury by oxidative stress, and oligodendrocyte death leads to neuronal dysfunction. Both neurons and oligodendrocytes are killed by mechanisms involving calcium overload in stroke, but new studies suggest that the upstream mechanisms differ between those two cell types. A major part of this project was to develop human cerebral organoids to be used as our model in order to investigate the potential effect the TRPA1 receptor has on oligodendrocyte death, together with the glutamate receptor known to cause calcium influx in neurons. Many potential neuroprotective drugs have been tested in clinical trials to treat ischemic stroke, but have failed when tested in humans (46). Therefore, there is a need for human in vitro models of ischemic stroke that potentially can fill the gap between animal models and the human brain. This study aims studying to test the involvement of three ionotropic receptors (TRPA1, NMDA and AMPA) on oligodendrocyte survival after *in vitro* ischemia in human cerebral organoids. This was performed with the aim of exploring a potential different death mechanism from that in neurons. In addition, we measured the total cell number, axonal quality, and apoptosis level to gain an overall understanding of how inhibition of these receptors affected the organoids.

5.1 Cerebral organoid as a model for of the human brain

Growing cerebral organoids from hiPSC was a part of this project and were used as our model to investigate possible mechanisms of oligodendrocyte death. This includes feeding the cells/organoids with nutrition regularly and quality checks for normal and healthy development (see section 3.2). As mentioned previously, some organoids exposed to the same factors developed differently regarding size and unique structures. Ventricular-like cavities are to be seen in the organoids containing no cells but had well-defined cell walls. Vertebrates CNS have ventricles that are areas of connected cavities where cerebrospinal fluid circulates and contributes to normal CNS development by regulation of the homeostasis and mechanical protection (101, 102). Although ventricular-like cavities resemble prober cerebral development, organoids containing these structures could allow stored cerebral differentiation mediums within the organoids. This could have an impact on the result of the ischemia experiment when the aim is to remove any glucose from the environment. In addition to the ventricular structures, areas of (most likely) cells not differentiated into neuroepithelial tissue were found within some organoids, revealed by immunohistochemistry. Both of these areas were taken into

considerations when analysing and were excluded in immunohistochemistry analysis to limit the impact it could have on the results. There is also a known issue that cerebral organoids have a relative variable outcome for the generation of diverse brain regions and the differentiation of cells, even though they are derived from the same cell line under the same conditions. Since it is a biological material, there will result in variations between the organoids showing spatial and cellular heterogeneity (103) and thereby introducing variations into the experiments. Some organoids for the IHC analysis had to be excluded due to the rate of non-neuroepithelial areas. This reduced the n-number in our analysis. The combination of a large variation between organoids and the fact that we had to exclude some organoids from the analyses, limited the changes of achieving statistically differences between experimental groups. Accordingly, there is a chance of a type-2 error in my results. However, as these phenomena are now known, we will include larger sample sizes to overcome this problem in future experiments.

Culturing cerebral organoids are both expensive, time-consuming and stretches over several month and the number of healthy, developed organoids is low compared with the starting point due to strict quality control along the way. Only approximately 60-80% of the EBs showing acceptable quality will exhibit neuroectoderm differentiation (67), and therefore, large batches are needed to achieve enough organoids for statistical analysis. Even though culturing cerebral organoids have these practical limitations, this model has given researchers a new tool in understanding the development of the central nervous system and the impact of diseases and trauma. Organoids have a self-organizing capacity where hiPSC grows and differentiates into 3D brain organoids upon timely application of components and environmental factors. This generates a broad diversity of cells a cellular composition with structural features that resemble the developing brain and can be used to model tissue physiology and pathology and discover of new drugs (95, 104). Since these organoids resemble the developing brain at the fatal stage, our ischemia model will perhaps be more suitable when examining prenatal or neonatal ischemia than ischemic stroke in adults (67). However, we can assume that the cellular mechanisms are approximately the same thereby giving us insight in the molecular mechanisms happening during stroke.

Research on cerebral organoids as a model for the human brain has been escalated over the past years. Still, some essential aspects distinguish them from the human brain and cannot fully replace animal models. As they are made from human tissue and use gene expression programs remarkably similar to those of the tissues from fetals (105), the lack of vascularisation and

blood supply is a limitation. This absence decreases the rate of nutrients and oxygen being able to diffuse into the centre of the organoids and thereby reaches a size and differentiation limit. The necrotic core will, therefore, in almost all cases be found in the centre of the organoids (106). This needs to be taken under consideration when doing quantitative analysis by IHC to avoid false-negative results when the centre most likely contains dead cells. When studying vascular diseases such as stroke, this critical lack of vascularisation will have impact on the organoids regardless of treatment. To solve this problem, some researchers have been implanting cerebral organoids into the mouse brain and bypassing this vascularization problem. By connecting the organoids to the mouse´s vascular system, the organoids resulted in enhanced survival and successful vascularization (71). However, the model will no longer be a pure human *in vitro* model, one of the desired aspects of this model.

Since the vascular system is absent in the cerebral organoid model, this also results in a lack of immune system defence occurring after stroke to the injury site. Both the innate and adaptive immune responses are involved in the ischaemic stroke pathology resulting from cellular stress and will emerge from minutes to even months after injury (107). Ischemic cells will release damage-associated molecular patterns, such as ROS, which influence microglia and infiltrating leukocytes to produce cytokines that affect the stroke pathology (107). Microglia are the CNS' macrophage-like cells and are rapidly activated during a stroke and release both pro-and anti-inflammatory mediators to help facilitate apoptosis and survivability of neurons (108-110). The role of which the immune system is beneficial or detrimental to the damaged tissue are still not clear (107), but needs to be taken under consideration when using cerebral organoids as a model. However, lacking this effect may also help investigate specific cellular responses to ischemia when the immune system cannot influence the outcome.

Even though the cerebral organoids form some distinct cell layers that resembles that of the human cerebral cortex, they do not grow to form networks in the same dimension or have the same laminar organization as the human brain. Moreover, they lack signalling proteins from the extracellular matrix to guide their morphological development, which can influence how the organoids respond to ischemic events (111, 112). However, an important feature that has been reported in cerebral organoids is the generation of an outer subventricular zone (OSVZ) containing an abundant population of outer radial glia (oRG) progenitor cells. These cells are considered being a central aspect of the increase in human cortex size and complexity. oRGs

are mainly missing in mouse brain development (111), and cerebral organoids provide a unique opportunity to study these cells.

Some ethical aspects of this model have to be taken into account. Even though cerebral organoids are not made from embryonic-derived stem cells, they are still artificially created structures of human brain tissue and considered of human origin. Until now, no studies have shown that these organoids do or will have consciousness, but as we increase the complexity of the model, the question of when the organoids develop consciousness will become a critical question (113). A positive aspect of using organoids as a research model is the reduction of animal models when the number of lab animals has increased worldwide with the advancement of the development and research in medical technology (114). One of the most debating arguments against animal models is the pain, distress and death experience by the animals during scientific experiments. Arguments is that being alive, animals have the right against pain and distress (115), something they do not always have in a laboratory setting. Cerebral organoids are not sufficient in replacing animal models today when they do not give complete answers to disease and developmental issues. But, the organoid model could in the future reduce the number of animals needed in research by bridging the gap between preliminary animal testing and clinical trials on human (114).

5.2 The effect of glutamate and TRPA1 receptor inhibition

In order to evaluate the effect of ischemia and how receptor inhibition influenced the general cell viability, we investigated the number of cells, nucleus size, and the level of apoptosis between the differently treated organoids. Surprisingly, the immunolabeling with DAPI showed no significant decrease in the number of cells between the ischemic durations. Even though the ischemia model did not show decreased cell number, we did detect increased fragmentation of cell nuclei with increased ischemia. We found smaller nucleus size where 11h of ischemia had almost half of the size compared with the non-ischemia group, and after 5h of ischemia the size was something between these two groups. Fragmentation of the DNA is a typical incident during apoptosis (34, 48), and could explain these observations. To further evaluate this finding, immunostaining with cleaved caspase-3 was therefore carried out. This experiment revealed a significant increase in the number of caspase-3 positive cells in both the ischemic groups for organoids only treated with DMSO, which could explain the observation of no significantly

reduced cell number, but instead fragmentation of the nuclei. In addition, it confirmed that our ischemia model did lead to cell death in our organoids.

We included antagonists in the experimental groups to investigate the role the glutamate and ionotropic receptors had on total cell number and fragmentations. Neither nor of the antagonists treated organoids had a significant difference in the total number of cells or the mean nucleus size in neither non-ischemia nor ischemic conditions. Although this finding was not significant, glutamate receptor inhibition showed a trend in larger mean nucleus size in the 5h ischemic group and had a somewhat higher mean cell density. However, the use of trend is not recommended for any not-statistically significant data and will be cautiously used (116). As described previously, NMDA and AMPA receptors are activated by glutamate which are in excessive levels during stroke, leading to a toxic rise of intracellular Ca^{2+} in the neurons and potentially in the oligodendrocytes (29). Therefore, by blocking these receptors with the antagonist could explain the trend in less nuclei fragmentation while these receptors are involved in neuronal death and neurons are in an excess in our organoids. When immunostained with caspase 3 for detection of the apoptotic levels in the organoids, we expected to find a significant decreased level based on this theory. However, organoids treated with glutamate antagonists did not had a significant decreased number of apoptotic cells, and the reason for this is a matter of speculations. The observed variations in the organoids could led to diverse outcome and influence the analysis. Another factor can be caused by the differences in in human and mouse tissue, when studies have shown glutamate inhibition effect on cell death only in mice and other mammals, but not specific in human tissue (46). Additionally, inhibition of both NMDA and AMPA receptors might be somewhat excessive and could result in the opposite consequence, thereby losing the potential neuroprotective effect. Regardless, further experiments should include organoids treated with only NMDA or AMPA antagonists to assess the receptor effect individually.

To further assess whether the glutamate receptor antagonists affected the neuronal quality, qualitative analysis was carried out. While many studies have shown neuroprotective effects when blocking glutamate receptors in mice, this has failed in human clinical trials (49). A reason could be, as described above, that the mouse brains have a lower ratio of white matter (3) and could subsequently explain the positive effect in animals only. Nevertheless, we wanted to examine how these receptor antagonists affected the neurons in human tissue by assessing the quality of TUJ-1 positive neuronal axons. As the qualitative analysis was carried out, we

detected a significant decrease in tissue quality after five and eleven hours of ischemia compared with the control group without any antagonists. This indicated that the ischemia model did kill or at least damaged the cells when introducing ischemia.

When introducing glutamate antagonists to the organoids, the general axonal quality decreased, as for the DMSO treated group. This was surprising when we would expect better neuron survival as studies have shown reduction in excitotoxity when inhibiting glutamate receptors in neurons (29). Although qualitative analysis provides a good measure of the extent of both intact and degenerated axons, there will be some insecurity using this method when we manually score the axon quality. Therefore, future investigations should co-localize neuron markers with caspase-3 or other apoptotic or cell death markers. This could give us more information and performed quantitative measurement on the neurons' viability with the additional antagonists. The neuron marker NeuN was carried out in this project to accomplish this wish, which stains the nucleus in mature neurons. However, as the organoids resemble young, developing brains, few NeuN cells were detected in our organoids (not shown). Anyway, optimalisation of automatic quantification of neurons using ImageJ should be carried out in future experiments.

Oligodendrocytes and their myelin are highly vulnerable to ischemic stroke, as for other brain injuries, and after an acute phase of ischemic stroke, oligodendrocytes are damaged, leading to demyelination of the axons and impaired neuronal signalling (12). We therefore wanted to investigate how these receptors specifically affected the oligodendrocyte lineage cells, although another study has shown different mechanism to calcium overload in oligodendrocytes than for neurons (38). IHC was performed with antibodies for oligodendrocyte lineage cells, and the number of cells positive for the marker SOX10 was quantified. We did not detect any significant differences in the number of SOX10 positive cells without receptor antagonists, although the mean density of oligodendrocytes was somewhat decreased as we increased the ischemia. Anyway, organoids treated with glutamate receptor antagonists did not reveal any significant difference in neither of the ischemia groups. This suggests that the mechanisms leading to oligodendrocyte death does not depend alone on the NMDA and AMPA receptors.

Generation of new cells is essential for the brain tissue repair process following brain injury, such as ischemic stroke (12). Zhang et al. demonstrated in a mice model study from 2013 that mice after a cerebral ischemia event showed an increase in oligodendrogenesis (117). Mature oligodendrocytes cannot proliferate in the adult brain. Therefore, the ischemic event tends to

give rise to a proliferation of precursor oligodendrocytes, likely to initiate remyelinating events after myelin loss or damage (35, 117). As mature oligodendrocytes arise from OPCs, we wanted to investigate whether the glutamate receptors had any involvement on these precursor cells. Surprisingly, we did not detect any significant increase in OPCs between the ischemic durations with only DMSO treatment. We expected to see an increase when, as mention above, remyelination events occur after injury, and OPCs respond to demyelination and damage by activation, proliferation, and migration (118). On the other hand, the ischemic model might be too harsh. When inducing 11h of ischemia to the organoids, this could result in more cell death and thereby being too harsh. Having additionally ischemic time points between 0h and 11h would help us in achieving a better result.

Interestingly, in the non-ischemic group there was a trend towards higher NG2+ cells in the organoids treated with NMDA and AMPA antagonists. As expression of neurotransmitter receptor decreases during oligodendrocyte differentiation, this suggests that these have a specific role in the OPCs. Studies from Gautier and Gudz et al. both showed that OPCs are recruited by neuronal activity (65, 119). And, that demyelinated axons generate synapses with recruited OPCs through AMPA receptors by glutamate signalling to instruct OPCs to differentiate into mature, myelinated oligodendrocytes. Gautier et al. (65) further detected a six-fold increase of OPCs around demyelinated axons when blocking the neuronal activity. These OPCs did not differentiate further to mature myelinated oligodendrocytes, and thereby suggest that neuronal activity and the release of glutamate instruct OPCs to differentiate into myelinating oligodendrocytes. This can explain our result when the cerebral organoids resemble developing brains containing mostly unmyelinated axons and the AMPA receptor (and NMDA) was inhibited in the organoids, thereby blocking the neuronal activity. Even so, this is a matter of speculations. We neither detected any significant difference nor had the organoids large variations between them and therefore need larger sample sizes to confirm any hypothesis.

The glutamate inhibition had neither effect on the number of OPCs when we introduced ischemia to the organoids, detected organoids have numbers close to zero. This can might be explained when oligodendrocytes and its precursor cells, in general, are vulnerable to ischemia when rat oligodendrocytes showed rapidly death after a brief global ischemia and were more sensitive than neurons (36). In addition, the theory of that the calcium overload mechanisms

differ between oligodendrocytes and neurons (38) might explain why inhibition of glutamate receptor did not influence the OPCs density.

As Hamilton et al. showed a different mechanism leading to Ca2+ overload in oligodendrocytes through the TRPA1 receptor in mice (38), we further investigated the effect of inhibiting these receptors. TRPA1 receptor inhibition in the no-ischemia group detected no significant differences in neither total cell number nor the mean nucleus size. Interesting, a significant increase in apoptotic cells was detected when immunostained with caspase 3, compared with the DMSO treated group. This might reveal that the TRPA1 receptor has distinct roles in the variety of cell types in the CNS and seems to have an undesired effect when inhibited in physiological conditions. This could also have impact on the potential clinical relevance when the TRPA1 antagonists showed to kill a subset of cell when the aim is to rescue the tissue from dying after a stroke. However, when increasing the ischemia, this effect slowly turned when the IHC analysis detected no longer any significant increase in apoptotic cells. Although, the level was still high (in all groups) indicating dying cells. Further analysis should therefore supplement more organoids in addition to evaluate which cell type underwent apoptosis. This can be achieved by co-staining caspase-3 and oligodendrocytes markers as for other CNS´ cells to conduct more information and bringing more power to the observation.

To assess whether the TRPA1 had any involvement on the number oligodendrocyte lineage cells, we preformed IHC analysis with SOX10 markers on organoids treated with TRPA1 antagonists. As mentioned, we did not detect any differences in the number of oligodendrocytes between the different ischemic durations with only DMSO. However, organoids treated with TRPA1 antagonists had a significant increase with a three- and a four-fold increase in SOX10 positive cells after 5h and 11h of ischemia, respectively, compared with their DMSO group. These levels were equal or even higher than the non-ischemic group, suggesting two things; TRPA1 inhibition increases proliferation of new OPCs or reduce the death of oligodendrocytes during ischemic stroke. The latter has been shown in studies tested on mice, where TRPA1 receptor inhibition led to a 70% reduction of intracellular Ca2+ in oligodendrocytes (38), making the TRPA1 receptor the dominant contributor to the ischemia evoked Ca2+ rise. Our data suggest that a similar mechanism takes place in human nervous tissue, but this needs to be tested further.

In order to investigate whether the TRPA1 receptor also influenced the OPCs, we conducted IHC with NG2 markers. Organoids treated with TRPA1 antagonists showed a significant increase in NG2 positive cells after 11h of ischemia. Furthermore, the number of OPCs was somewhat even higher than in the non-ischemic group, having about 10-fold more NG2 positive cells. As this observation also was seen in the SOX10 experiment, we suggest that the TRPA1 receptor might be a dominant contributor to calcium influx in oligodendrocyte lineage cells, leading to either cell death or that inhibition of this receptor influence the proliferation of OPCs. To evaluate whether this high level of SOX10 and NG2 positive cells was due to new, proliferating OPCs, co-staining of SOX10 or NG2 with the proliferation marker bromodeoxyuridine (BrdU) can be performed in future experiments (120).

Since we found a significant difference in the number of oligodendrocytes with TRPA1 antagonist treatment, we also investigate its role on neurons. Surprisingly, organoids treated with TRPA1 receptor antagonist showed a significant reduction in tissue quality in the non-ischemic group by having 20-40% more damaged axonal tissue when compared with both the non-treated group and glutamate inhibited group. TRPA1 is known to be located on sensory neurons and plays a role in the pathogenesis of pain and inflammation. With the unique role of processing noxious stimuli (121), this might suggest a link between the lower axon quality when inhibiting this receptor. As the cell death analysis by caspase staining also showed an increase in apoptotic cells in the non-ischemic group treated with TRPA1 antagonists, this might suggest that a significant portion of the caspase-positive cells were neurons. However, more studies are needed to confirm this hypothesis.

When introducing ischemia to the organoids, the general neuronal quality decreased in all groups. By reducing calcium influx into oligodendrocytes through the TRPA1 receptors would suggest that it might helped the neurons' survivability since oligodendrocytes allow efficient axon potential propagation and provide metabolic support to the underlying axon (16). Anyway, as our organoids resembles a developing brain, there will be few myelinated axons which might explain why we do not see any effect of this treatment. As mentioned above, improved analysis of the neurons together with apoptotic markers are needed to reveal more information.

To substantiate the findings detected with TRPA1 inhibition on oligodendrocytes, we wanted to localize the TRPA1 receptor in the cerebral organoids. While the presence and functions of the TRPA1 receptor in sensory neurons are today well-known as a chemosensory receptor (97,

98), new studies have revealed its location and its potential function in the CNS glial cells, even though its pathophysiological role remains unclear (43, 99). As the TRPA1 receptor has shown a potential effect in oligodendrocytes, few studies have shown its location in human CNS and exhibited its role in humans stoke events. Therefore, cerebral organoids were used to localize the receptor in human tissue, and co-staining with oligodendrocyte and neuron markers was implemented in the RNA-FISH protocol. Unfortunately, co-staining with antibodies did not work when implemented in the protocol. Nevertheless, TRPA1 mRNA expression was seen in a subset of cells in the organoids, indicating that the receptor is present in our organoids. More optimisation and test of different antibodies in needed to determine the identity of the TRPA1-expressing cells in the organoids. TRPA1 mRNA expression was detected in mouse sections, as Hamilton et al. showed in their study from 2016 (38), and thereby confirming TRPA1 presence in mouse oligodendrocytes.

To explore whether the same trends were seen at the mRNA level as for the protein (IHC), we experimented with RT-qPCR analysis for SOX10, NG2, TUJ-1 and the TRPA1 mRNA expression. The cerebral organoids used for this experiment was induced to either non or 5h of ischemia and where only treated with one of the antagonists to investigate more specific each receptor. Unfortunately, the limited access of organoids for these experiments resulted in only two biological replicates, and therefore, no statistical analysis could be performed. In addition, the organoids showed high and noticeable variations between them where some of the organoids showed even opposite trends and did therefore make the results less reliable. The divergence between organoids and particular between batches is a general problem in organoid research (103), and we need larger sample sizes to conduct any significantly differences or exclude potential outliers.

However, the mRNA expression of both SOX10 and NG2 did not revealed the same trend as in IHC, showing lower mRNA expression with TRPA1 antagonist after 5h of ischemia when compared with the DMSO 0h ischemia group. A possibility that we did not see the same line as in IHC could be that the antagonist was in this experiment separated. In addition, the HC-3 antagonists did not reveal any mRNA after isolation and the A96 antagonist alone might not be sufficient enough. For the TRPA1 mRNA expression, we did not detect any spectacular difference from the control (DMSO 0h), in addition to showing large variances between the organoids. Although we cannot conclude anything form this experiment, we did detect up to 28-fold increase in TUJ-1 expression after 5h of ischemia, which might indicate higher

expression after ischemic events. As neurogenesis happens after brain injury and results in increased proliferation, we would expect some higher level of TUJ-1 mRNA, as TUJ-1 is expressed in developing and mature neurons (96).

However, no conclusion can be made, and we cannot indicate if any of these antagonists had any influence on the neurons, or neither on the oligodendrocytes or the TRPA1 expression before larger sample sizes are conducted bringing more power to these observations. Further experiments should also test other HK genes than GAPDH when the enzyme is involved in glycolysis. Its activity can be intensified by the ischemia itself, thereby affecting the gene expression and disrupting the endogenous control function, which further contributes to variations between treatments groups (122).

Further improvements

Further experiments using human cerebral organoids as an *in vitro* model need to consider for the variance in organoid development, either by improving the quality control or by making sure of include large enough sample sizes in the experimental groups. While our project detected positive effects on oligodendrocyte density by some treatments, we also found high levels of apoptotic cells in all the experimental groups. To further asses which cell types died from the ischemic events, immunostaining with oligodendrocyte and neuron markers combined with an apoptosis marker should be tested to determine the viability. Flowcytometry could also be a potential option to contribute to more robust test results when the whole organoids will be investigated. Since we found an increase in OPCs after 11h of ischemia with TRPA1 antagonists, it could be interesting to co-stain with the mitotic marker Ki-67 or BrdU that would determine whether these OPCs are newly formed, or this was a result of highly variable organoids.

In addition, it would have been interesting to co-localize the TRPA1 mRNA expression in the cerebral organoids with other cell types when it has shown to influence the number of oligodendrocytes after stroke (38), but also showed an increase in apoptotic cells in non-ischemic conditions. Therefore, the RNA-FISH protocol for cerebral organoids with implemented IHC needs to be improved to investigate the overall localization of TRPA1 in human CNS.

6. Conclusion

This project aimed at testing the involvement of ionotropic glutamate- and TRPA1 receptors in oligodendrocyte density and overall cell death in response to ischemia using human cerebral organoids as our model. Inhibition of glutamate receptors had no significant effect on the density of apoptotic cells, oligodendrocytes or neuronal TUJ-1-morphology. However, due to large variations between organoids, this should be tested further with a high n-number. Moreover, inhibition of the two glutamate receptor types, NMDA and AMPA, should be tested separately.

We have shown that cerebral organoids treated with TRPA1 receptor antagonists had as many oligodendrocyte lineage cells after an ischemic event as in non-ischemic conditions, indicating that the TRPA1 receptor is a dominant contributor to oligodendrocyte death after ischemia in human brains tissue *in vitro*. The number of precursor oligodendrocyte cells was also increased after 11h of ischemia with TRPA1 antagonists. Of note, in non-ischemic organoids, TRPA1 antagonists increased the density of apoptotic cells (all cell types) and worsened the morphology of TUJ-1-positive neurons. This suggests a damaging effect of TRPA1 receptor inhibition, which may limit its clinical potential. In line with the observed effects of TRPA1 receptor inhibition, we show that cerebral organoids express mRNA for the TRPA1 receptor, but unfortunately, we could not detect which cell types expressed the mRNA.

Summing up, this project confirms that TRPA1, previously shown to contribute to oligodendrocyte death in ischemic mice, are also involved in ischemic oligodendrocyte death in human nervous tissue *in vitro*. This identifies an interesting field for further research on protective agents after stroke.

7. References

1. Joan Stilies TLJ. The Basics og Brain Development Neuropsychology Review 2010;20(4):327-48.
2. Goldberg JL. How does an axon grow? Genes Dev. 2003;17(8):941-58.
3. von Bartheld CS, Bahney J, Herculano-Houzel S. The search for true numbers of neurons and glial cells in the human brain: A review of 150 years of cell counting. J Comp Neurol. 2016;524(18):3865-95.
4. Schmidt H, Knösche TR. Action potential propagation and synchronisation in myelinated axons. PLoS Comput Biol. 2019;15(10):e1007004.
5. Gonzalez-Perez O. Neural stem cells in the adult human brain. Biol Biomed Rep. 2012;2(1):59-69.
6. Duan X, Kang E, Liu CY, Ming GL, Song H. Development of neural stem cell in the adult brain. Curr Opin Neurobiol. 2008;18(1):108-15.
7. J. Bradley Zuchero, Barres BA. Glia in mammalian development and disease. 2015.
8. Barres BA. The mystery and magic of glia: a perspective on their roles in health and disease. Neuron. 2008;60(3):430-40.
9. Liebner S, Dijkhuizen RM, Reiss Y, Plate KH, Agalliu D, Constantin G. Functional morphology of the blood-brain barrier in health and disease. Acta Neuropathol. 2018;135(3):311-36.
10. Tognatta R, Karl MT, Fyffe-Maricich SL, Popratiloff A, Garrison ED, Schenck JK, et al. Astrocytes Are Required for Oligodendrocyte Survival and Maintenance of Myelin Compaction and Integrity. Front Cell Neurosci. 2020;14:74.
11. V. Hugh Perry, Teeling J. Microglia and macrophages of the central nervous system: the contribution of microglia priming and systemic inflammation to chronic neurodegeneration. 2013.
12. Kuhn S, Gritti L, Crooks D, Dombrowski Y. Oligodendrocytes in Development, Myelin Generation and Beyond. Cells. 2019;8(11).
13. Bergles QE, Richardson WD. Oligodendrocyte Development and Plasticity. 2016.
14. Simons M, Nave KA. Oligodendrocytes: Myelination and Axonal Support. Cold Spring Harb Perspect Biol. 2015;8(1):a020479.
15. Rosko L, Smith VN, Yamazaki R, Huang JK. Oligodendrocyte Bioenergetics in Health and Disease. Neuroscientist. 2019;25(4):334-43.
16. Marin MA, Carmichael ST. Stroke in CNS white matter: Models and mechanisms. Neuroscience Letters. 2018;684:193-9.
17. Rinholm JE, Vervaeke K, Tadross MR, Tkachuk AN, Kopek BG, Brown TA, et al. Movement and structure of mitochondria in oligodendrocytes and their myelin sheaths. Glia. 2016;64(5):810-25.
18. Sommer I, Schachner M. Monoclonal antibodies (O1 to O4) to oligodendrocyte cell surfaces: An immunocytological study in the central nervous system. Developmental Biology. 1981;83(2):311-27.
19. Bhat RV, Axt KJ, Fosnaugh JS, Smith KJ, Johnson KA, Hill DE, et al. Expression of the APC tumor suppressor protein in oligodendroglia. Glia. 1996;17(2):169-74.
20. Dimou L, Gallo V. NG2-glia and their functions in the central nervous system. Glia. 2015;63(8):1429-51.
21. Ma Y, Liu T, Zhang Z, Yang G-Y. Significant of Complement System in Ischemic Stroke: A Comprehensive Review. 2019.

22. Feigin VL, Krishnamurthi RV, Parmar P, Norrving B, Mensah GA, Bennett DA, et al. Update on the Global Burden of Ischemic and Hemorrhagic Stroke in 1990-2013: The GBD 2013 Study. Neuroepidemiology. 2015;45(3):161-76.
23. Mergenthaler P, Lindauer U, Dienel GA, Meisel A. Sugar for the brain: the role of glucose in physiological and pathological brain function. Trends Neurosci. 2013;36(10):587-97.
24. Raichle ME, Gusnard DA. Appraising the brain's energy budget. Proc Natl Acad Sci U S A. 2002;99(16):10237-9.
25. Kaufmann AM, Firlik AD, Fukui MB, Wechsler LR, Jungries CA, Yonas H. Ischemic core and penumbra in human stroke. Stroke. 1999;30(1):93-9.
26. Lau A, Tymianski M. Glutamate receptors, neurotoxicity and neurodegeneration. Pflügers Archiv - European Journal of Physiology. 2010;460(2):525-42.
27. Allen NJ, Káradóttir R, Attwell D. Reversal or reduction of glutamate and GABA transport in CNS pathology and therapy. Pflügers Archiv. 2004;449(2):132-42.
28. Sloan Steven A, Barres Ben A. The Detrimental Role of Glial Acidification during Ischemia. Neuron. 2014;81(2):221-3.
29. Bano D, Ankarcrona M. Beyond the critical point: An overview of excitotoxicity, calcium overload and the downstream consequences. Neuroscience Letters. 2018;663:79-85.
30. Ankarcrona M, Dypbukt JM, Bonfoco E, Zhivotovsky B, Orrenius S, Lipton SA, et al. Glutamate-induced neuronal death: a succession of necrosis or apoptosis depending on mitochondrial function. Neuron. 1995;15(4):961-73.
31. Tsujimoto Y. Apoptosis and necrosis: Intracellular ATP level as a determinant for cell death modes. Cell Death & Differentiation. 1997;4(6):429-34.
32. Liu F, Lu J, Manaenko A, Tang J, Hu Q. Mitochondria in Ischemic Stroke: New Insight and Implications. Aging Dis. 2018;9(5):924-37.
33. Wyllie AH, Kerr JFR, Currie AR. Cell Death: The Significance of Apoptosis. In: Bourne GH, Danielli JF, Jeon KW, editors. International Review of Cytology. 68: Academic Press; 1980. p. 251-306.
34. Broughton BRS, Reutens DC, Sobey CG. Apoptotic Mechanisms After Cerebral Ischemia. Stroke. 2009;40(5):e331-e9.
35. Bradl M, Lassmann H. Oligodendrocytes: biology and pathology. Acta Neuropathol. 2010;119(1):37-53.
36. Petito CK, Olarte JP, Roberts B, Nowak TS, Jr., Pulsinelli WA. Selective glial vulnerability following transient global ischemia in rat brain. J Neuropathol Exp Neurol. 1998;57(3):231-8.
37. Pantoni L, Garcia JH, Gutierrez JA. Cerebral White Matter Is Highly Vulnerable to Ischemia. Stroke. 1996;27(9):1641-7.
38. Hamilton NB, Kolodziejczyk K, Kougioumtzidou E, Attwell D. Proton-gated Ca(2+)-permeable TRP channels damage myelin in conditions mimicking ischaemia. Nature. 2016;529(7587):523-7.
39. Káradóttir R, Cavelier P, Bergersen LH, Attwell D. NMDA receptors are expressed in oligodendrocytes and activated in ischaemia. Nature. 2005;438(7071):1162-6.
40. Micu I, Jiang Q, Coderre E, Ridsdale A, Zhang L, Woulfe J, et al. NMDA receptors mediate calcium accumulation in myelin during chemical ischaemia. Nature. 2006;439(7079):988-92.
41. Salter MG, Fern R. NMDA receptors are expressed in developing oligodendrocyte processes and mediate injury. Nature. 2005;438(7071):1167-71.

42. Cheli VT, Correale J, Paez PM, Pasquini JM. Iron Metabolism in Oligodendrocytes and Astrocytes, Implications for Myelination and Remyelination. ASN Neuro. 2020;12:1759091420962681.
43. Lyngsie G, Krumina L, Tunlid A, Persson P. Generation of hydroxyl radicals from reactions between a dimethoxyhydroquinone and iron oxide nanoparticles. Scientific Reports. 2018;8(1):10834.
44. Zhao Z. Iron and oxidizing species in oxidative stress and Alzheimer's disease. Aging Med (Milton). 2019;2(2):82-7.
45. Taha TA, Mullen TD, Obeid LM. A house divided: ceramide, sphingosine, and sphingosine-1-phosphate in programmed cell death. Biochim Biophys Acta. 2006;1758(12):2027-36.
46. Casals JB, Pieri NC, Feitosa ML, Ercolin AC, Roballo KC, Barreto RS, et al. The use of animal models for stroke research: a review. Comp Med. 2011;61(4):305-13.
47. Sommer CJ. Ischemic stroke: experimental models and reality. Acta Neuropathol. 2017;133(2):245-61.
48. Sekerdag E, Solaroglu I, Gursoy-Ozdemir Y. Cell Death Mechanisms in Stroke and Novel Molecular and Cellular Treatment Options. Curr Neuropharmacol. 2018;16(9):1396-415.
49. Macrae IM, Allan SM. Stroke: The past, present and future. Brain Neurosci Adv. 2018;2:2398212818810689.
50. Neuhaus AA, Couch Y, Hadley G, Buchan AM. Neuroprotection in stroke: the importance of collaboration and reproducibility. Brain. 2017;140(8):2079-92.
51. Sherwood CC, Stimpson CD, Raghanti MA, Wildman DE, Uddin M, Grossman LI, et al. Evolution of increased glia–neuron ratios in the human frontal cortex. Proceedings of the National Academy of Sciences. 2006;103(37):13606-11.
52. Perlman RL. Mouse models of human disease: An evolutionary perspective. Evol Med Public Health. 2016;2016(1):170-6.
53. Carmichael ST. Rodent models of focal stroke: size, mechanism, and purpose. NeuroRx. 2005;2(3):396-409.
54. Onwuekwe I, Ezeala-Adikaibe B. Ischemic stroke and neuroprotection. Ann Med Health Sci Res. 2012;2(2):186-90.
55. Muir KW. Glutamate-based therapeutic approaches: clinical trials with NMDA antagonists. Current Opinion in Pharmacology. 2006;6(1):53-60.
56. Horn J, Limburg M. Calcium antagonists for acute ischemic stroke. Cochrane Database of Systematic Reviews. 2000(1).
57. Gandolfo C, Sandercock PAG, Conti M. Lubeluzole for acute ischaemic stroke. Cochrane Database of Systematic Reviews. 2002(1).
58. Hill MD, Martin RH, Mikulis D, Wong JH, Silver FL, terBrugge KG, et al. Safety and efficacy of NA-1 in patients with iatrogenic stroke after endovascular aneurysm repair (ENACT): a phase 2, randomised, double-blind, placebo-controlled trial. The Lancet Neurology. 2012;11(11):942-50.
59. Singh P, Talwar P. Exploring putative inhibitors of Death Associated Protein Kinase 1 (DAPK1) via targeting Gly-Glu-Leu (GEL) and Pro-Glu-Asn (PEN) substrate recognition motifs. Journal of Molecular Graphics and Modelling. 2017;77:153-67.
60. Shuaib A, Lees KR, Lyden P, Grotta J, Davalos A, Davis SM, et al. NXY-059 for the Treatment of Acute Ischemic Stroke. New England Journal of Medicine. 2007;357(6):562-71.
61. Follett PL, Rosenberg PA, Volpe JJ, Jensen FE. NBQX attenuates excitotoxic injury in developing white matter. J Neurosci. 2000;20(24):9235-41.

62. Tekkök SB, Goldberg MP. Ampa/kainate receptor activation mediates hypoxic oligodendrocyte death and axonal injury in cerebral white matter. J Neurosci. 2001;21(12):4237-48.
63. Manning SM, Talos DM, Zhou C, Selip DB, Park HK, Park CJ, et al. NMDA receptor blockade with memantine attenuates white matter injury in a rat model of periventricular leukomalacia. J Neurosci. 2008;28(26):6670-8.
64. Yuan X, Eisen AM, McBain CJ, Gallo V. A role for glutamate and its receptors in the regulation of oligodendrocyte development in cerebellar tissue slices. Development. 1998;125(15):2901-14.
65. Gautier HOB, Evans KA, Volbracht K, James R, Sitnikov S, Lundgaard I, et al. Neuronal activity regulates remyelination via glutamate signalling to oligodendrocyte progenitors. Nature Communications. 2015;6(1):8518.
66. Wilson HV. A NEW METHOD BY WHICH SPONGES MAY BE ARTIFICIALLY REARED. Science. 1907;25(649):912-5.
67. Madeline A Lancaster JAK. Generation of cerebral organoids from human pluripotent stem cells Nature Protocols. 2014;9:2329-40.
68. The Nobel Prize in Physiology or Medicine 2012 2021 [Available from: https://www.nobelprize.org/prizes/medicine/2012/press-release/.
69. Yakoub AM, Sadek M. Development and Characterization of Human Cerebral Organoids: An Optimized Protocol. Cell Transplant. 2018;27(3):393-406.
70. Kirk RGW. Recovering The Principles of Humane Experimental Technique: The 3Rs and the Human Essence of Animal Research. Sci Technol Human Values. 2018;43(4):622-48.
71. Daviaud N, Friedel RH, Zou H. Vascularization and Engraftment of Transplanted Human Cerebral Organoids in Mouse Cortex. eNeuro. 2018;5(6).
72. Quadrato G, Nguyen T, Macosko EZ, Sherwood JL, Min Yang S, Berger DR, et al. Cell diversity and network dynamics in photosensitive human brain organoids. Nature. 2017;545(7652):48-53.
73. Ryou M-g, Mallet RT. An In Vitro Oxygen–Glucose Deprivation Model for Studying Ischemia–Reperfusion Injury of Neuronal Cells. In: Tharakan B, editor. Traumatic and Ischemic Injury: Methods and Protocols. New York, NY: Springer New York; 2018. p. 229-35.
74. Albert B, Johnson A, Lewis J, Morgan D, Raff M, Roberts K, et al. Molecular Biology og the cell. Sixth ed2015.
75. Immunocytochemical Methods and Protocols. Totowa, New Jersey: Humana Press Inc; 1999.
76. A. Berod BKH, J-F. Pujol. Importance of fixation in Immunohistochemistry. 1980. In: The Journal of Histochemistry and Cytochemistry [Internet]. [844-50].
77. Chen X, Cho D-B, Yang P-C. Double staining immunohistochemistry 2010.
78. Renshaw S. Immunohistochemistry and immunocytochemisrty Oxford: Elsevier; 2013.
79. Ramos-Vera JA, Miller MA. When Tissue Antigens and Antibodies Get Along; Revisiting the Technical Aspects of Immunohistochemistry - The Red, Brown, and Blue Technique. 2013.
80. Igor Buchwalow VS, Werner Boecker, Markus Tiemann. Non-specific binding of antibodies in immunohistochemistry: fallacies and facts. Scientific reports 2011.
81. Im K, Mareninov S, Diaz MFP, Yong WH. An Introduction to Performing Immunofluorescence Staining. Methods Mol Biol. 2019;1897:299-311.
82. Paddock SWF, T. J. Davidson, M. W. Introductory Confocal Concepts [Available from: https://www.microscopyu.com/techniques/confocal/introductory-confocal-concepts.

83. Johannes Schindelin CTR, Mark C. Hiner, Kevin W. Eliceiri. The ImageJ ecosystem: an open platform for biomedical image analysis. Molecular Reproduction and development. 2015;82(7-8):518-29.
84. Collins TJ. ImageJ for microscopy. Biotechniques. 2007;43:25-30.
85. G Felsenfeld a, Miles HT. The Physical and Chemical Properties of Nucleic Acids. Annual Review of Biochemistry. 1967;36(1):407-48.
86. Young AP, Jackson DJ, Wyeth RC. A technical review and guide to RNA fluorescence in situ hybridization. PeerJ. 2020;8:e8806.
87. Pardue ML, Gall JG. Molecular hybridization of radioactive DNA to the DNA of cytological preparations. Proc Natl Acad Sci U S A. 1969;64(2):600-4.
88. Rudkin GT, Stollar BD. High resolution detection of DNA-RNA hybrids in situ by indirect immunofluorescence. Nature. 1977;265(5593):472-3.
89. Singer RH, Ward DC. Actin gene expression visualized in chicken muscle tissue culture by using in situ hybridization with a biotinated nucleotide analog. Proc Natl Acad Sci U S A. 1982;79(23):7331-5.
90. Fabre A-L, Colotte M, Luis A, Tuffet S, Bonnet J. An efficient method for long-term room temperature storage of RNA. European Journal of Human Genetics. 2014;22(3):379-85.
91. Kubista M, Andrade JM, Bengtsson M, Forootan A, Jonák J, Lind K, et al. The real-time polymerase chain reaction. Mol Aspects Med. 2006;27(2-3):95-125.
92. Russell JN, Clements JE, Gama L. Quantitation of gene expression in formaldehyde-fixed and fluorescence-activated sorted cells. PLoS One. 2013;8(9):e73849.
93. Palavicini JP, Lloyd BN, Hayes CD, Bianchi E, Kang DE, Dawson-Scully K, et al. RanBP9 Plays a Critical Role in Neonatal Brain Development in Mice. PLoS One. 2013;8(6):e66908.
94. Giandomenico SL, Mierau SB, Gibbons GM, Wenger LMD, Masullo L, Sit T, et al. Cerebral organoids at the air–liquid interface generate diverse nerve tracts with functional output. Nature Neuroscience. 2019;22(4):669-79.
95. Amin ND, Paşca SP. Building Models of Brain Disorders with Three-Dimensional Organoids. Neuron. 2018;100(2):389-405.
96. Alexander JE, Hunt DF, Lee MK, Shabanowitz J, Michel H, Berlin SC, et al. Characterization of posttranslational modifications in neuron-specific class III beta-tubulin by mass spectrometry. Proc Natl Acad Sci U S A. 1991;88(11):4685-9.
97. Kneynsberg A, Collier TJ, Manfredsson FP, Kanaan NM. Quantitative and semi-quantitative measurements of axonal degeneration in tissue and primary neuron cultures. J Neurosci Methods. 2016;266:32-41.
98. Dent EW, Baas PW. Microtubules in neurons as information carriers. J Neurochem. 2014;129(2):235-9.
99. Hilliard MA. Axonal degeneration and regeneration: a mechanistic tug-of-war. Journal of Neurochemistry. 2009;108(1):23-32.
100. Fernandes ES, Fernandes MA, Keeble JE. The functions of TRPA1 and TRPV1: moving away from sensory nerves. Br J Pharmacol. 2012;166(2):510-21.
101. Fame RM, Cortés-Campos C, Sive HL. Brain Ventricular System and Cerebrospinal Fluid Development and Function: Light at the End of the Tube: A Primer with Latest Insights. Bioessays. 2020;42(3):e1900186.
102. Stratchko L, Filatova I, Agarwal A, Kanekar S. The Ventricular System of the Brain: Anatomy and Normal Variations. Seminars in Ultrasound, CT and MRI. 2016;37(2):72-83.
103. Di Lullo E, Kriegstein AR. The use of brain organoids to investigate neural development and disease. Nature Reviews Neuroscience. 2017;18(10):573-84.

104. Kardia E, Frese M, Smertina E, Strive T, Zeng X-L, Estes M, et al. Culture and differentiation of rabbit intestinal organoids and organoid-derived cell monolayers. Scientific Reports. 2021;11(1):5401.
105. Camp JG, Badsha F, Florio M, Kanton S, Gerber T, Wilsch-Bräuninger M, et al. Human cerebral organoids recapitulate gene expression programs of fetal neocortex development. Proceedings of the National Academy of Sciences. 2015;112(51):15672-7.
106. Lancaster MA, Renner M, Martin C-A, Wenzel D, Bicknell LS, Hurles ME, et al. Cerebral organiods model human brain development and microcephaly. 2014.
107. Rayasam A, Hsu M, Kijak JA, Kissel L, Hernandez G, Sandor M, et al. Immune responses in stroke: how the immune system contributes to damage and healing after stroke and how this knowledge could be translated to better cures? Immunology. 2018;154(3):363-76.
108. Schilling M, Besselmann M, Leonhard C, Mueller M, Ringelstein EB, Kiefer R. Microglial activation precedes and predominates over macrophage infiltration in transient focal cerebral ischemia: a study in green fluorescent protein transgenic bone marrow chimeric mice. Experimental Neurology. 2003;183(1):25-33.
109. Patel AR, Ritzel R, McCullough LD, Liu F. Microglia and ischemic stroke: a double-edged sword. Int J Physiol Pathophysiol Pharmacol. 2013;5(2):73-90.
110. Xing C, Arai K, Lo EH, Hommel M. Pathophysiologic cascades in ischemic stroke. Int J Stroke. 2012;7(5):378-85.
111. Wang H. Modeling Neurological Diseases With Human Brain Organoids. Front Synaptic Neurosci. 2018;10:15.
112. Pașca AM, Park J-Y, Shin H-W, Qi Q, Revah O, Krasnoff R, et al. Human 3D cellular model of hypoxic brain injury of prematurity. Nature Medicine. 2019;25(5):784-91.
113. Sawai T, Sakaguchi H, Thomas E, Takahashi J, Fujita M. The Ethics of Cerebral Organoid Research: Being Conscious of Consciousness. Stem Cell Reports. 2019;13(3):440-7.
114. Doke SK, Dhawale SC. Alternatives to animal testing: A review. Saudi Pharm J. 2015;23(3):223-9.
115. Rollin BE. Toxicology and New Social Ethics for Animals. Toxicologic Pathology. 2003;31(1_suppl):128-31.
116. Gibbs NM, Gibbs SV. Misuse of 'trend' to describe 'almost significant' differences in anaesthesia research. BJA: British Journal of Anaesthesia. 2015;115(3):337-9.
117. Zhang R, Chopp M, Zhang ZG. Oligodendrogenesis after cerebral ischemia. Front Cell Neurosci. 2013;7:201.
118. Franklin RJM, ffrench-Constant C. Remyelination in the CNS: from biology to therapy. Nature Reviews Neuroscience. 2008;9(11):839-55.
119. Gudz TI, Komuro H, Macklin WB. Glutamate stimulates oligodendrocyte progenitor migration mediated via an alphav integrin/myelin proteolipid protein complex. J Neurosci. 2006;26(9):2458-66.
120. Taupin P. BrdU immunohistochemistry for studying adult neurogenesis: Paradigms, pitfalls, limitations, and validation. Brain Research Reviews. 2007;53(1):198-214.
121. Wang XL, Cui LW, Liu Z, Gao YM, Wang S, Li H, et al. Effects of TRPA1 activation and inhibition on TRPA1 and CGRP expression in dorsal root ganglion neurons. Neural Regen Res. 2019;14(1):140-8.
122. Williamson JR. Glycolytic control mechanisms. II. Kinetics of intermediate changes during the aerobic-anoxic transition in perfused rat heart. J Biol Chem. 1966;241(21):5026-36.

8. Appendix

Section A

Reagents, kits, consumables, instruments and softwares

Table S1: Reagents, producers and catalogue numbers

Reagent	Producer	Catalogue nr
Geltrex, LDEVFree, hESCQualified, Reduced Growth Factor Basement Membrane Matrix	Thermo Fisher Scientific, Waltham, MA, USA	A1413301
DMEM/F12 medium	Thermo Fisher Scientific, Waltham, MA, USA	11330-057
Essential 8 medium	Thermo Fisher Scientific, Waltham, MA, USA	A1517001
Accutase	Stemcell Technologies, Vancouver, Canada	07920
ROCK inhibitor Y27632	Sigma-Aldrich®, Darmstadt, Germany	SCM075
KnockOut Serum Replacement (KOSR)	Thermo Fisher Scientific, Waltham, MA, USA	10828-028
Hyclone Fetal Bovine Serum	Thermo Fisher Scientific, Waltham, MA, USA	SH30070.03
GlutaMAX Supplement	Thermo Fisher Scientific, Waltham, MA, USA	35050-061
MEM NonEssential Amino Acids Solution	Thermo Fisher Scientific, Waltham, MA, USA	11140-050
2mercaptoethanol	Thermo Fisher Scientific, Waltham, MA, USA	21985023
Penicillin Streptomycin Solution 100X	VWR, Pennsylvania, USA	30002CI
Recombinant human FGFbasic	Peprotech, Cranbury, NJ, USA	10018B
N2 supplement 100X	Thermo Fisher Scientific, Waltham, MA, USA	17502048
Heparin	Sigma-Aldrich®, Darmstadt, Germany	21103-049
Neurobasal Medium	Thermo Fisher Scientific, Waltham, MA, USA	21103-049
Insulin	Sigma-Aldrich®, Darmstadt, Germany	I9278
B27 without Vitamin A	Thermo Fisher Scientific, Waltham, MA, USA	12587010
B27	Thermo Fisher Scientific, Waltham, MA, USA	17504044
Matrigel matrix gel	Corning, Tewksbury, MA, USA	356234

Recombinant Human BDNF	Peprotech, Cranbury, NJ, USA	45002B
T3 (60 ng/mL)	Sigma-Aldrich®, Darmstadt, Germany	T2877
HGF (5 ng mL)	Peprotech, Cranbury, NJ, USA	315-23
IGF-1 (10 ng/mLl)	VWR, Pennsylvania, USA	100-11
PDGF-AA (10 ng ml−1)	R&D Systems, Minnesota, USA	221-AA
NT-3 (20 ng ml−1)	Peprotech, Cranbury, NJ, USA	450-03
cAMP (1 µM)	Sigma-Aldrich®, Darmstadt, Germany	D0627
D-AP5 (50 µM I water)	Abcam, Cambridge, UK	Ab 120003
NBQX (µM in DMSO)	Abcam, Cambridge, UK	Ab 120046
HC-030031 (80 µM in DMSO)	Abcam, Cambridge, UK	Ab 120554
A967079 (10 µM in DMSO)	Abcam, Cambridge, UK	Ab 144580
Paraformaldehyde (PFA)(4% and 0,4 %)	Santa Cruz, Dallas, UDA	281692
Tween®20	Sigma-Aldrich®, Darmstadt, Germany	P1379
10% Neutral Buffered Formalin (NBF)	Sigma-Aldrich®, Darmstadt, Germany	HT501128-4L
Sucrose in PBS (10%, 20% and 30%)	Sigma-Aldrich®, Darmstadt, Germany	110M00382V
Neg-50 frozen section mounting medium	Mercedes Scientific	FIS 22046511
Phosphate-buffered saline (PBS) (0,01 M, pH 7,4)	Oslo Universury Hospital, department of Microbiology	20060301
DAPI (1:5000)	Sigma-Aldrich®, Darmstadt, Germany	D-9542-1MG
ProLong™ Glass Antifade Mountant	Thermo Fisher Scientific, Waltham, MA, USA	P36981
10% Normal goat serum (NGS)	Sigma-Aldrich®, Darmstadt, Germany	69023
1% Bovine serum albumin (BSA)	Saween & Werner, Limhamn, Sweden	B2000-500
Triton™ X-100	Sigma-Aldrich®, Darmstadt, Germany	T8787
PowerUp™ SYBR™ Green Master Mix	Thermo Fisher Scientific, Waltham, MA, USA	4367659
RNase free water	Thermo Fisher Scientific, Waltham, MA, USA	10977-035
TRIzol RNA Isolation Reagents	Thermo Fisher Scientific, Waltham, MA, USA	15596026
Neutral Buffered Formalin (NBF)	Chemi-Teknik AS, Oslo, Norway	21254

Table S2: Antibodies used in immunohistochemistry

Primary antibodies	Dilution	Manufacturer	Catalogue number
Rabbit anti-GFAP	1:400	Thermo Fisher Scientific, Waltham, MA, USA	
Rabbit anti-SOX10	1:400	Abcam, Cambridge, UK	AB155279
Mouse anti-NG2	1:200	Merck Millipore, Darmstadt, Germany	MAB2029
Mouse anti-TUJ-1	1:1000	R&D systems/ BIO Techne, Minneapolus, UAS	MAB1195
Rabbit anti- Cleaved caspase-3	1:400	Cell Signaling Technology, Inc, Danvers, MA, USA	ASP 175
Secondary antibodies	**Dilution**	**Manufacturer**	**Catalogue number**
Goat anti-mouse Alexa Fluor 488	1:400	Thermo Fisher Scientific, Waltham, MA, USA	A11029
Goat anti-mouse Alexa Fluor 555	1:400	Thermo Fisher Scientific, Waltham, MA, USA	A21424
Goat anti-rabbit Alexa Fluor 488	1:400	Thermo Fisher Scientific, Waltham, MA, USA	A11034
Goat anti-rabbit Alexa Fluor 555	1:400	Thermo Fisher Scientific, Waltham, MA, USA	A21429

Table S3: Antibodies used in FISH

Primary antibodi	Dilution	Manufacturer	Catalogue number
Rabbit anti-Olig2	1:100	R&D systems/ BIO Techne, Minneapolus, UAS	MAB9610
Mouse anti-TUJ-1	1:500	R&D systems/ BIO Techne, Minneapolus, UAS	MAB1195
Secondary antibodies	**Dilution**	**Manufacturer**	**Catalogue number**
Goat anti-mouse Alexa Fluor 488	1:400	Thermo Fisher Scientific, Waltham, MA, USA	A11029
Goat anti-mouse Alexa Fluor 555	1:400	Thermo Fisher Scientific, Waltham, MA, USA	A21070

Table S4: Kits, producers and catalogue number

Kit	Producer	Catalogue number
RNeasy Plus Micro Kit	QIAGEN, Hilden, Germany	74004
High-Capacity cDNA Reverse Transcription Kit	Thermo Fisher Scientific, Baltics, Vilnius	4368814
RNAscope® Multiplex Fluorescent Reagents Kit v2	ACD Bio-techne Newark, CA, USA	323100

Table S5: Consumables, producers and catalogue number

Consumable	Producer	Catalogue number
Superfrost™ Microscope Slides	Thermo Fisher Scientific, Waltham, MA, USA	12372098
Menzel-Glaser	Thermo Fisher Scientific, Waltham, MA, USA	11778691
Absolute alcohol prima ren	Antibac, Asker, Norge	600068
Immersol™ Immersion Oil	Thermo Fisher Scientific, Waltham, MA, USA	10539438
ImmEdge™ Hydropfobic Barrier PAP Pen	Maravai LifeScience	H-4000
Tissue Culture Plate 6 well	Corning, Tewksbury, MA, USA	-
Tissue Culture Plate 24 well	Corning, Tewksbury, MA, USA	-
Tissue Culture Plate 96 well	F Corning, Tewksbury, MA, USA	-
MicroAmp® Fast 96-well Reaction Plate	Thermo Fisher Scientific, Waltham, MA, USA	4346907
Optical Adhesive Covers	Thermo Fisher Scientific, Waltham, MA, USA	4360954

Table S6: Equipment and instruments

Equipment and instruments	Producer	Catalogue number
StepOnePlusTM Real-Time PCR System	Thermo Fisher Scientific, Waltham, MA, USA	4376600
Microcentrifuge 5424 R	Eppendorf®, Hamburg, Germany	Z722960
NanoDrop™ Spectrophotometer	Thermo Fisher Scientific, Waltham, MA, USA	13-400-518
Applied Biosystems™ 2720 Thermal Cycler	Thermo Fisher Scientific, Waltham, MA, USA 1	12313653
Leica TCS SP8 gSTED microscopy	Leica Microsystems, Santa Clara, CA, USA	-
Immuno Slide Staining Tray, Moisture chamber	Pyramid Innovation, Polegate, Engalnd	-
Hypoxia Induction Chamber	Stemcell Technologies, Vancouver, Canada	27310
Heating incubator	Termaks AS, Bergen, Norway	390-0750NO

Table S7: Softwares and developmers

Software	Developer
Fiji/Image J	Rasband, National Institutes of Health (NIH), Maryland, USA
LASX software	Leica Microsystems, Santa Clara, CA, USA
Microsoft® Excel	Microsoft, Redmond, WA, USA

GraphPad Software Prism	GraphPad Software, San Diego, CA, USA
StepOne™ Software	ThermoFisher (qPCR pcen)

Table S8: PCR program

Temperatur	Time
25 °C	10 min
37 °C	120 min
85 °C	5 min
4 °C	∞

Table S9: RT-qPCR set-up

Temperature	Time
95 °C	10 min
95 °C	15 sec x 40
58°C	1 min x 40
95°C	15 sec
60°C	1 min
95°C	15 sec

Table S10: RT-qPCR primer sequences

Gene	Forward/Reverse	Sequence
GAPDH	Forward	CCACATCGCTCAGACACCAT
	Reverse	GCGCCCAATACGACCAAAT
SOX10	Forward	CCAGGCCCACTACAAGAGC
	Reverse	CTCTGTCTTCGGGGTGGTTG
NG2	Forward	CTGGTCCGGCACAAGAAGAT
	Reverse	ATACGATGTCTGCAGGTGGC
TUJ-1	Forward	GCAACTACGTGGGCGAC
	Reverse	TCGAGGCACGTACTTGT
TRPA1	Forward	AGCTGTGCAGGGCATGAATA
	Reverse	TTTGTGGTGCACGCAATGAT

Table S11: RNA-FISH probes.

Species	RNA Scope Probe	Accession number
Human	Hs-TRPA1-O1-C3	NM 007332.2
Mouse	Mm-TRPA1-01	NM 177781.5

Section B

Mediums, solutions, buffers and reaction volumes

Mediums for organoid setup

Embryoid body medium – EBM (~40 mL)
- DMEM-F12 (30 mL)
- KOSR (7,5 mL)
- Fetal Bovine Serum (1 mL)
- GlutaMAX (0,4 mL)
- MEM-NEAA (0,4 mL)
- 2-mercaptoethanol (10 µL)

Day 0 to 4 included:
- iROCK 50µM (150 µL)
- FGF 4 ng/µL (150ng/10µL)

Neural Induction Medium – NIM (~50 mL)
- DMEM-F12 (without Glutamin & Hepes) (48,5 mL)
- N2 supplement (0,5 mL)
- GlutaMAX (0,5 mL)
- MEM-NEAA (0,5 mL)
- Heparin (50 µL)

Neuronal differentiation medium – NDM (~50 mL)
- DMEM-F12 (wo Glutamin & Hepes) (25 mL)
- Neurobasal medium (25 mL)
- N2 supplement (0,25mL)
- GlutaMAX (0,5 mL)
- MEM-NEAA (0,25 mL)
- Insulin (12,5 µL)
- 2-mercaptoethanol (17,5 µL)
- B27 with or without vitamin A (0,5 mL)

OPC medium 1 - OPCM1 (~50 mL)
- DMEM-F12 (wo Glutamin & Hepes) (25 mL)
- Neurobasal medium (25 mL)
- N2 supplement (0,25mL)
- GlutaMAX (0,5 mL)
- MEM-NEAA (0,25 mL)
- Insulin (12,5 µL)
- 2-mercaptoethanol (17,5 µL)
- B27 with vitamin A (0,5 mL)
- BDNF (20 ng/mL) (1µg)
- cAMP (1µM) (24,6 µg)
- T3 (60 ng/mL) (3µg)
- Hepatocytt growth factor (5ng/mL) (250ng)
- Insulin-like growth factor 1 (10 ng/mL) (500ng)
- PDGF-AA (10ng/mL) (500ng)
- NT-3 (20 ng/mL) (1µg)

OPC medium 2 – OPCM2 (~50 mL)
- DMEM-F12 (wo Glutamin & Hepes) (25 mL)
- Neurobasal medium (25 mL)
- N2 supplement (0,25mL)
- GlutaMAX (0,5 mL)
- MEM-NEAA (0,25 mL)
- Insulin (12,5 µL)
- 2-mercaptoethanol (17,5 µL)
- B27 with vitamin A (0,5 mL)
- BDNF (20 ng/mL) (1µg)
- cAMP (1µM) (24,6 µg)
- T3 (60 ng/mL) (3µg)

Mediums for ischemia experiment
Ischemia medium (10 mL):
- DMEM/F-12 Flex media, ÷ glucose, + phenol red + penicillin-streptomycin (5 mL)
- Neurobasal -A medium, ÷ D-glucose, ÷ sodium pyruvate added penstrep and phenol red (4.85 mL)
- N2 supplement (50 µl)
- MEM-NEAA (50 µl)
- B27 supplement + Vit A (100 ul)
- 2-mercaptoethanol (3.5 µl)
- NaCl (50 ul from 2 M stock)

Control medium (10 mL):
- DMEM/F-12 Flex media, ÷ glucose, + phenol red + pencillin-streptomycin (5 mL)
- Neurobasal -A medium, ÷ D-glucose, ÷ sodium pyruvate + penicillin-streptomycin (4.6 mL)
- N2 supplement (50 µL)
- MEM-NEAA (50 µL)
- GlutaMAX (100 µL)
- B27 supplement + Vit A (100 µL)
- 2-mercaptoethanol (3,5 µL)
- Glucose (0.3 mL)

Antagonists:
- NMDA antagonist: D-AP5 (50 µM).
10 mg D-AP5 in 507 µL water = 100mM. 10µL per 20 mLOPCM2 medium gives 50µM.
- AMPA antagonist: NBQX (25 µM in DMSO).
10 mg NBQX in 297µL DMSO = 100 mM (5µL per 20mL OPCM2 medium gives 25 µM).
- TRPA1 antagonist: HC-030031 (80 µM in DMSO).
10 mg HC-030031 in 282µL = 100mM (16µL per 20mL OPCM2 medium gives 80µM).
- TRPA1 antagonist: A967979 (10 µM in DMSO).
10mg A967079 in 483µL DMSO = 100mM (2µL per 20mL OPCM2 medium gives 10µM).

Sucrose feeding solutions
Sucrose in PBS (10 %, 20 % and 30 %):
- 10% = 20g sucrose + PBS that make in total 200mL solution

- 20% = 40g sucrose + PBS that make in total 200mL solution
- 30% = 60g sucrose + PBS that make in total 200mL solution

Solutions for immunohistochemistry:
- PBS (0,01 M, pH 7,4)
- Citrate buffer (10 mM, pH 6.0)

Block solutions:
- 10 % Normal goat serum
- 1 % Bovine serum albumin
- 0,5 % Triton X-100
- Diluted in PBS

Primary and secondary antibody solution:

- 3 % Normal goat serum
- 1 % Bovine serum albumin
- 0,5 % Triton X-100
- Diluted in PBS

Table S12: Reagents and amount per reaction in synthesis of cDNA.

Reagents	**Amount (µL)**
Buffer	2
dNTPs	0,8
Randome primers	2
MultiScribe Reverse transcriptase	1
sH_20	4,2
Total RNA 10 ng/ µL	10

Table S13: RT-qPCR mixture reagents and volume per reaction.

Reagent	**Amount (µL)**
PowerUp SYBR Green Master mix 2X	5
Primer Forward 10 µM	0,2
Primer Reverse 10 µM	0,2
sH_2O	2,6
cDNA 1:8	2

Norges miljø- og biovitenskapelige universitet
Noregs miljø- og biovitskapelege universitet
Norwegian University of Life Sciences

Postboks 5003
NO-1432 Ås
Norway